10 EUR

HUNGARIAN GROUP OF *fib*

CONCRETE STRUCTURES

ANNUAL TECHNICAL JOURNAL

2022

Vol. 23


FERROBETON
A CRH COMPANY
safe basis provided by concrete
www.ferrobeton.hu

CONCRETE STRUCTURES
Journal of the Hungarian Group of ***fib***

Founded by: Hungarian Group of ***fib***
Publisher: Hungarian Group of ***fib***
(***fib*** = International Federation for Structural Concrete)

Editorial office:
Budapest University of Technology and Economics (BME)
Department of Construction Materials and Engineering Geology
Műegyetem rkp. 3., H-1111 Budapest
Phone: +36-1-463 4068
Fax: +36-1-463 3450
WEB http://www.fib.bme.hu
WEB editor: András Bíró

Layout and print: Csaba Halmai, Navigar Ltd.

Price: 10 EUR, Printed in 1000 copies

HU ISSN 2062-7904
online ISSN: 1586-0361

Cover photo:
Construction of Tisza bridge at M44 expressway between Lakitelek and Tiszakürt

Photos by: Zoltán Kispéter

CONTENT

Sponsors:

Railway Bridges Foundation, ÉMI Nonprofit Ltd., HÍDÉPÍTŐ Co., Holcim Hungary Co., MÁV Co., MSC Consulting Co., Lábatlani Vasbetonipari Co., Pont-*TERV* Co., UVATERV Co., MÉLYÉPTERV KOMPLEX Engineering Co., SW Umwelttechnik Hungary Ltd., Betonmix Consulting Ltd., BVM Épelem Ltd., CAEC Ltd., Pannon Freyssinet Ltd., STABIL PLAN Ltd., UNION PLAN Ltd., DCB Consulting Ltd., BME Dept. of Structural Engineering, BME Dept. of Construction Materials and Technologies

CONSTRUCTION WORKS OF THE TISZA BRIDGE IN THE M 44 EXPRESSWAY SECTION BETWEEN LAKITELEK-TISZAKÜRT


István Lakatos - Zoltán Kispéter

https://doi.org/10.32970/CS.2022.1.1

Work commenced in the first half of 2019 on the newest section of the M 44, connecting Nagykőrös to Békéscsaba, between Lakitelek and Tiszakürt. A new 556-metre-long Tisza bridge was built here by A-Híd Zrt., based on the plans of Uvaterv Co. (professional designer), with a maximum span of 152 metres. The project is implemented by National Infrastructure Development Ltd., the main contractor was Duna Aszfalt Ltd. The traffic started on the superstructure in December 2021 (Fig. 1).

KEY DATA OF THE TISZA BRIDGE:

Crossing angle:	90°
Span:	45.00+76.00+152.00+76.00+40.40+40.40+40.40+39.05 m
Riverbed span:	147.90 m
Superstructure length:	556.55 m
Deck slab width:	23.12 m
Superstructure surface:	12,867 m^2
Foundation:	bored pile foundation
Superstructure:	cable-stayed bridge with composite superstructure; reinforced steel girders and reinforced concrete slab

Fig. 1: Tisza bridge

RIVER BRIDGE – SUPERSTRUCTURE

The riverbed bridge is a three-span cable-stayed bridge with a maximum span of 152.00 m. Steel – concrete composite superstructure, with two steel box girder and a reinforced concrete slab with a parallel belt, is suspended on the outside by stay cables on half-elliptical reinforced concrete pylons.

The superstructure consists of a main girder, pylons, and stay cables. The steel main girder consists of two single-celled box girders with sloping webs, and function as a composite superstructure with an on-site concrete slab.

PYLONS

The cross-sectional area of the pylon is 3.00 x 2.50 m, with the highest point at 37.64 m above the track level and the highest point above 52 m above the ground level. The cables are symmetrically spaced, spaced evenly along the elliptical axis of the pylon at the top and located at 8 m intervals along the length of the superstructure at the bottom. The tension cables were leaded through the saddles in the pylon.

Custom-made Ø40 rebars were an essential part of the reinforcement. Due to the limited cross-section (there was no space for conventional couplers in most parts of the superstructure), special reinforcing steel couplers had to be used. *(Fig. 2).*

The pylon was built in thirteen concreting phases, with climbing formwork. In total, around 70 tonnes of formwork material were used to construct the arches. The height of the strokes varied between 3 and 4 metres, closely matching the phases of the reinforcement. For each phase, detailed formwork plans have been drawn up, taking particular care to manage the constant deformation due to the special shape of the pylon. Plenty of custom-made formwork panels and boxes were needed.

In order to work efficiently and safely, it was expected that in addition to the current working level, technological working

Fig. 2: Pylons

Fig. 3: Working platform

levels would be established at the upper and lower levels of the formwork.

With this system, phases I-X could be completed.

The connecting fittings in the pylon (saddles, flight direction lights, etc.) made our task even more difficult.

A new solution was needed for the formwork of the pylons in phases XI-XIII, as the previously used formwork system was no longer usable due to the high inclination. *(Fig. 3,4)* A-Híd Zrt. Technical Department and the colleagues working on the site have designed and developed a working platform consisting of modular elements created by the pylon legs being supported together. This platform provided both safe working conditions and adequate support. The scaffolding and formwork system for the upper phases were completed from this working level.

The pylon construction works were served by 1 Wolff WK 91 SL type tower crane, respectively.

During the break between the two phases of the tensioning works, the painting of the pylon in "pigeon blue" colour was also started, partly using the alpine technique.

MAIN BRIDGE

The steel superstructure of the riverbed bridge under the slab, connected by cross girders, was erected and pushed from both flood plains towards the middle of the bridge. After the steel superstructure was completed and adjusted, the cables were installed and tensioned simultaneously with the on-site concrete slab in several phases. The factory and on-site joints were made by welding. *(Fig. 5)*

In order to serve the formwork of the slab, it was necessary to build a temporary moving working level between the box girders. The formwork wagons were in operation all day, as the formwork of the slab, the concreting and the reinforcing works were continuously. The concreting was carried out in five steps according to the phasing diagrams provided by the designer - in co-ordination with the tensioning of the stay

Fig. 4: Working platform

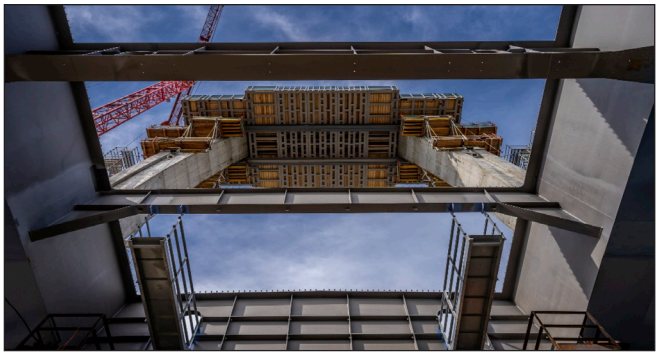

Fig. 5: Erecting area

cables. The concreting of Phase I (one field on the right and one on the left bank) was a spectacular operation, as it was carried out in synch with 4 concrete pumps. With the next concreting phase (also two segments), followed by the placement of the joints, the riverbed bridge slab was connected to the floodplain bridges on both the right and left banks. Concreting works of the riverbed bridge slab continued after the 2nd tensioning step (last two cable groups).

APPROACH BRIDGES

The pillars are made with a 7.70 m wide 1.50 m high pile head beam and 1.80 m diameter columns.
Superstructure of the approached bridges were made with using prefabricated prestressed reinforced concrete beams.

The approach bridge superstructure is an on-site concrete slab with composite precast prestressed reinforced concrete bridge girders. A total of 127 bridge beams were built for the two floodplain bridges. Due to the limited working space, the lifting of the beams had to be carried out with 2 cranes in several cases. *(Fig. 6)*

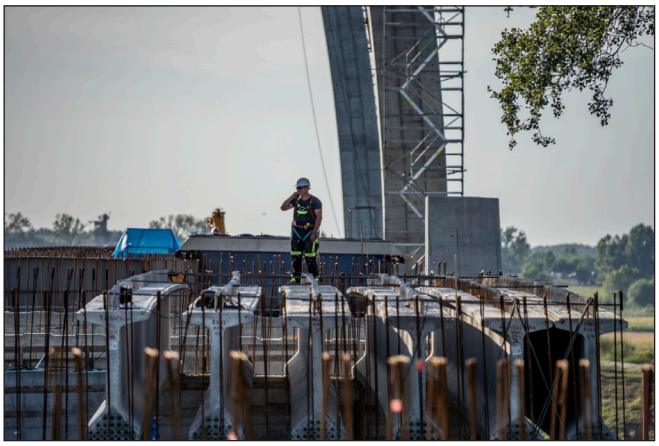

Fig. 6: bridge beams

István Lakatos, project leader (1973) He graduated as a civil engineer at the Institute of Water Management of the Pollak Mihály Technical College, Baja. He has been working for A-Híd Zrt. for 25 years. As a project leader he is typically working on Civil Engineering, Structural Engineering and Bridge Constructions.

Zoltán Kispéter, chief engineer (1980) He graduated as an Engineer from the Faculty of Engineering, University of Szeged. He has been working for A-Híd Zrt. for 10 years. As a chief engineer, he is typically involved in Civil Engineering, Structural Engineering and Bridge Construction works.

EXTENDED RANKINE FAILURE CRITERIA FOR CONCRETE

Andor Windisch

https://doi.org/10.32970/CS.2022.1.2

As possible failure criteria MC2010 refers to those of Rankine, Drucker-Prager and Mohr-Coulomb, respectively, and to modifications or combinations of them. After a brief overview of these failure criteria the characteristics of Mohr-circle are described. Next chapter discusses why the Modified Mohr–Coulomb failure criterion fails in case of concrete. Displaying the Mohr-circles of different bi- and triaxial test series reveal that neither the straight nor the parabolic failure criteria fit. The failure patterns of uniaxial compressive and tensile test specimens prove that concrete fails due to principal tensile stresses/strains in separation and concrete is not a frictional material. The proposed Extended Rankine failure criteria are based directly on the principal stresses.

The criteria limit the greatest- and the actual smallest principal stress, respectively. This latter is function of the two other principal stresses. It is shown that the Ultimate Strength Surface cannot be properly described as stated by CEB Bulletin Nr. 156

Keywords: failure criterion, Rankine, Mohr-circle, Mohr-Coulomb criterion, friction, sliding, separation, principal stress, shear stress

1. INTRODUCTION

MC2010 5.1.8.3 gives the following guidelines about the possible yield functions of concrete under multiaxial states of stresses:

"Basically, yield functions *f* and plastic potentials *g* can be chosen based on multi-axial failure criteria for concrete. These criteria should depend not only on shear stresses, but also on the first invariant I_1 of the stress tensor to consider the influence of the hydrostatic pressure on the ductility of the material. Thus, formulations as the

- Rankine criterion, where tensile failure occurs when the maximum principal stress reaches the uniaxial tensile strength f_{ct}; refer to Rankine, W.J.M., "A Manual of Applied Mechanics", (London, 1868)
- Drucker-Prager criterion, which is the modification of von Mises criterion including the influence of hydrostatic pressure on yielding; refer to Drucker, D.C.; Prager, W., "Soil mechanics and plastic analysis of limit design" (Quarterly of Applied Mechanics, Vol. 10, 1952),
- Mohr-Coulomb criterion, where the maximum shear stress is the decisive measure of yielding, and the critical shear stress value depends on hydrostatic pressure; refer to Mohr, O., "Scientific paper on the area of technical mechanics " (Ernst & Sohn, Berlin, 1906; in German),

and modifications or combinations of them can be used in concrete plasticity models."

After a brief overview about the different failure criteria and about the characteristics of Mohr-circle we discuss why the modified Mohr–Coulomb failure criterion does not fit in case of concrete. Thereafter an extended Rankine failure criterion is proposed. This criterion is based directly on the principal stresses for both, the tensile and the compression failure and is valid in case of triaxial states of stress, too.

2. BRIEF PRELIMINARY OVERVIEW

2.1 Failure criteria

Here are the relevant failure criteria briefly recalled.
Coulomb presented in 1776 his frictional hypothesis: failure often occurs along certain sliding planes, the resistance of which is determined by a parameter termed the cohesion and an internal friction, the magnitude of which depends on the normal stress in the sliding plane (*Figure 1*).

Note: Coulomb dealt with friction between two independent solid bodies separated already through a plane surface. His hypothesis does not apply to separate (fail) a solid body into two parts. After the force parallel to the contact surface has overcome the resting frictional force, the two bodies slide on each other.

Rankine stated in his 1876 published model that a body fails when any of the three principal stresses exceeds the ultimate tensile strength, regardless of the magnitude of the other principal stresses.

In 1868 Tresca postulated for mild steel that failure occurs when the maximum value of the shear stress is exceeded.

In 1882 Mohr assumed that failure occurs when the stresses in a section satisfy the condition:

$$f(\sigma, \tau) = 0 \qquad (1)$$

This function displaced in the σ, τ coordinate system yields Mohr's failure envelop (*Figure 2*). Its simplest form can be got as it just touches the Mohr's circles corresponding to the uniaxial tensile strength (σ_1, 0) and uniaxial compressive strength (σ_3, 0).

Leon (1935) realized that some test results of Mörsch on concrete specimens were in contradiction to the failure crite-

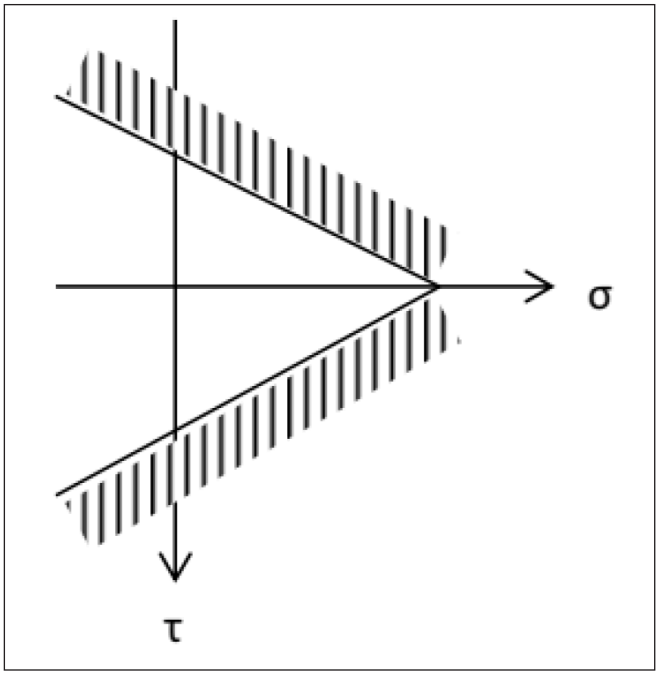

Figure 1: Coulomb´s frictional hypothesis

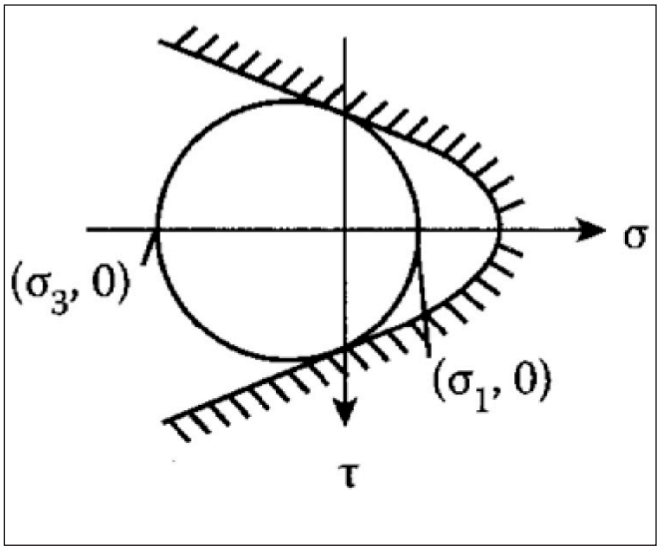

Figure 2: Mohr´s failure envelope

rion of Mohr with the straight envelop. This would anticipate that the failure section at tensile test occurs under the same inclination φ/2 as in case of compression, which is not the case. A parabolic envelop was introduced: it is symmetric to σ-axis, its apex touches the circle corresponding to the uniaxial tensile test at f_t. In addition, the parabola tangents the Mohr-circle of the uniaxial compression test. *Figure 3* shows this parabola corresponding to the ratio $f_c/f_t = 14$, and three circles representing some tests of Mörsch.

The equation of the envelop is:

$$\sigma(\tau) = -\frac{1}{2f_t + f_c - \sqrt{f_t(f_t + f_c)}} \cdot \tau^2 + f_t \qquad (2)$$

Both, Coulomb's hypothesis and Leon's parabola are defined by two parameters only, which generally are not sufficient to fit the experimental data. The simplest extension (one more parameter) is the tension cutoff: the greatest tensile principal stress is limited: a combination of Coulomb's friction hypothesis with Rankine's principal stress hypothesis to describe a separation failure (*Figure 4*). An advantage of this

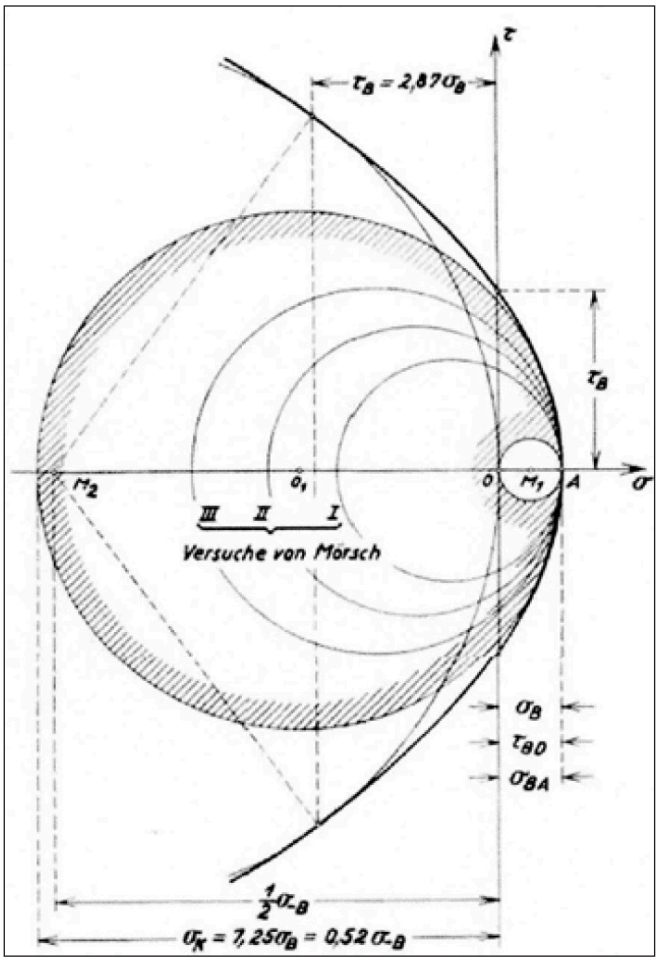

Figure 3: Parabolic rupture criterion for concrete in plane stress coordinate system as presented by Leon

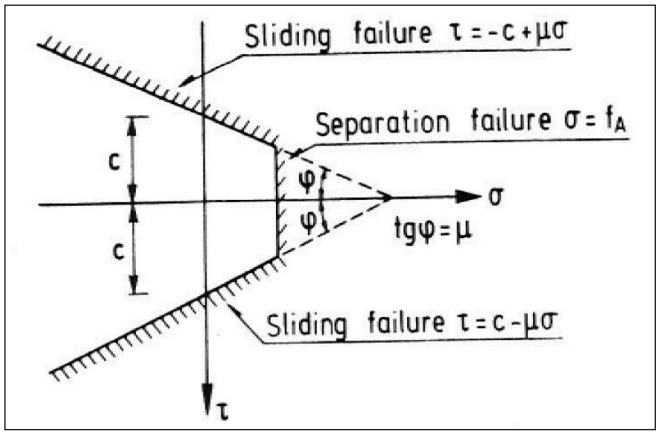

Figure 4: Modified Coulomb rupture criterion

Modified Coulomb Criteria is that the tensile strength (the third parameter) may be varied independently of the two others.

A Modified Coulomb Material can reveal sliding failure and separation failure (*Figure 4*). At sliding failure a motion parallel to the failure surface occurs, while the relative motion at separation failure is perpendicular to the failure surface.

2.2 Mohr´s Circle

As Mohr's circle plays a central role in this proposal some of its characteristics shall be brush up here.

Mohr's circle is a two-dimensional graphical representation of the transformation law for the Cauchy stress tensor. It is used for calculating stresses at a particular material point

with respect to a coordinate system in many planes by reducing them to vertical and horizontal components. These are called principal planes in which principal stresses are calculated; Mohr's circle can also be used to find the principal planes and the principal stresses in a graphical representation and is one of the easiest ways to do so.

The abscissa and ordinate (σ, τ) of each point on the circle are the magnitudes of the normal stress and shear stress components, respectively, acting on the rotated coordinate system. In other words, the circle is the focus of points that represent the state of stress on individual planes at all their orientations, where the axes represent the principal axes of the stress elements.

Note: for a Mohr's circle for plane stress state three stress components are needed: σ_x, σ_y and τ_{xy}, i.e. two (σ, τ) are not enough.

Note: Having a Mohr-circle which pertains to a failure then in principle each point on this circle represents the failure. The point where the circle touches the (correct?) Modified Coulomb border line (which needs not to be straight) has no privileged importance. Concrete does not fail in shear/sliding but in all cases in tension/tensile cracking/separation.

Note: the 'shear stress' is an auxiliary parameter only, a stress component. It characterizes the stress in the structural material at a given point only in conjunction with the normal stress components. Concrete has no shear strength. The loading pattern 'pure shear' results in two principal stresses of the same size as the shear stress, acting in ±45° planes. The separation failure occurs when the size of principal tensile stress reaches the actual tensile strength. No sign of shear failure or of sliding!

For a general three-dimensional case of stresses at a point, the values of the principal stresses (σ_1, σ_2, σ_3) and their principal directions (n_1, n_2, n_3) must be first evaluated. Based on the three principal stresses the three Mohr-circles having their centers on the σ_n axis between the points with the abscissas σ_1 vs. σ_2, σ_1 vs. σ_3 and σ_2 vs. σ_3 resp. can be drawn.

3. WHY THE MODIFIED MOHR–COULOMB FAILURE CRITERION FAILS IN CASE OF CONCRETE?

It is generally accepted that the failure criterion of concrete is well described as a Modified Coulomb Material. The Mohr–Coulomb failure criterion represents the linear envelope that is obtained from a plot of the shear strength of a material versus the applied normal stress. This relation is expressed as

$$\tau = \sigma \cdot tan\varphi + c \qquad (3)$$

where τ is the shear stress, σ is the normal stress, c is the intercept of the failure envelope with the τ axis, and tanφ is the slope of the failure envelope. The quantity c is often called the cohesion and the angle **φ is called the angle of internal friction.** Compression is assumed to be positive in the following discussion. (If compression is assumed to be negative then σ should be replaced with − σ)

If φ = 0, the Mohr–Coulomb criterion reduces to the Tresca criterion. On the other hand, if φ = 90° the Mohr–Coulomb model is equivalent to the Rankine model. Higher values of φ are not allowed.

Important note: in case of φ < 90° sliding failure should occur whereas at φ = 90° separation failure appears! An odd change!

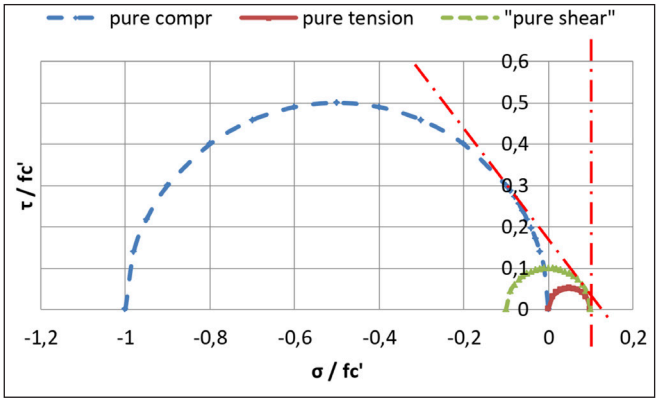

Figure 5: *Normalized Mohr-circles define the Modified Coulomb failure criteria*

Figure 5 presents the Mohr-circles (normalized with f_c') for uniaxial compression, uniaxial tension and 'pure shear' of a concrete with f_{ct} / f_c' = 0.1 (approx. C30) and the lines corresponding to 'separation' and 'sliding', resp. The figure reveals that the "cohesion" – implied at Coulomb's friction law – is in case of concrete not a material characteristic. It is simply only the length of a section along the shear – axis cut by a trend line (which is maybe even not straight) which cannot be determined in a test. Please note that – as the ratio f_{ct}/f_c' changes acc. to the class of concrete – both lines of the Modified Coulomb failure criteria (the abscissa of separation and the inclination, tanϕ, of segregation) differ acc. to the concrete class.

The use of Modified Coulomb Material is forced by researchers of shear and torsion design who apply in their models stress fields with uniaxial pressure which fail in inclined sliding. They must adhere to the existence of inclined cracks to load direction (see *Figure 6*), even in case of uniaxial tension (besides 'normal' separation cracks *Figure 7*).

Note: inclined cracks to load direction can have two sources:

- Some 'subversive' influences e.g. friction between loading plate and specimen: the tensile crack develops well perpendicular to the real tensile principal stresses, or
- Tensile cracks developed during an independent, previous loading situation. Here we remind you that the theory of plasticity is valid only if all external loads increase in proportion to one another, one-parametric loading!

The appearance of a sliding failure along a surface inclined to the axis of the in compression loaded specimen may have arisen at ordinary loading tests where the friction between the metal loading plate and the specimen hindered the lateral deformation of the specimen thus producing a shear-like supplementary loading which turned the direction of the principal stresses. Remember: in order to minimize this friction Kupfer (1973) loaded his test specimens through a metal brush thus reduced the shear stresses there. The failures of his specimens occurred as tensile (separation) failures in form of discrete cracks parallel to the plane of loading.

From Mohr's circle we have:

$$\sigma = \sigma_m - \tau_m \cdot sin\varphi; \qquad \tau = \tau_m \cdot cos\varphi \qquad (4)$$

where

$$\tau_m = \frac{\sigma_1 - \sigma_3}{2}\ ;\ \sigma_m = \frac{\sigma_1 + \sigma_3}{2} \qquad (5)$$

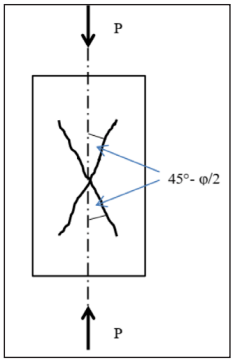

Figure 6: Sliding failure in case of pure compression as presented by Nielsen (2011)

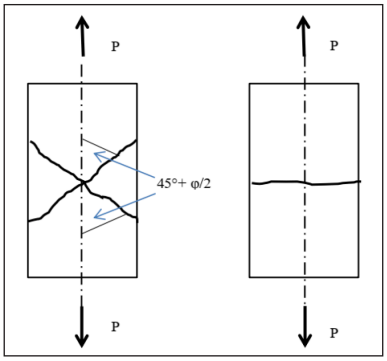

Figure 7: Sliding (left) and separation (right) failure, both might occur in case of pure tension acc. to Nielsen, (2011)

and σ_1 is the maximum principal stress and σ_3 is the minimum principal stress.

Note: σ_m is the abscissa of the center of Mohr-circle whereas τ_m is its radius.

In the following the Mohr-circles of well-known results of Kupfer's biaxial tests should be presented in Modified Coulomb rupture criterion for concrete, see Fig. 8.

Kupfer's tests can be classified into three groups:

- tension-tension
- tension-compression
- compression-compression

Please note: there is no word about 'pure shear' or shear strength.

With reference to the χ-ratio proposed by Windisch (2021) the relationship f_{ct}^* vs. f_c^* can be reasonably well described with

$$\left(\frac{f_c'^*}{f_c'}\right)^2 + \left(\frac{f_{ct}^*}{f_{ctm}}\right)^2 = 1 \qquad (6)$$

Applying $\chi = f_c' / f_{ctm}$ we get

$$\left(\frac{f_c'^*}{f_c'}\right)^2 + \left(\frac{\chi \cdot f_{ct}^*}{f_c'}\right)^2 = 1 \qquad (6a)$$

or

$$(f_c'^*)^2 + (\chi \cdot f_{ct}^*)^2 = f_c'^2 \qquad (6b)$$

Figure 8 shows the Mohr-circle representations of the tension-compression region of Kupfer's (1973) biaxial tests. It is clear: here separation failures occur.

Note: the sizes of the biaxial tensile strengths depend on the size of the compressive stress hence the three Mohr-circles intersect the $+\sigma_1$ axis at different abscissas.

Figure 9 presents the Mohr-circles of the compression-compression region of Kupfer's biaxial tests. Here it becomes clear that all three principal stresses ($\sigma_1 = 0$, too) need to be taken into account for the Mohr-circle representation otherwise the Mohr-circle of the biaxial compressive stress state will shrink to a point.

Showing the Mohr-circles for different $\boldsymbol{\sigma}_1/f_c'$ vs. $\boldsymbol{\sigma}_3/f_c'$ ratios *Figure 9* reveals that in the compression-compression region the Modified Coulomb rupture criterion does not apply (no common tangent line is possible). In fact, in all loading cases not sliding failures but separation failures occur.

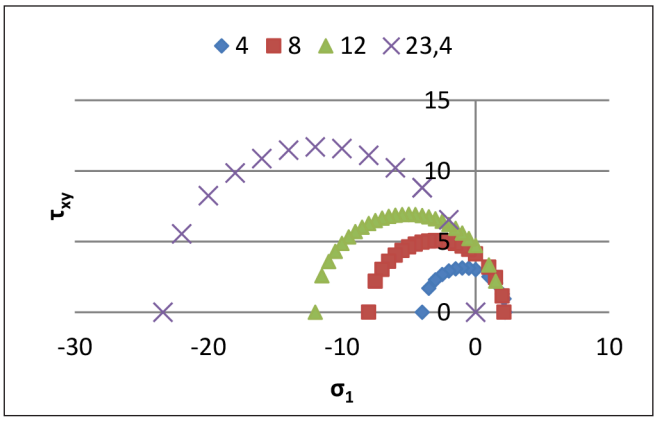

Figure 8: Mohr-circles of biaxial tension-compression and $\sigma_1 = \sigma_2$ compression-compression tests with different σ_{2u}-values as tested by Kupfer ($f_c' = 20$ N/mm²)

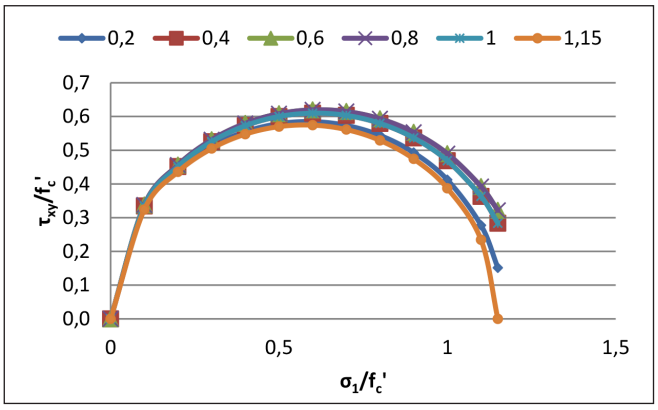

Figure 9: Normalized Mohr-circles of compression-compression tests with different σ_2/f_c' ratios by Kupfer ($f_c' = 20$ N/mm²)

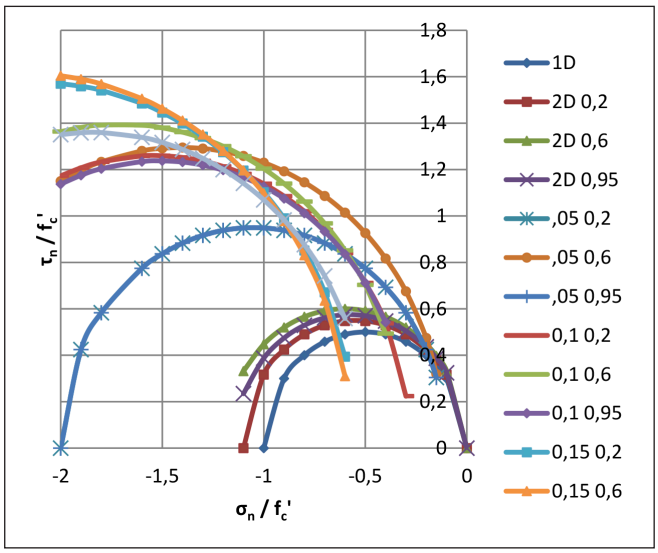

Figure 10: Mohr-circles of compression-compression bi- and triaxial tests of Speck ($f_c' = 72$ N/mm²)

Figure 10 shows the $\sigma_n / f_c' \geq -2$ region ($f_c' = 72$ N/mm²) of the Mohr-circles as measured by Speck (2007) in her 1D - 3D tests. The markings in Fig. 10 mean: 1D: uniaxial; 2D 0.2: biaxial, $\sigma_{2n}/\sigma_{3u} = 0.2$; .05 0.2: 3D, $\sigma_{1n}/\sigma_{3u} = 0.05$, $\sigma_{2n}/\sigma_{3u} = 0.2$. The positions of the circles reveal that neither the Mohr-Coulomb criterion (straight tangenting each circle) nor the Leon criterion (parabola with its tip at the tensile strength) could function as general failure criterion. It must be once more be emphasized that both, Mohr-Coulomb and Leon with their sliding failures are valid when the solid body is already separated in two parts through cracking, that contradicts the fundamental assumption (one parametric loading) of plastic theory.

4. EXTENDED RANKINE FAILURE CRITERIA FOR CONCRETE

The proposed Extended Rankine failure criteria are based directly on the principal stresses.

The Mohr-circle is applied acc. to its original purpose: a transparent geometrical method to determine the size and direction (inclination) of the principal stresses from the stress components given in a global coordinate system.

The Extended Rankine failure criteria are

- the greatest (>0) principal stress, σ_1, cannot be greater than the actual tensile strength (its size depends on the size of the σ_2 and σ_3 principal stresses if at least one of them is compressive stress. (In case of the original Rankine criterion one (fix) tensile strength governed.)
- the triple of the compressive principal stresses $\sigma_3 = \Phi(\sigma_1, \sigma_2)$ cannot be smaller than the actual smallest principal strength, σ_3, which is function of the two other principal stresses:

$$\sigma_3 = \Phi(\sigma_1, \sigma_2) \qquad (7)$$

Note: In this paper the data measured by Speck (2007) in her multiaxial compressive tests were evaluated. The results of the bi- and triaxial compression tests of the literature are evaluated and discussed in a next paper of the author.

It is known that lateral compressive stresses and/or hindered transverse deformations (confinement) let increase the compressive strength in the longitudinal direction. Ottosen (1977) and other researcher (CEB 1983) who use the hydrostatic- and deviatory stresses (octahedral normal- and shear stresses) claim that the form of the Ultimate Strength Surface (USS) can be calibrated with four strength values: the uniaxial tensile strength, the uniaxial compressive strength (point on the compressive meridian), the biaxial compressive strength (point on the tensile meridian), and a triaxial compressive strength at one point on the compressive meridian ($\sigma_1 = \sigma_2 > \sigma_3$).

Figure 11 should reveal that the three a.m. calibrating strength values (marked with the red arrows) cannot properly characterize the monotone increasing, continuous function of the USS (as deduced from the test results of Speck, 2007).

Figure 11 shows the local ordinates of normalized $\sigma_3/f_c' = \Phi(\sigma_1/f_c', \sigma_2/f_c')$ function as deduced from the bi- and triaxial tests measured by Speck on $f_c' = 72$ N/mm² test specimens.

Figure 12 presents the USS in another form: the abscissa is $\gamma = \sigma_1 / \sigma_3$, the ordinate is $\lambda = \sigma_2 / \sigma_3$. The USS increases monotonic in the γ-direction, whereas increases up to $\lambda = 0.5 \sim 0.6$ then decreases moderately.

Having determined the relevant failure causing principal stresses the corresponding normal- and shear stress components in the global coordinate system can be determined using Mohr-circles of the tensor calculus. Note: the global shear stress components calculated from the failure causing principal stresses refer by no means to shear failure!

Concrete fails due to the tensile deformations perpendicular to the axis with the maximum principal stress (smallest compressive stress).

Figure 11: *Relative increase of the bi- and triaxial compressive strength as function of both other relative compressive stresses*

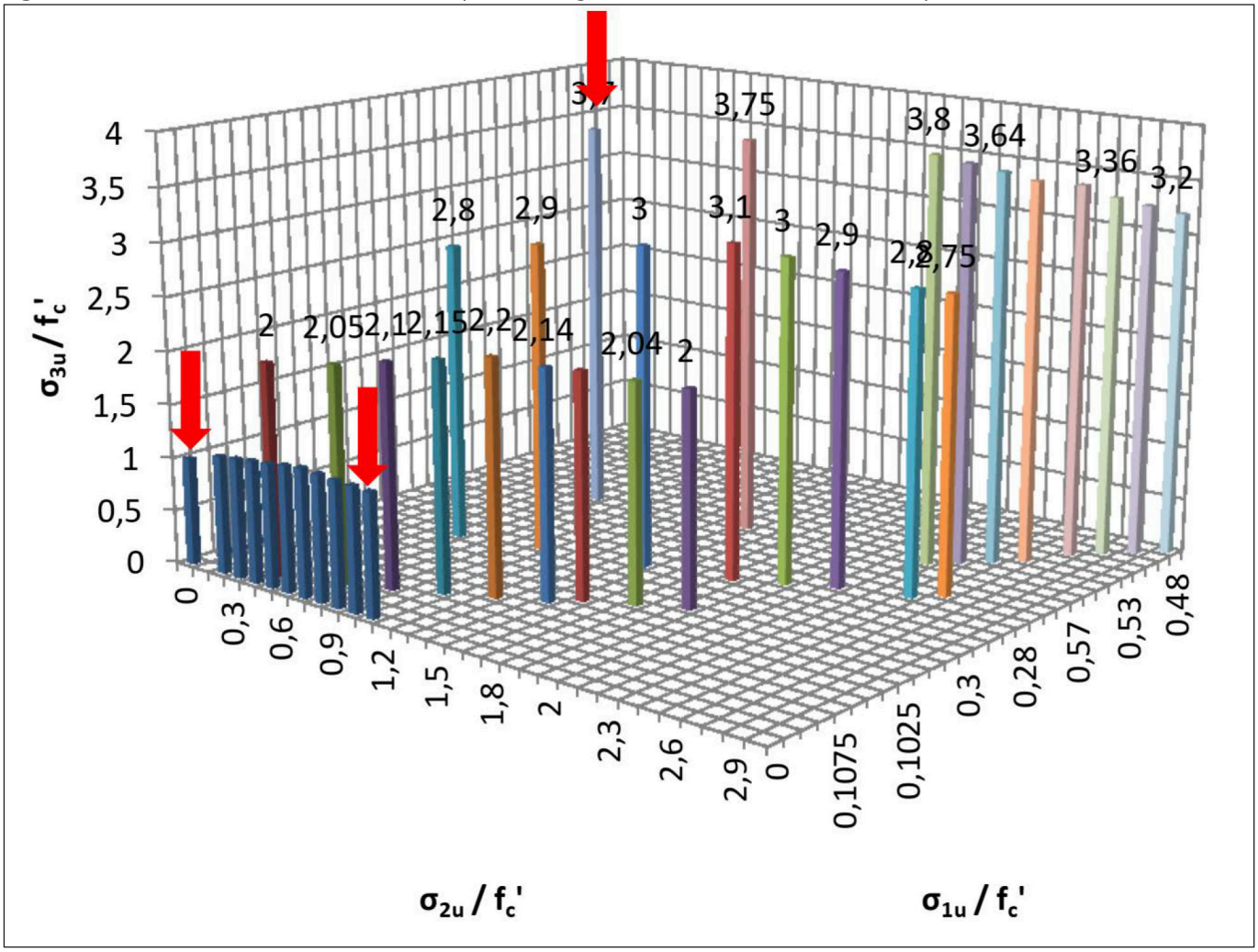

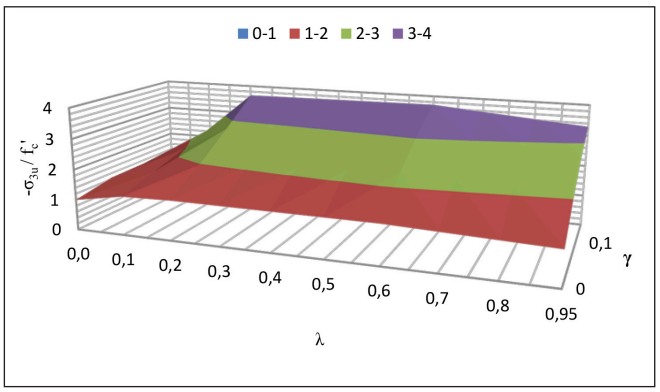

Figure 12: *The Ultimate Strength Surface compiled from the data measured by Speck (2007)*

The type of failure is in all cases separation, i.e. discrete cracks occur perpendicular to the direction of the greatest and possibly of the intermediate principal stress, resp.

In biaxial compression tests the direction of the transverse tensile deformations is given: the "third" axis (here it should be marked as axis 1). In case of Kupfer's biaxial panel tests the cracks developed perpendicular to the panel and parallel with the middle plane, resp.

Speck, who paid great attention to reduce the friction between the loading device and the test specimens, in all loading cases –whether uni,- bi- or triaxial loading, compression or tension, or mixed- found always separation failures (*Figure 13*), and she is right.

Separation failure (in form of discrete tensile cracks) occurs when the greatest of the principal stresses equals with the actual tensile strength or the smallest (greatest negative) principal stress reaches the actual 2D or 3D compressive strength. The failure occurs along the principal plane which is at an angle ϕ with axis x (this is the third component of the Mohr-circle besides the two principal stresses.

The Mohr-Coulomb failure criteria are not valid for concrete. Concrete is definitely not a frictional material.

The author hopes that with introduction of the failure criterion based on the principal stresses the wrong ways caused by the central reference to the sliding failures and ultimate shear stresses, a better and material appropriate description of the damage-theory etc. can be developed.

5. CONCLUSIONS

The Mohr-Coulomb failure criteria are inadequate to describe the bi- and triaxial failure characteritics of concrete.

Applying them for the evaluation of the test results given in the literature proves that neither a straight nor a curved line can be fitted to the Mohr-circles representing the 2D and 3D strength values.

Further problems are:

- the Coulomb-criteria refers to already existing failure surfaces only.
- The Mohr-circles are a useful and visually attractive geometrical interpretation of the stress-transformation between different axis-systems, moreover in 2D only, not more.
- The Mohr failure criterion does not consider the intermediate stress component which is an important influencing factor of the ultimate failure strength
- The "shear stress" is "produced" by our hugging to the global coordinate system. Nature and concrete do not "know" it.

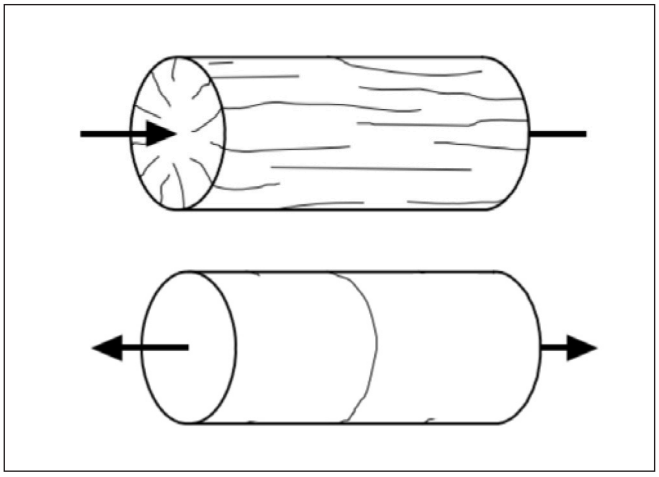

Figure 13: *Separation failures in case of uniaxial compression- and tensile tests as presented by Speck (2007)*

- Concrete obeys principal stresses only.
- Concrete fails in tension, in form of separation cracks.
- Concrete has no shear strength!
- The researchers were misled by the failure patterns of the specimens loaded with friction between its surface and the loading plate.

Summarizing: for concrete the Mohr-Coulomb failure criteria cannot be applied and concrete is definitely not a frictional material.

Extended Rankine failure criteria based directly on the principal stresses are proposed:

- the greatest (>0) principal stress, σ_1, cannot be greater than the actual tensile strength (its size depends on the size of the σ_2 and σ_3 principal stresses if at least one of them is compressive stress. (In case of the original Rankine criterion one (fix) tensile strength governed.)
- the triple of the compressive principal stresses $\sigma_3 = \Phi(\sigma_1, \sigma_2)$ cannot be smaller than the actual smallest principal strength, σ_3, which is function of the two other principal stress components, $\sigma_3 = \Phi(\sigma_1, \sigma_2)$.

The author hopes that with introduction of the Extended Rankine failure criteria based on the principal stresses a material-appropriate description of the damage-theory etc. can be developed.

6. REFERENCES

Comité Euro-international du Béton, (1983), Bulletin d'information N° 156: "Concrete under multiaxial states of stress. Constitutive equations for practical design", Contribution à la 23e Session plenière du C.E.B. Prague – Juin 1983, p. 149.

Drucker, D. C., Prager, W. (1952), "Soil Mechanics and Plasticity Analysis of Limit Design", *Quarterly of Applied Mathematics*, Vol. 10, No. 2, 157-165.

fib Model Code for Concrete Structures 2010 (MC2010) (2013), Fédération international du béton, Oct. 2013, Ernst & Sohn, Berlin, p. 434.

Kupfer, H. (1973), „Das Verhalten des Betons unter mehrachsiger Kurzzeitbelastung unter besonderer Berücksichtigung der zweiachsigen Beanspruchung", *Deutscher Ausschuss für Stahlbeton*, Heft 229, Ernst und Sohn, Berlin, p. 105.

Leon, A., (1935), "Über die Scherfestigkeit des Betons", *Beton und Eisen* 34, Heft 8, pp. 130-135.

Mohr, O. (1906), "Scientific paper on the area of technical mechanics", *Ernst & Sohn*, Berlin, 1906, (in German)

Nielsen, M. P., Hoang, L. C. (2011), "Limit Analysis and Concrete Plasticity", 3rd edition, CRC *Press Taylor & Francis Group*, p. 796.

Ottosen, N.S. (1977), "A Failure Criterion for Concrete", *Journal of Engineering Mechanics*, Div. ASCE, Vol 103, EM4.

Rankine, W.J.M., (1868), "A Manual of Applied Mechanics", London

Speck, K. (2007), "Beton unter mehraxialer Beanspruchung. Ein Materialgesetz für Hochleistungsbetone unter Kurzzeitbelastung, Concrete under multiaxial loading conditions. A Constitutive Model for Short-Time Loading of High Performance Concretes" Dissertation, TU Dresden, p. 224.

Windisch A. (2021), "The tensile strength: the most fundamental mechanical characteristics of concrete" Concrete Structures, 2021 pp. 1-4. https://doi.org/10.32970/CS.2021.1.1

7. NOTATIONS

c	cohesion
f	yield function (MC2010)
f_c, f_c'	concrete compressive strength
f_c*, f_{ct}*	ultimate strength (compression and tension resp.) in 2D and/or 3D loading
f_{ct}, f_t, f_A	tensile strength
f_{ctm}	mean tensile strength
g	plastic potential (MC2010)
φ	inclination of the sliding surface
ϕ	angle of internal friction
$\gamma = \sigma_1 / \sigma_3$	loading parameter
$\lambda = \sigma_2 / \sigma_3$	loading parameter
$\chi = f_{ck}/f_{ctm}$	ratio of characteristic concrete compressive strength to mean tensile strength
σ_1, σ_2, σ_3	principal stresses ($\sigma_1 \geq \sigma_2 \geq \sigma_3$)
σ_{3u}	ultimate strength measured in test
σ_{com}	hydrostatic normal stress
μ	friction coefficient
σ, σ_n	normal stress component
τ, τ_n	shear stress component

Andor Windisch PhD, Prof. h.c. retired as Technical Director of DYWIDAG-Systems International in Munich, Germany. He made his MSc and PhD at Technical University of Budapest, Hungary, where he served 18 years and is now Honorary Professor. Since 1970 he is member of different commissions of FIP, CEB, *fib* and ACI. He is author of more than 190 technical papers. *Andor.Windisch@web.de*

APPLICATION OF THE WEIBULL DISTRIBUTION TO THE DESCRIPTION OF THE SKEW DISTRIBUTION OF CONCRETE COMPRESSIVE STRENGTH

Hon. Prof. Tibor Kausay

https://doi.org/10.32970/CS.2022.1.3

The extremal distribution is noteworthy because, unlike the normal distribution (Gaussian distribution) and t-distribution (Student distribution) prevalent in engineering, it is generally asymmetric, and therefore is well suited for modeling the actual compressive strength distribution of concrete.

Keywords: Weibull distribution, extremal distribution, density funciton, concrete, compressive strength, skewness

1. INTRODUCTION

Misték wrote in his studies (1974, 1977, 2000, 2001) that the distribution function of maximum loads follows the upper Weibull distribution, while that of the minimum strength of loadbearing materials follows the lower third extreme (Weibull) distribution. In accordance with *Misték, Ujhelyi* (1978, 1985) wrote that probability distribution of the compressive strength for an average quality level concrete production in the lower concrete class range (below C16/20) or for the highly plastic consistency may be approximated by the log-normal distribution with right skewness (extending to the right with positive skewness), while in the higher compressive strength range (beyond C20/25) or for plastic consistency it may be approximated by the lower extremal distribution with skewness to the left (extending to the left with negative skewness). Compressive strength in the middle strength range (C16/20 – C20/25) may be considered to follow the normal distribution.

2. EXTREME VALUE DISTRIBUTIONS (EVD)

An extreme value is either very small or very large value in a probability distribution. These extreme values are found in the tails of a probability distribution (i.e. the distribution's extremities).

Extreme value analysis (EVA) is a branch of statistics dealing with the extreme deviations from the median of probability distributions. EVD has three types which are named after their most famous researchers and each type can be an upper (maximum) and lower (minimum), as can be seen in Table 1.

Based on experiments of *W. Weibull* (1939), for compressive strength distribution of brittle materials (such as for compressive strength distributions of higher strength concretes) the lower *Weibull* extremal value distribution proved to be right from among the three lower extremal value distribution functions *(Rinne*, 2009).

Table 1: Density function of reduced extreme value distributions (Rinne, 2009)

Type	Upper or maximum extreme value distribution	Lower or minimum extreme value distribution
I.	$g_{\ \mathrm{f}}(u\ \|0;1) = \mathrm{e}^{-u\ -\mathrm{e}^{-u}}$ upper *Gumbel* distribution	$g_{\ \mathrm{a}}(u\ \|0;1) = \mathrm{e}^{u\ -\mathrm{e}^{u}}$ lower *Gumbel* distribution
II.	$f_{\mathrm{Fr,f}}(u\|0;1;\mathrm{c}) = = \mathrm{c} \times u^{-\mathrm{c}-1} \times \mathrm{e}^{-u^{-\mathrm{c}}}$ upper *Fréchet* distribution	$f_{\mathrm{Fr,a}}(u\|0;1;\mathrm{c}) = = \mathrm{c} \times (-u)^{-\mathrm{c}-1} \times \mathrm{e}^{-(-u)^{-\mathrm{c}}}$ lower *Fréchet* distribution
III.	$w_{\mathrm{f}}(u\|0;1;\mathrm{c}) = = \mathrm{c} \times (-u)^{\mathrm{c}-1} \times \mathrm{e}^{-(-u)^{\mathrm{c}}}$ upper *Weibull* distribution	$w_{\mathrm{a}}(u\|0;1;\mathrm{c}) = = \mathrm{c} \times u^{\mathrm{c}-1} \times \mathrm{e}^{-u^{\mathrm{c}}}$ lower *Weibull* distribution

3. THE WEIBULL DISTRIBUTION

In probability theory and statistics, the Weibull distribution - named after the Swedish mathematician *Weibull* (1951) - is a continuous probability distribution.

The most general form of Weibull's probability density function has three parameters: γ - shape parameter, μ - location parameter and α - scale parameter. The case where $\mu = 0$ and $\alpha = 1$ is called the standard Weibull distribution. The case where $\mu = 0$ is called the 2-parameter Weibull distribution. In the formulation of the single parameter Weibull distribution the only unknown parameter is the scale parameter, η, i.e. we assume that the shape parameter is known a priori from past experience with identical or similar products.

Note: in the literature different letters are used for the parameters. In this paper the shape parameter is marked with "c", the location parameter with "a" and the scale parameter with "b".

The skewness coefficient is the quotient of the third order moment of the area under the curve of the density function with respect to the center of gravity (μ_3) and the third power of the standard deviation (), *(Palotás*, 1979), (*Hartung* et al., 2009):

$$\gamma_{\text{skewness}} = \frac{\mu_3}{{s_n}^3} = \frac{\left(\frac{1}{n} \times \sum_{i=1}^{n}(x_i - \bar{x})^3\right)}{\sqrt[2]{\left(\frac{1}{n} \times \sum_{i=1}^{n}(x_i - \bar{x})^2\right)^3}}$$

4. DETERMINATION OF WEIBULL DISTRIBUTION PARAMETERS

To evaluate results of the compressive strength tests according to the *Mistéth* theory, values of location parameter „a", of scale parameter „b" (in the literature also λ) and shape parameter „c" (in literature also k) of the *Weibull* distribution must be known.

Our assumptions for their determination are that

- skewness factor of the single-parameter, simplified lower *Weibull* distribution equals the empirical skewness factor obtained from the measurements:

$$\gamma_{\text{skewness,Weibull,low}}(u|0;1;c) = \gamma_{\text{skewness,test}}$$

- standard deviation of the two-parameter semi-simplified lower *Weibull* distribution equals to the empirical standard deviation obtained from the measurements:

$$s_{\text{Weibull,low}}(z|0;b;c) = s_{\text{test}}$$

- mean value of the three-parameter lower *Weibull* distribution equals to the empirical average obtained from the measurements:

$$\mu_{\text{Weibull,low}}(x|a;b;c) = f_{\text{cm,test}},$$

Figure 1: Skewness factor of the single-parameter simplified Weibull distribution as a function of the shape parameter „c"

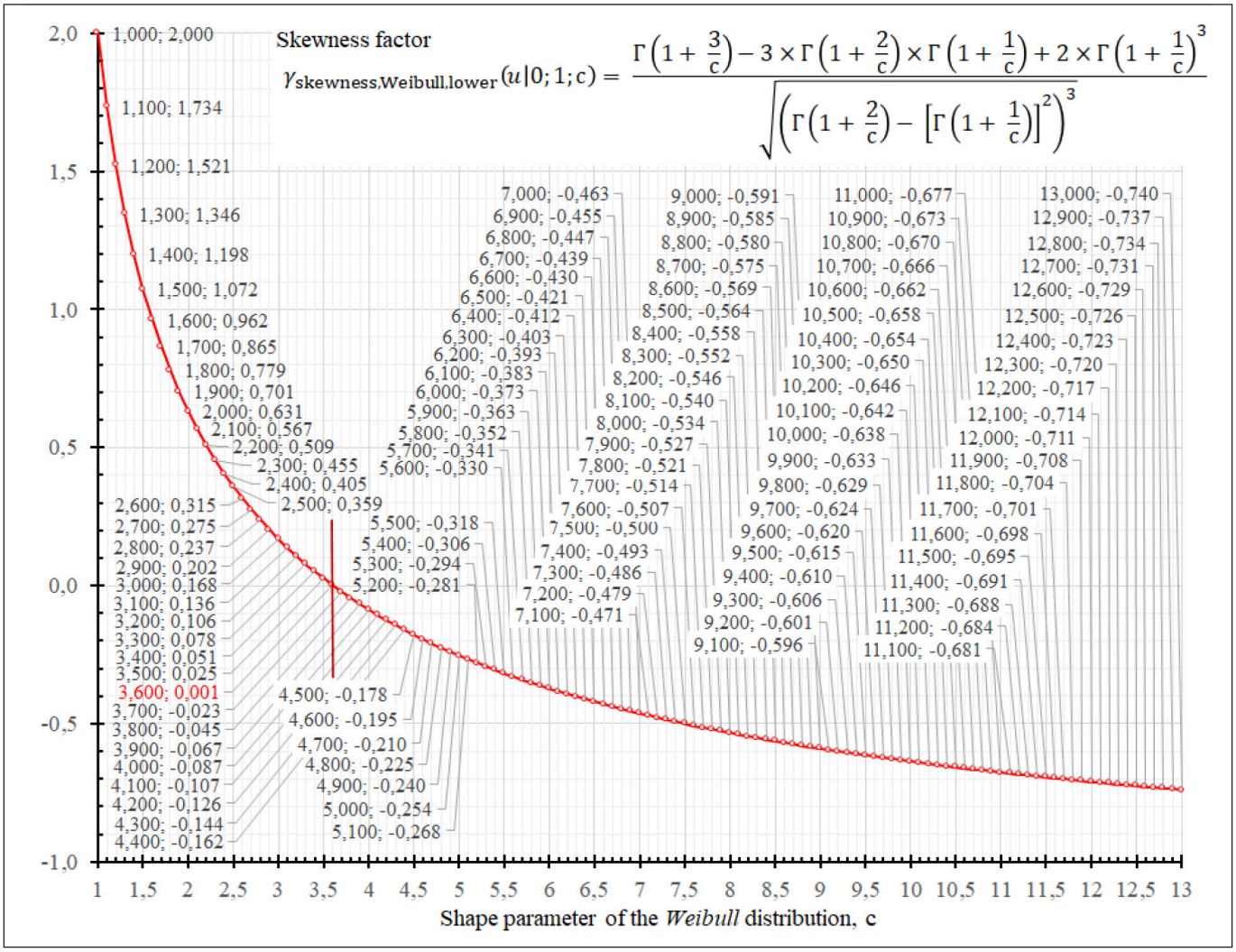

➢ difference between the mean value of the three-parameter lower *Weibull* distribution (which is considered equal with the empirical average) and the mean value of the two-parameter semi-simplified lower *Weibull* distribution equals to the value of the location parameter „a”:

$$a = f_{cm,test} - \mu_{Weibull,low}(z|0;b;c).$$

Recommended steps for the determination of the values of the location parameter „a”, scale parameter „b” and shape parameter „c” are the following:

- Step 1: Into the formula of skewness factor for the single-parameter, simplified lower *Weibull* distribution the empirical skewness factor obtained by the measurements ($\gamma_{skewness,test}$) is introduced and the shape parameter „c” value of the *Weibull* distribution pertinent to the empirical skewness factor is found by implicit iteration:

Figure 2: Standard deviation of the *z* independent variable of the two-parameter lower Weibull distribution semi-simplified assuming that location parameter a = 0, as a function of the scale parameter „b” and the shape parameter „c”, if 1.0 ≤ b ≤ 10.0 and if 1.0 ≤ c ≤ 10.0

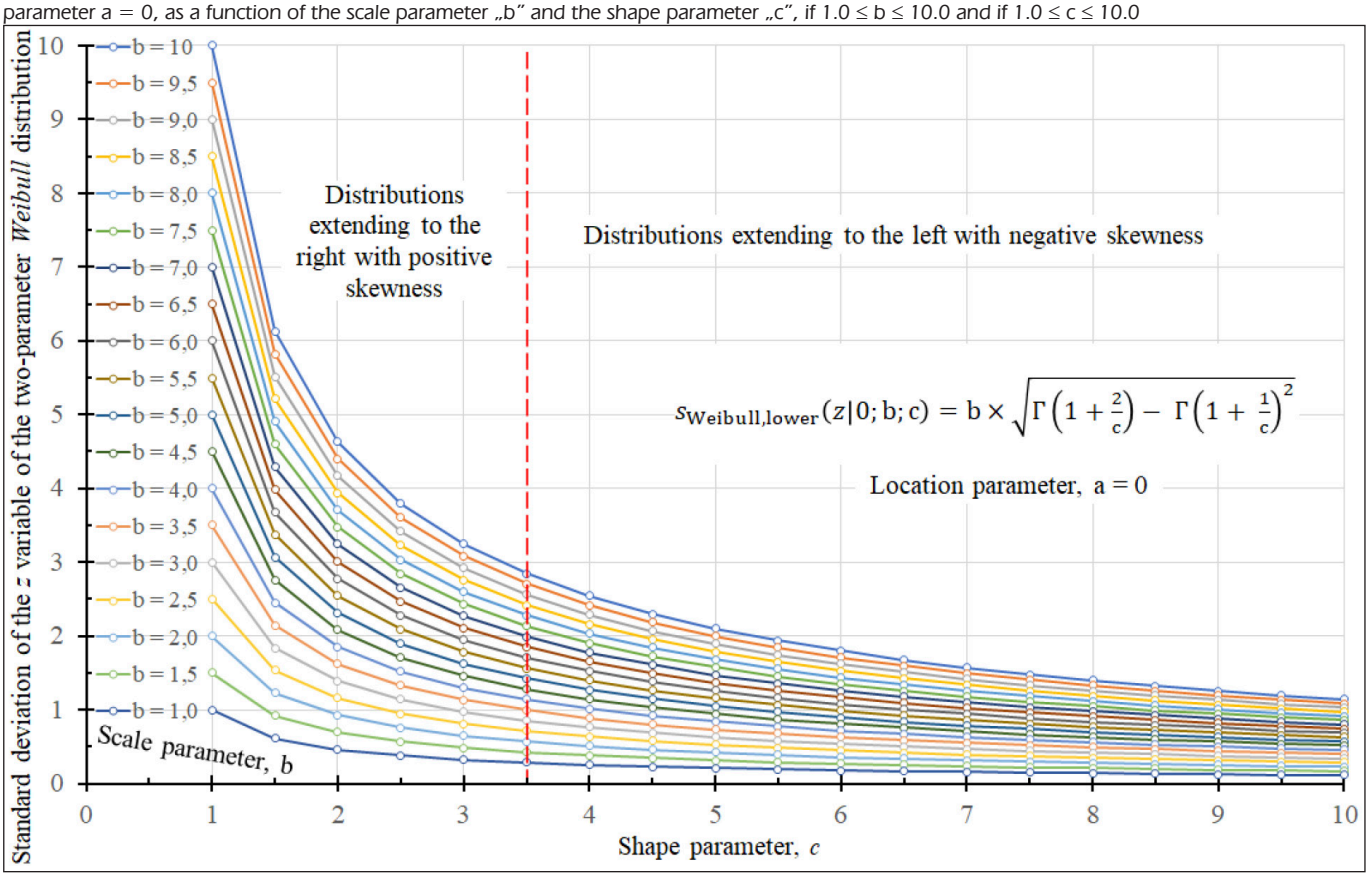

Figure 3: Standard deviation of the z independent variable of the two-parameter lower Weibull distribution semi-simplified by setting the location parameter „a” to 0, as a function of the scale parameter „b” and shape parameter „c”, if 10.0 ≤ b ≤ 50.0 and if 1.0 ≤ c ≤ 10.0

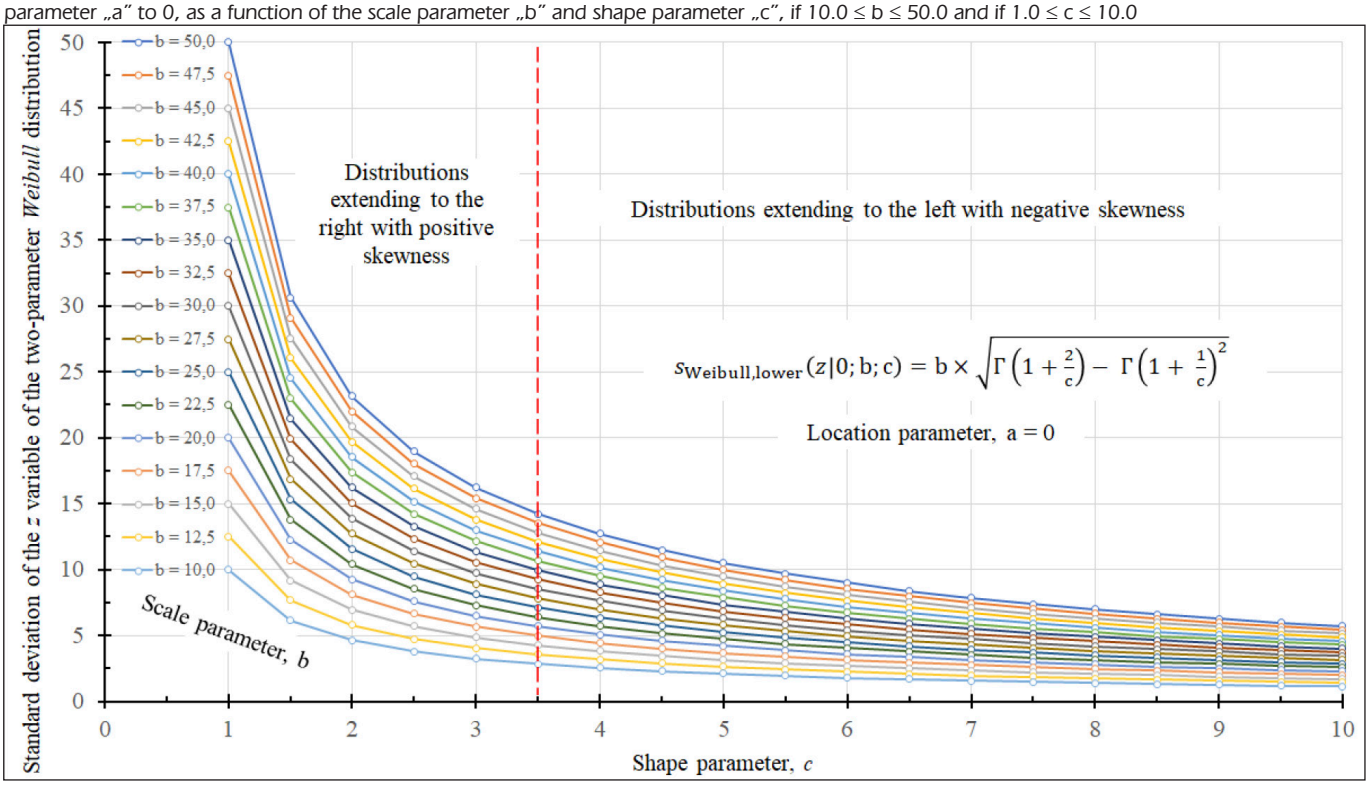

Figure 4: *The quotient of the standard deviation/scale parameter quotient (of the semi-simplified two-parameter lower Weibull distribution (which is proportional to the standard deviation) as function of the shape parameter „c"*

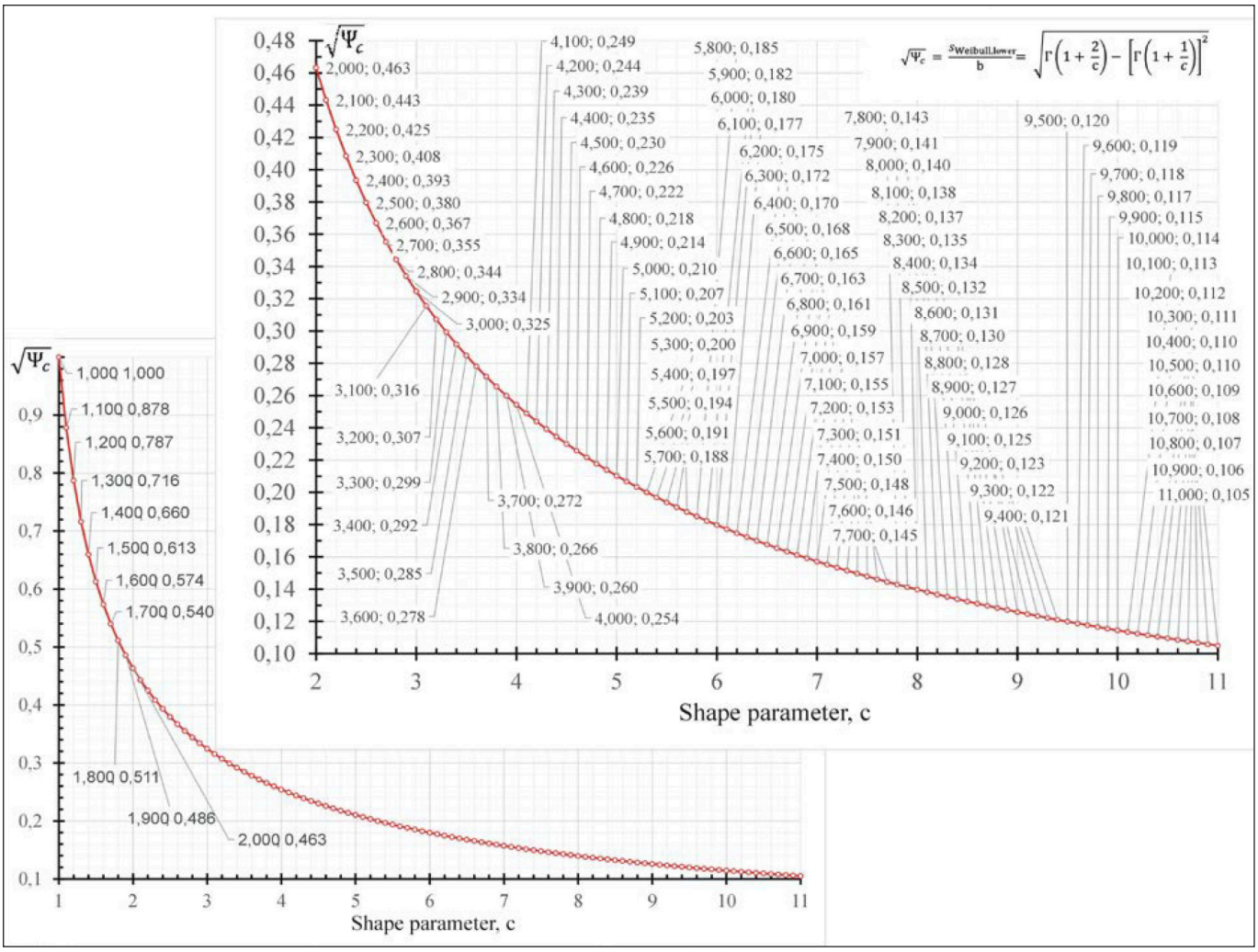

Figure 5: *Squared standard deviation/scale parameter quotient ($\sqrt{\Psi_c}$) of the semi-simplified two-parameter lower Weibull distribution proportional to the square of the standard deviation as a function of the shape parameter „c"*

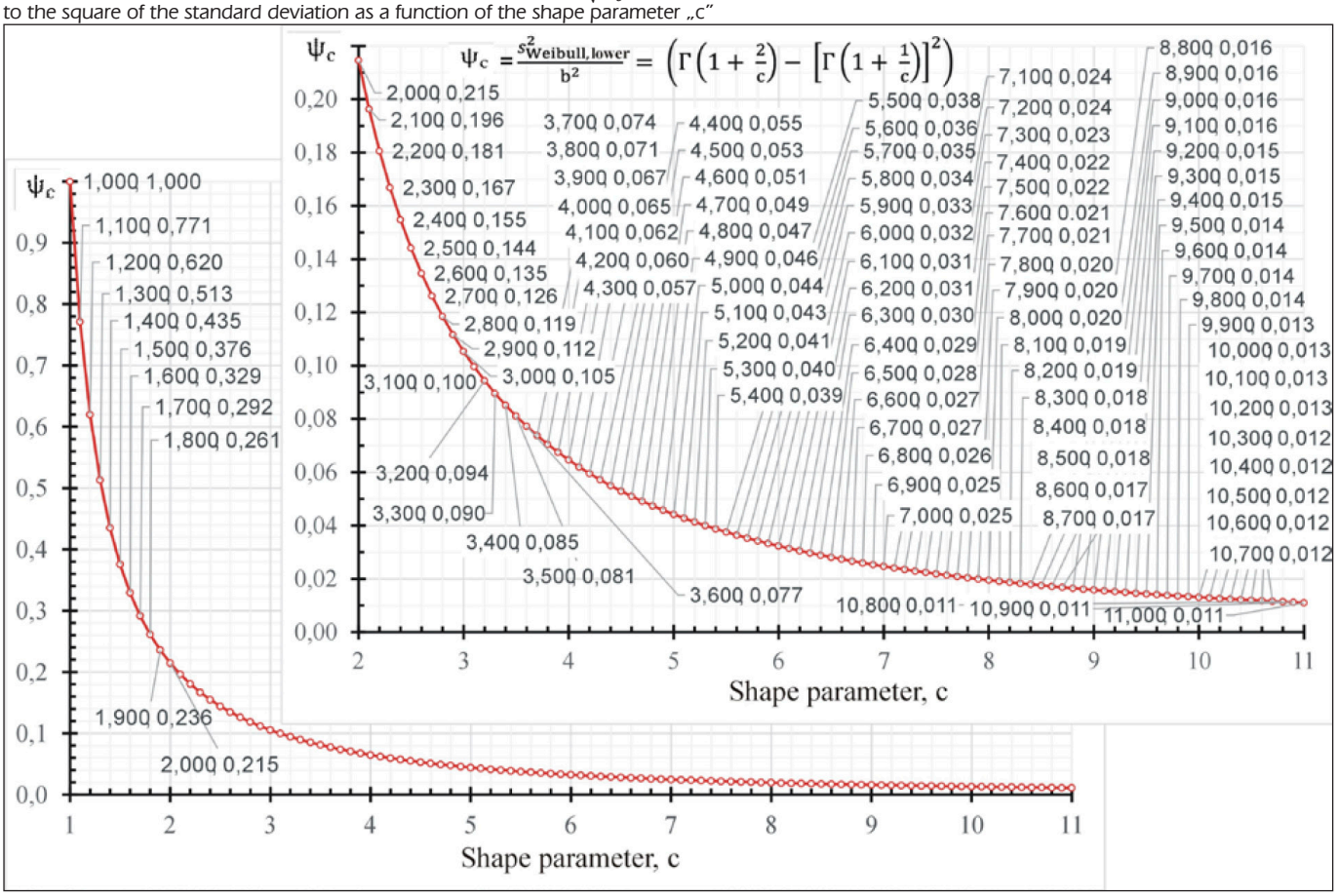

$$Y_{\text{skewness,Weibull,low}}(u|0;1;c) = \frac{\Gamma\left(1+\frac{3}{c}\right)-3\times\Gamma\left(1+\frac{2}{c}\right)\times\Gamma\left(1+\frac{1}{c}\right)+2\times\Gamma\left(1+\frac{1}{c}\right)^3}{\sqrt{\left(\Gamma\left(1+\frac{2}{c}\right)-\left[\Gamma\left(1+\frac{1}{c}\right)\right]^2\right)^3}} = Y_{\text{skewness,test}}$$

Upon the successive approximation (iteration), calculation of skewness factor of the single-parameter lower *Weibull* distribution is repeated until a value approaching the empirical skewness factor best (e.g. to three decimals) is obtained. *Figure 1* may assist this procedure.

- Step 2: Into the formula of the standard deviation of the two-parameter semi-simplified lower *Weibull* distribution the already known value of the shape parameter c and the value of the empirical standard deviation of the concrete

Figure 6: Expected mean value of the *z* independent variable of the two-parameter lower Weibull distribution semi-simplified by the location parameter „a" as a function of the scale parameter „b" and shape parameter „c", if 1.0 ≤ b ≤ 10.0 and if 1.0 ≤ c ≤ 10.0

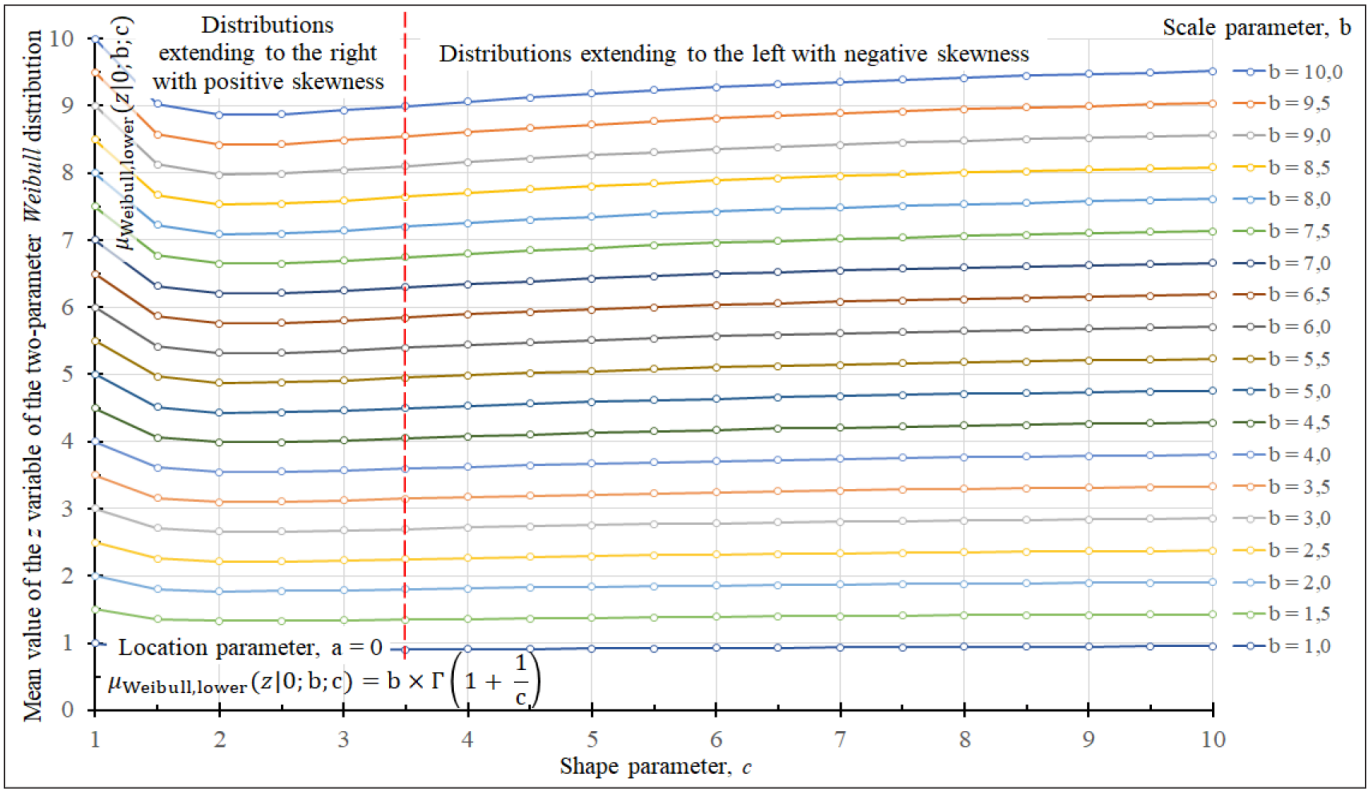

Figure 7: Expected mean value of the *z* independent variable of the two-parameter lower Weibull distribution semi-simplified by the location parameter „a" as a function of the scale parameter „b" and shape parameter „c", if 10.0 ≤ b ≤ 50.0 and if 1.0 ≤ c ≤ 10.0

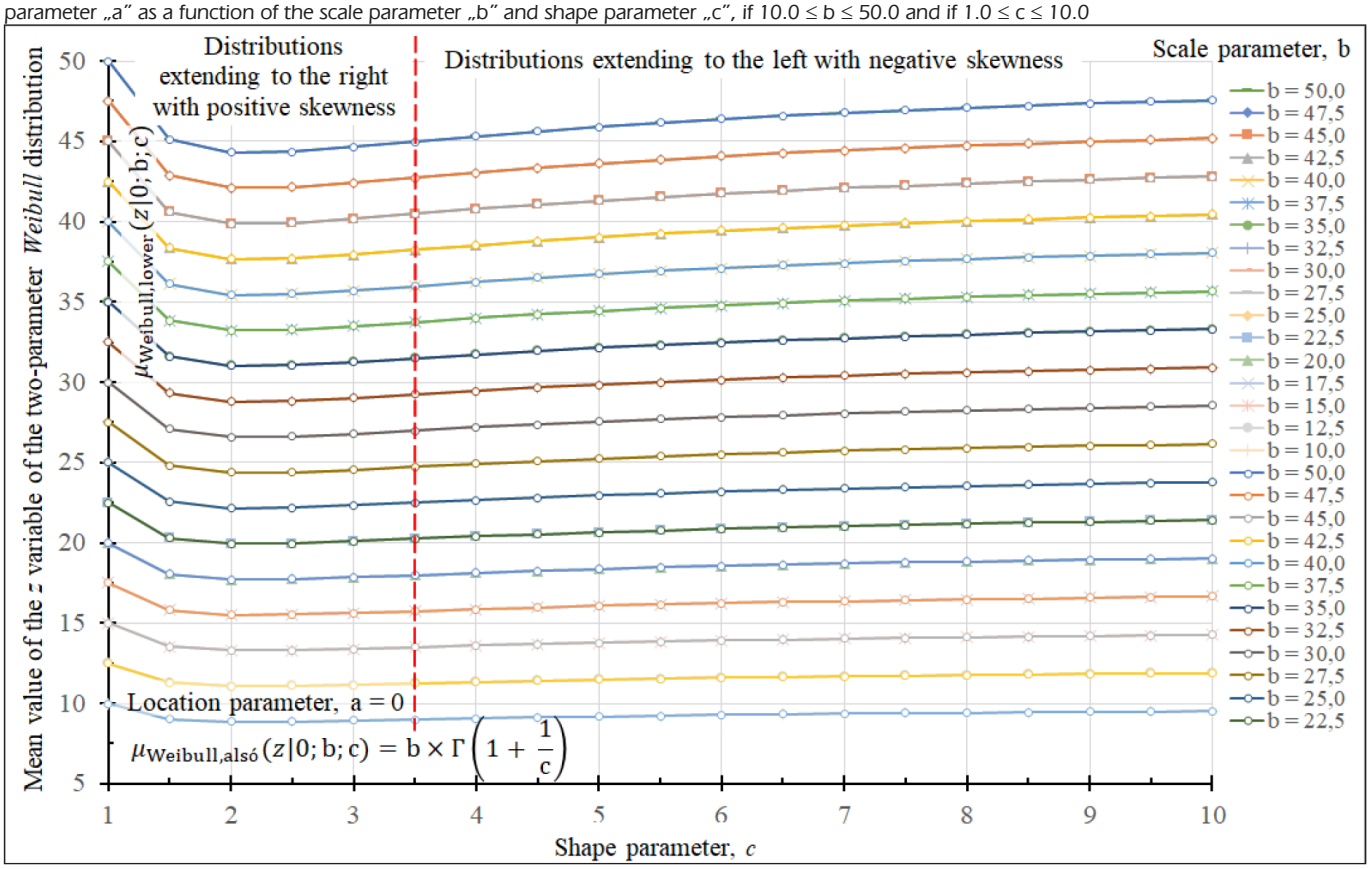

Figure 8: Nomogram for determination of parameters to the lower Weibull distribution

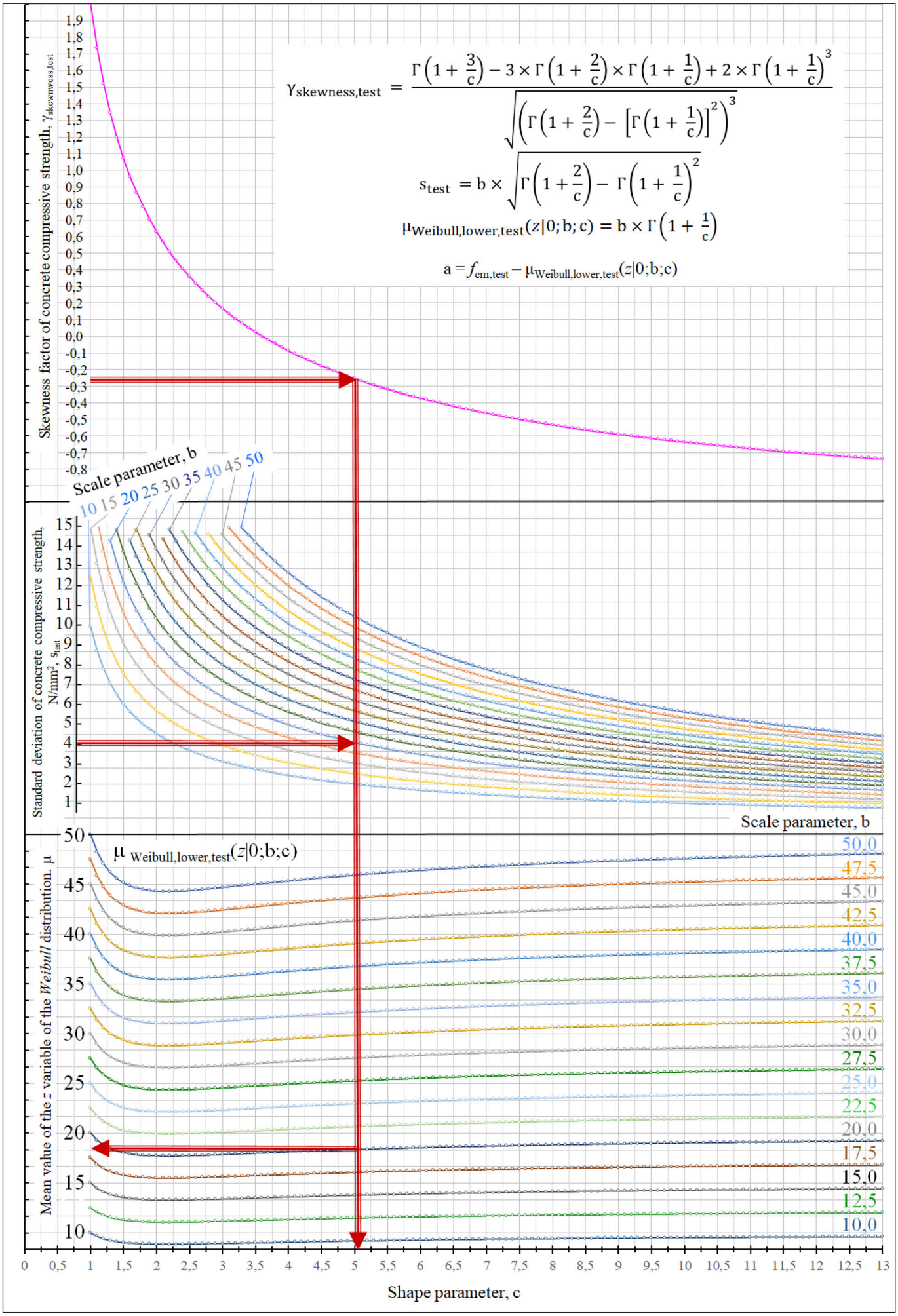

Figure 9: Demonstration for the solution process of the numerical examples in a nomogram

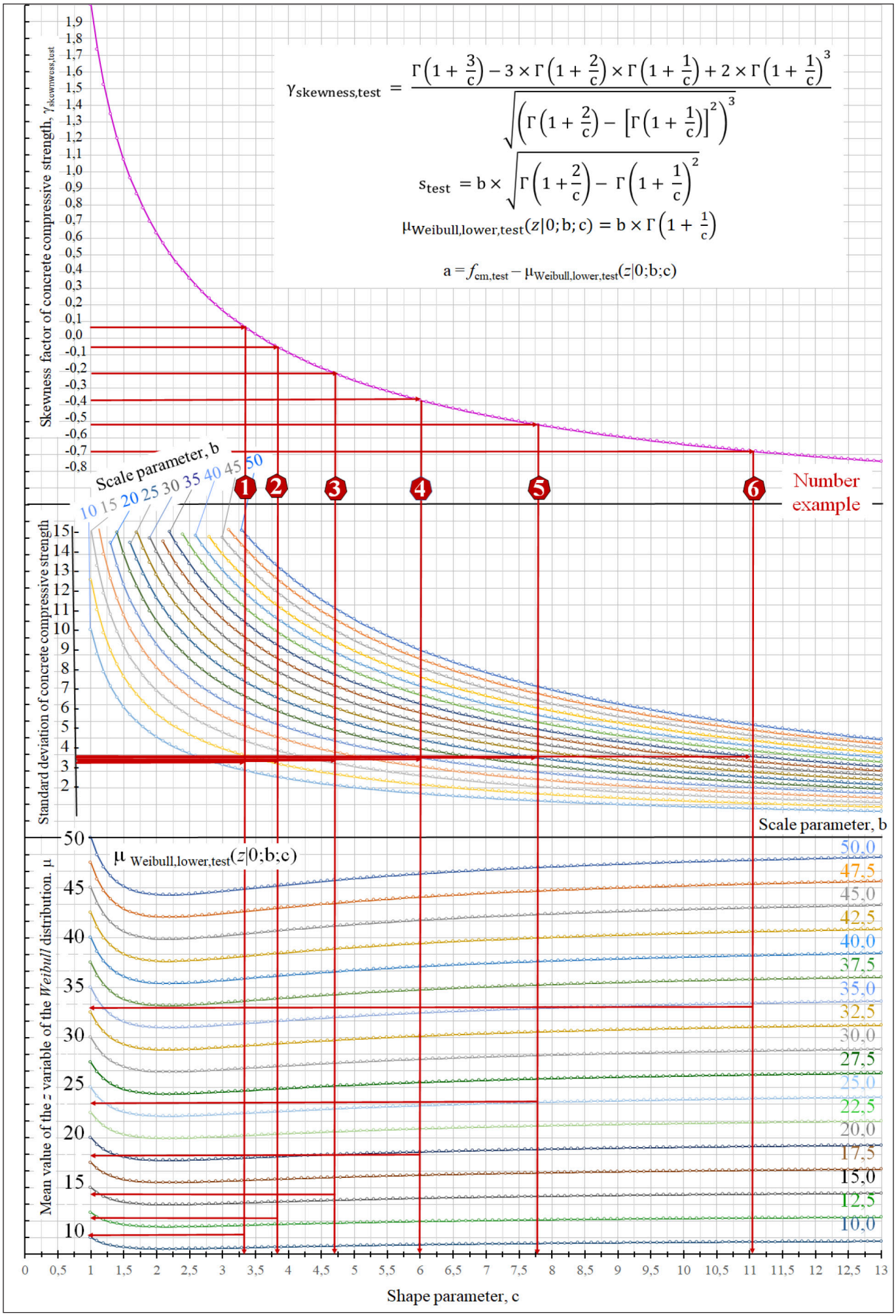

Table 2: Numerical examples for application of the lower Weibull extreme value distribution in case of concrete strength evaluation

Sign of the numerical example					
1.	2.	3.	4.	5.	6.
Initial data					
Concrete compressive strength class, EN 1992-1-1:2004+A1:2014 Eurocode 2					
C16/20	C20/25	C25/30	C30/37	C35/45	C40/50
Empirical average of concrete compressive strength, N/mm², $f_{cm,cyl,test}$ EN 1992-1-1:2004+A1:2014 Eurocode 2					
24	28	33	38	43	48
Empirical standard deviation of concrete compressive strength, N/mm², s_{test}					
3,40	3,45	3,50	3,55	3,60	3,65
Empirical relative standard deviation of concrete compressive strength, $s_{rel,test}$					
0,142	0,123	0,106	0,093	0,084	0,076
Empirical skewness factor of concrete compressive strength, $\gamma_{skewness,test}$					
+0,07	-0,05	-0,21	-0,37	-0,52	-0,68
Result of the calculation					
Mean value of the single-parameter simplified *Weibull* distribution,					
0,897	0,904	0,915	0,927	0,941	0,955
Mean value of the two-parameter semi-simplified *Weibull* distribution,					
10,271	11,802	14,436	18,230	23,660	33,430
Location parameter „a" of the *Weibull* distribution					
13,729	16,198	18,564	19,770	19,340	14,570
Scale parameter „b" of the *Weibull* distribution					
11,445	13,054	15,780	19,656	25,157	34,992
Shape parameter „c" of the *Weibull* distribution					
3,329	3,822	4,698	5,968	7,787	11,080
Empirical characteristic value of concrete compressive strength with *Weibull* distribution (5% quantile), N/mm², $f_{ck,test}$					
18,419	22,199	26,939	31,720	36,519	41,334
Empirical acceptance distance of concrete compressive strength with *Weibull* distribution, N/mm², $f_{cm,test} - f_{ck,test}$					
5,581	5,801	6,061	6,280	6,481	6,666
Acceptance constant of according to the number example (acceptance distance / standard deviation)					
1,641	1,681	1,732	1,769	1,800	1,826

compressive strength obtained from the measurements (s_{test}) are taken into account and the value of the scale parameter b of the *Weibull* distribution pertinent to the empirical standard deviation is found by implicit iteration:

$$s_{\text{Weibull,low}}(z|0;\mathrm{b};\mathrm{c}) = \mathrm{b} \times \sqrt{\Gamma\left(1+\frac{2}{\mathrm{c}}\right) - \Gamma\left(1+\frac{1}{\mathrm{c}}\right)^2} = s_{\text{test}}$$

Upon the successive iteration, calculation of skewness factor of the two-parameter lower *Weibull* distribution is repeated with input of different b values until a best value approaching the empirical skewness factor (e.g. to three decimals) is obtained. *Figures 2 and 3* can assist this procedure. These figures show diagrams of standard deviation for the *z* independent variable of the semi-simplified two-parameter lower *Weibull* distribution as a function of the scale parameter „b" and the shape parameter „c".
Figures 4 and 5 might also be of help: here diagrams for the *z* independent variable of the semi-simplified two-parameter lower *Weibull* distribution are shown: the standard deviation/ scale parameter quotient

$$\sqrt{\Psi_c} = \frac{s_{\text{Weibull,low}}}{\mathrm{b}} = \sqrt{\Gamma\left(1+\frac{2}{\mathrm{c}}\right) - \left[\Gamma\left(1+\frac{1}{\mathrm{c}}\right)\right]^2}$$

and the square of the standard deviation/scale parameter quotient

$$\Psi_c = \left(\frac{s_{\text{Weibull,low}}}{\mathrm{b}}\right)^2 = \left(\Gamma\left(1+\frac{2}{\mathrm{c}}\right) - \left[\Gamma\left(1+\frac{1}{\mathrm{c}}\right)\right]^2\right)$$

Calculated value of the shape parameter „c" can be refined by the use of the scale parameter „b", if required.

- Step 3: Mean value of $\mu_{\text{Weibull,low}}(z|0;b;c)$ for the two-parameter semi-simpified lower *Weibull* distribution is calculated by implicit iteration using the (already known) values of the scale parameter „b" and shape parameter „c" :

$$\mu_{\text{Weibull,low}}(z|0;\mathrm{b};\mathrm{c}) = \mathrm{b} \times \Gamma\left(1+\frac{1}{\mathrm{c}}\right)$$

Figures 6 and 7 show diagrams of the mean value $\mu_{\text{Weibull,low}}(z|0;b;c)$ for the two-parameter semi-simplified lower *Weibull* distribution, depicted as a function of scale parameter „b" and shape parameter „c".

Figure 10: Diagrams of Step 1 of the solution for the numerical examples. Curves for the single-parameter generalized (GEV) density function for the lower Weibull distribution

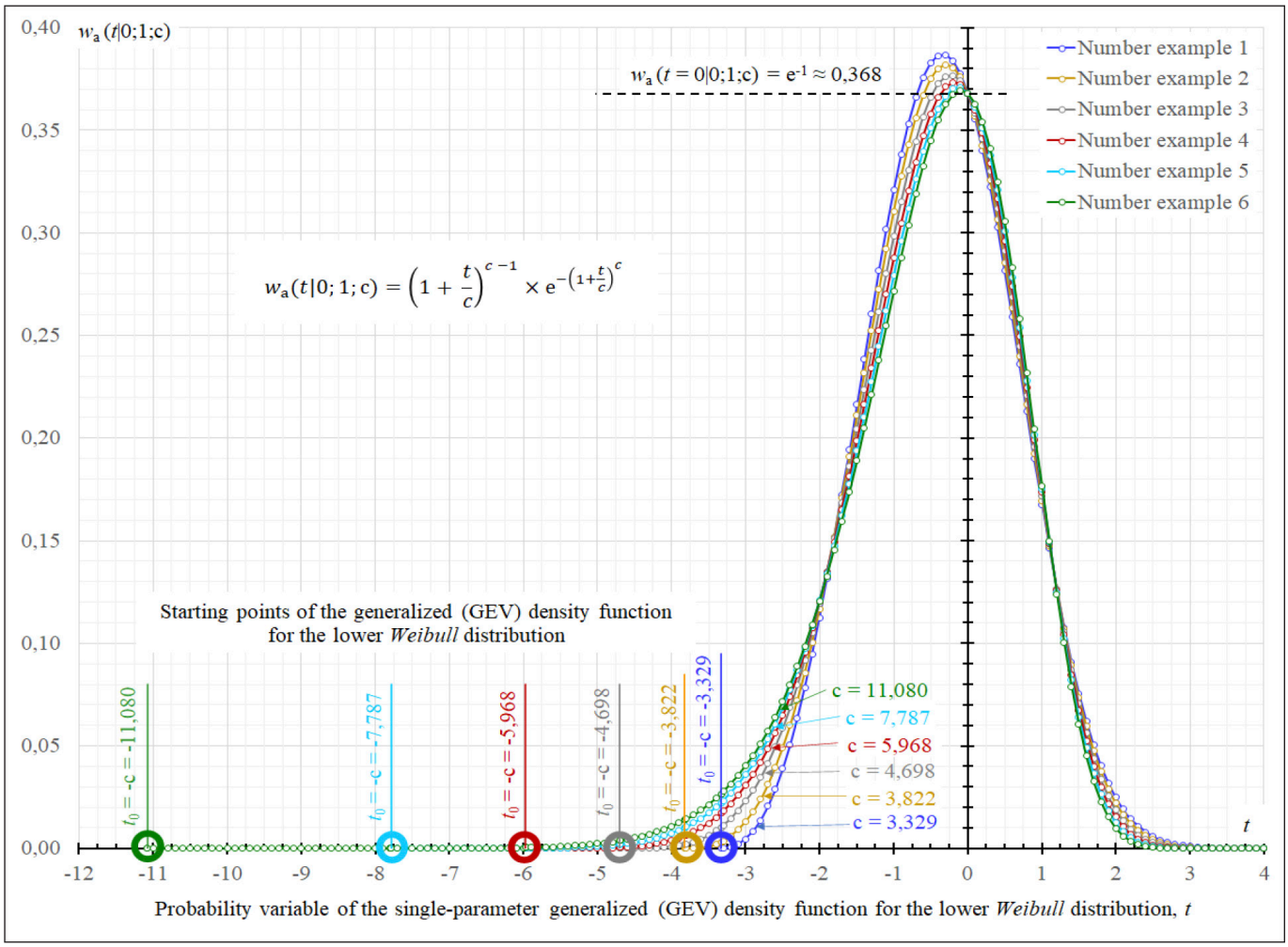

Figure 11: Diagrams of Step 1 of the solution procedure for the numerical examples. Curves of the single-parameter simplified density function for the lower Weibull distribution

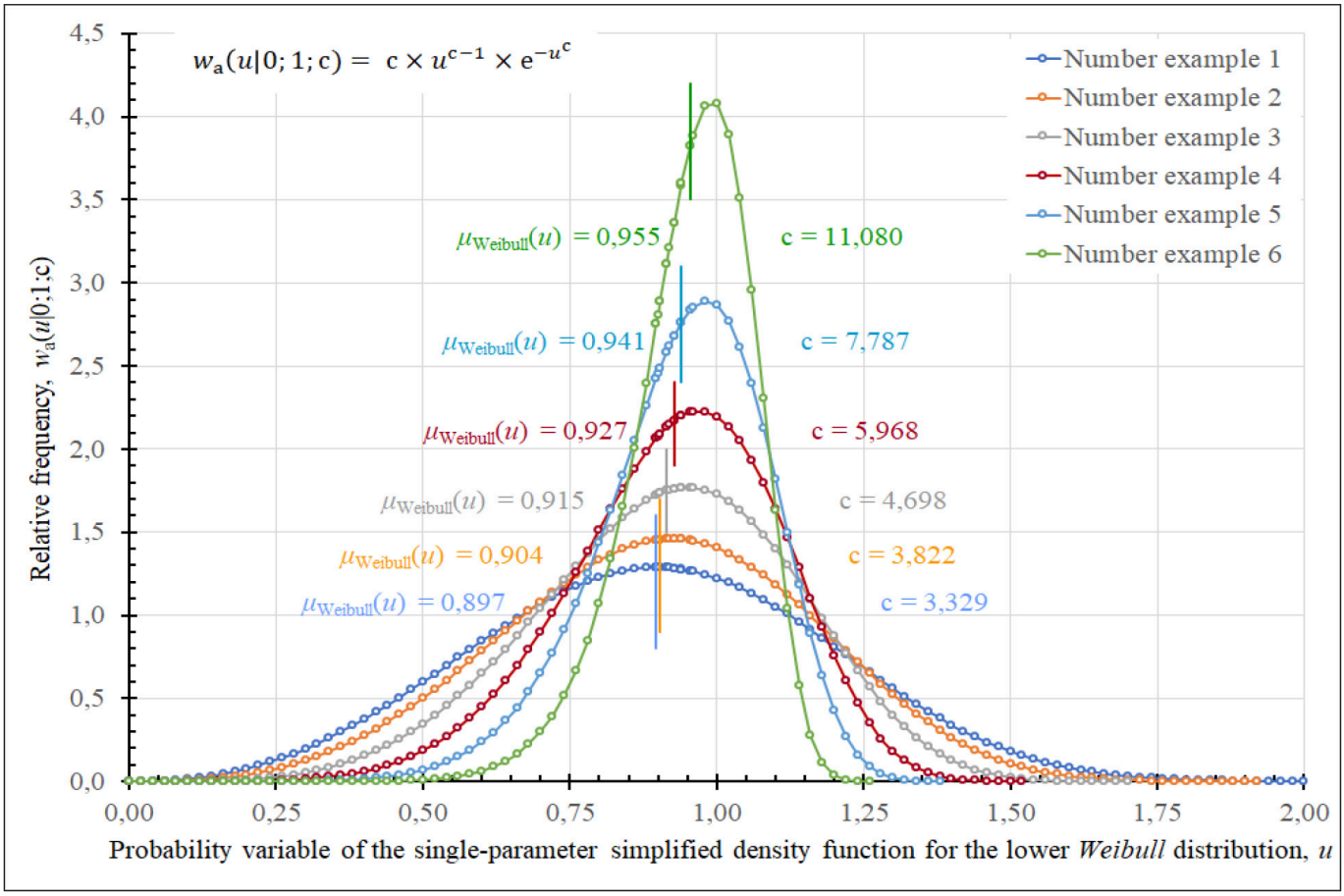

Figure 12: Diagrams for Step 2 of the solution procedure for the numerical examples. Curves of the two-parameter semi-simplified density function for the lower Weibull distribution

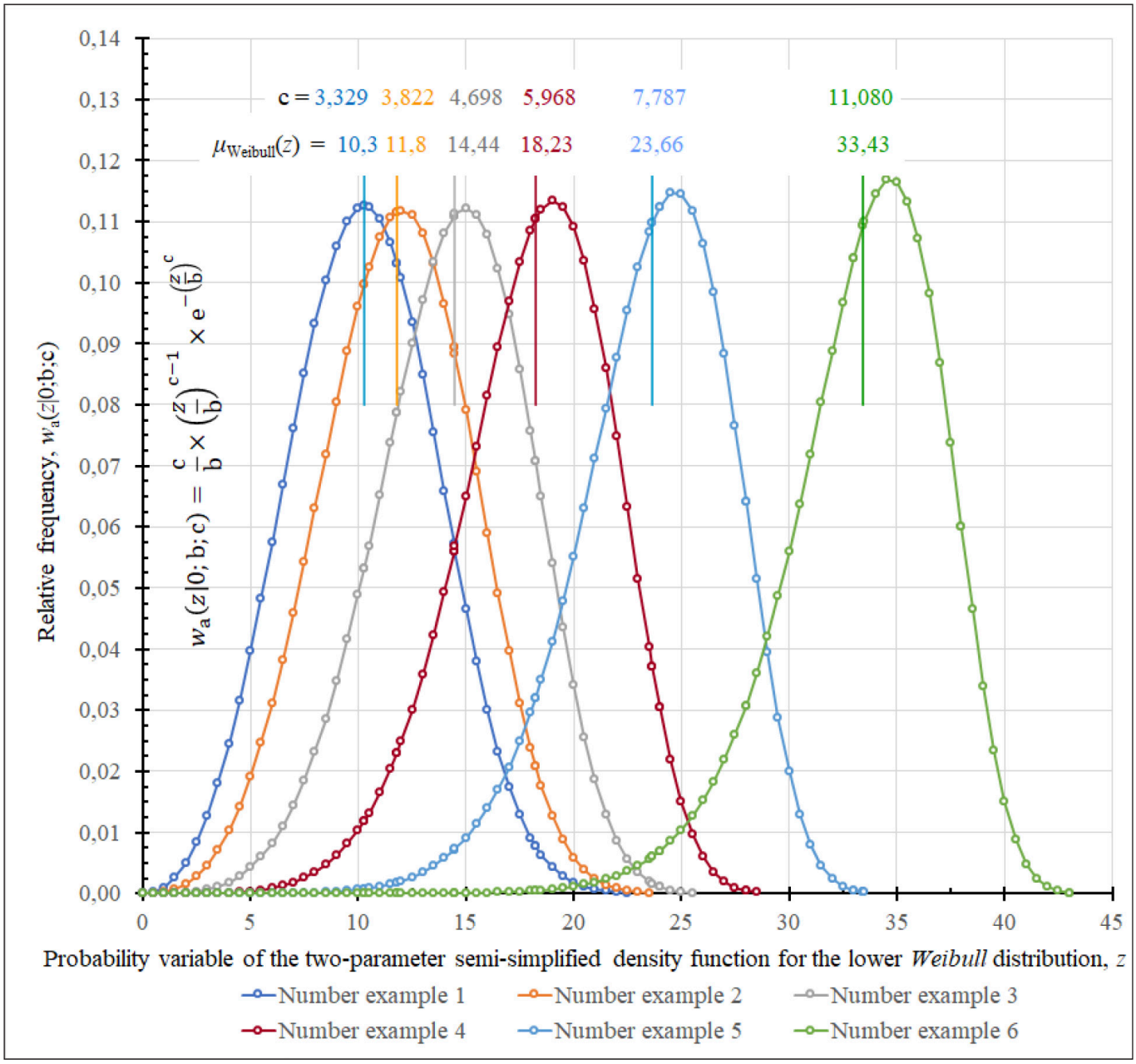

Value of the location parameter „a" can be obtained, when (corresponding to our basic assumption) the calculated mean value $\mu_{Weibull,low}(z|0;b;c)$ of the two-parameter semi-simplified lower *Weibull* distribution is subtracted from the empirical average value of the concrete compressive strength ($f_{cm,test}$):

$$a = f_{cm,test} - \mu_{Weibull,low}(z|0;b;c)$$

- Step 4: A nomogram (*Figure 8*) can be constructed using *Figures 1 - 7* in which calculated parameters of the *Weibull* distribution can be presented in their relations.

5. NUMERICAL EXAMPLE FOR EVALUATING THE COMPRESSIVE STRENGTH OF CONCRETE WITH WEIBULL DISTRIBUTION

Numerical examples have been solved by the calculation method of parameters to the *Weibull* distribution as recommended above. Initial data of the numerical examples are: empirical mean value of the concrete compressive strength, its empirical standard deviation and empirical skewness factor. Major results of the calculation are characteristics of the two-parameter *Weibull* distribution: the mean value, the values of the location parameter, the scale parameter, the shape parameter, as well as the empirical characteristic (5% fractile) value and the empirical acceptance distance of the concrete compressive strength following the *Weibull* distribution and its empirical acceptance distance. The initial data of the numerical examples based on older experimental results and result of the calculation are shown in Table 2. Solution process of the numerical examples is shown in *Figure 9*.

Curves have been drawn for the following cases applying the calculated data of the numerical examples: single-parameter generalized extreme value distribution (GEV) density function for the lower *Weibull* distribution (*Figure 10*), single-parameter simplified density function of the same (*Figure 11*), two-parameter semi-simplified density

Figure 13: Diagrams for Step 3 of the solution procedure for the numerical examples. Curves of the three-parameter simplified density function for the concrete compressive strength with the lower Weibull distribution

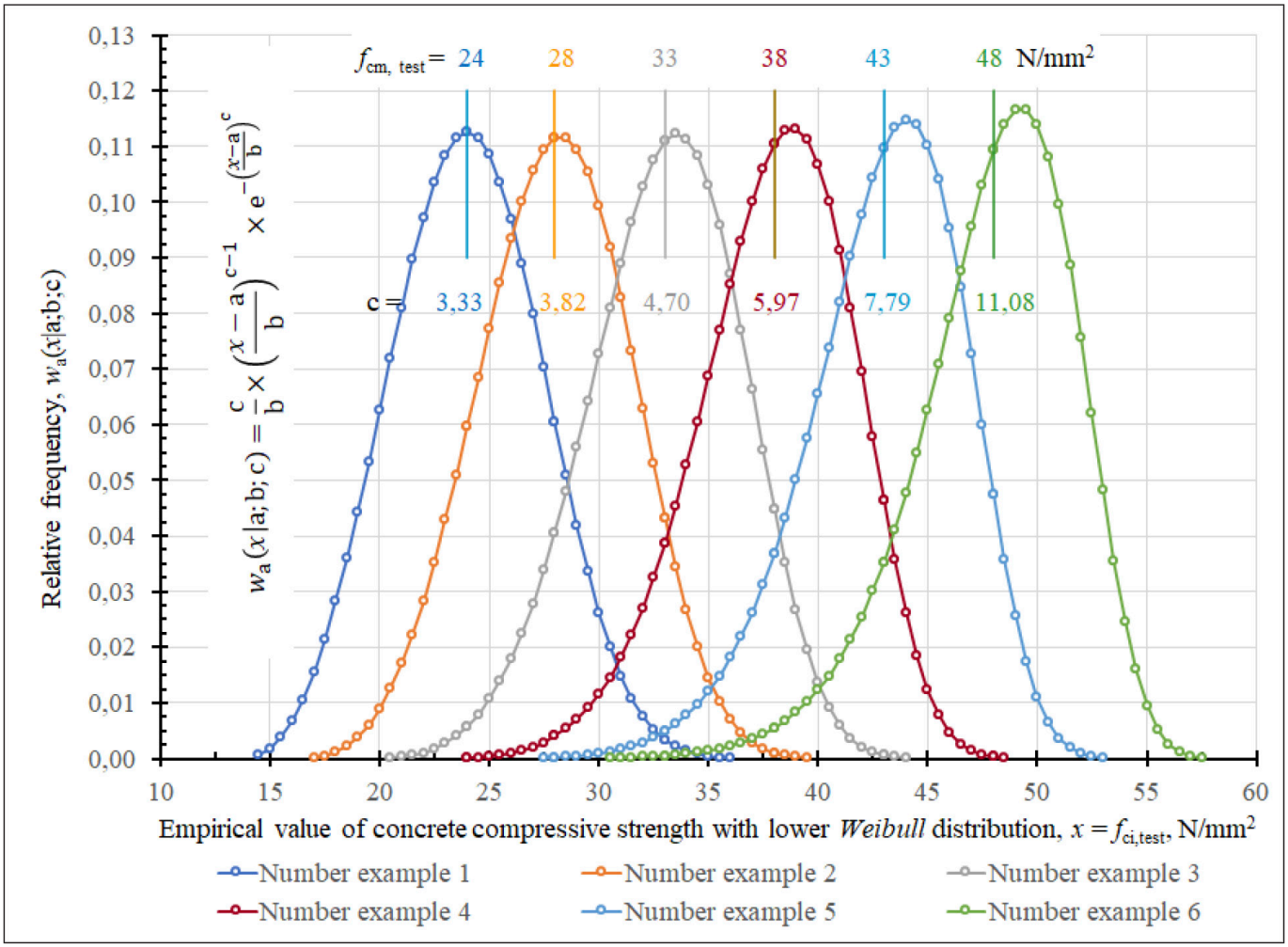

Figure 14: Diagrams for Step 3 of the solution for the numerical example. Curves of the three-parameter simplified distribution function for the concrete compressive strength with lower Weibull distribution

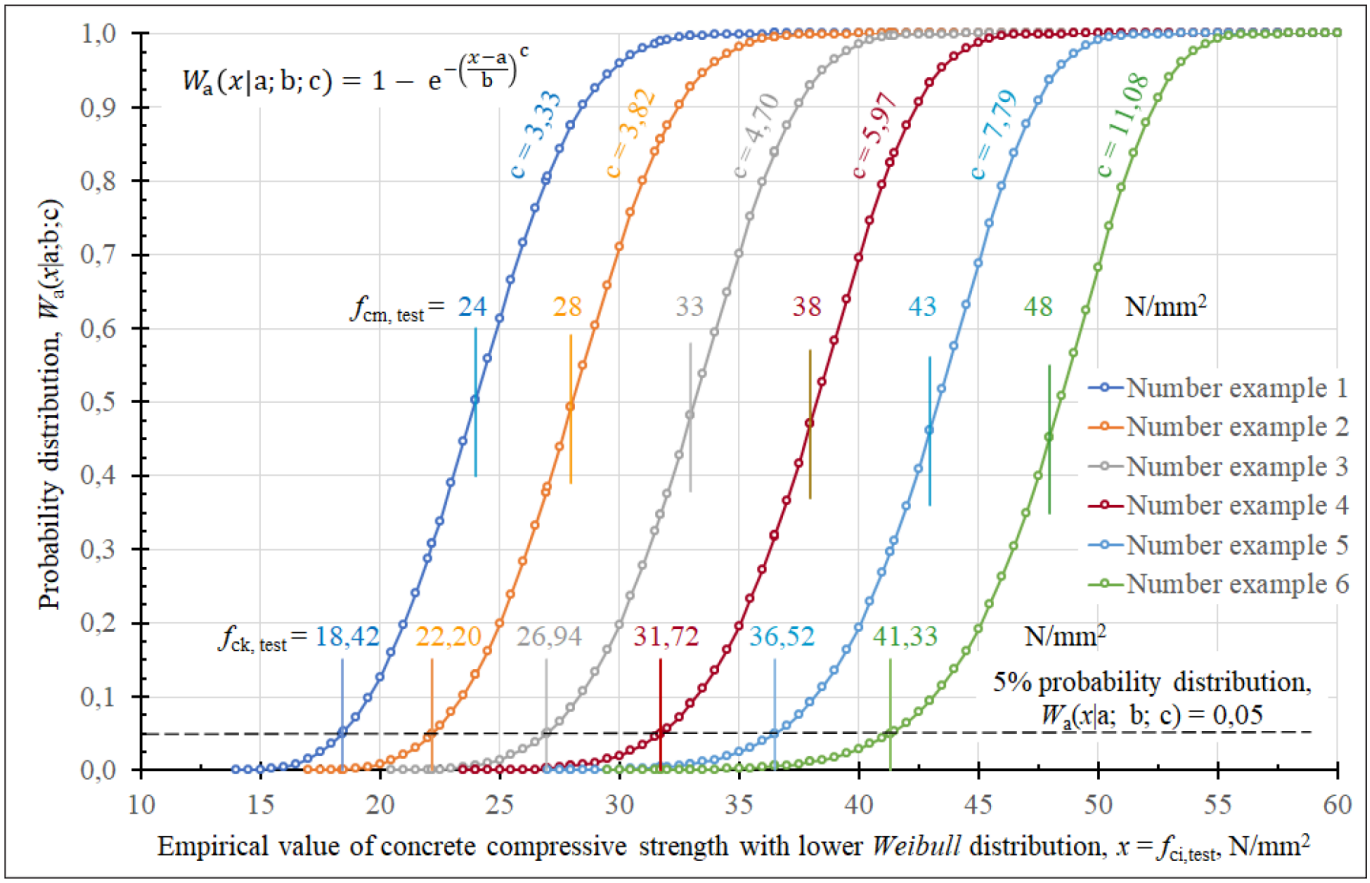

function of the same (*Figure 12*), as well as three-parameter density function and distribution function of the concrete compressive strength characterized with lower *Weibull* distribution (*Figures 13 and 14*, resp.).

The 5% empirical characteristic value for the concrete compressive strength represented with lower *Weibull* distribution was also shown in *Figure 14*. Empirical acceptance distance of the compressive strength ($f_{cm,test}$ – $f_{ck,test}$) is the difference of the empirical average ($f_{cm,test}$) and the empirical characteristic value ($f_{ck,test}$). Values of the difference in our numerical examples exceed 5.5 N/mm^2, in classes beyond C25/30 6 N/mm^2 (*Table 2*).

If the number n of the tested specimens is also considered, the acceptance distance is to be multiplied by the t_n/1,645 quotient, where t_n is *Student*'s t-value (*Federighi,* 1959), (*Stange* et al., 1966). Value of the quotient for a test size with n = 3 is e.g. 2.92/1.645 = 1.775, for a test size with n = 5 it is 2.132/1.645 = 1.296, for a test with n = 15 it is 1.761/1.645 = 1.071 or for a test with n = 35 it is 1.691/1.645 = 1.028.

6. CONCLUSIONS

1. Based on the last but one row of Table 2 we can conclude that the acceptance distance of the concrete compressive strength (performing a really skew distribution) calculated with the lower Weibull distribution is much higher than 4 N/mm^2 , as calculated corresponding to 8.2.1.3.2./Method A section of the EN 206:2013+A2:2021 standard pertinent to the initial production, and higher than 1.48×σ_{test} N/mm^2 corresponding to 8.2.1.3.2./Method B section (continuous production) of the same standard.
2. Consequetly, that according to the EN 206:2013+A2:2021 and the subsequent Hungarian product standard MSZ 4798:2016 with certain concrete compressive strength class (e.g. C40/50) has actually a lower average compressive strength – which is the basis for design of concrete composition – which takes into account the average compressive strength of the standards Eurocode (EN 1990:2002+A1:2005) and Eurocode 2 (EN 1992-1-1:2004+A1:2014, EN 1992-2:2005, EN 1992-3:2006) for the same concrete compressive strength class (Kausay et al., 2007).
3. This already unfavorable difference in acceptance factors (e.g. use of 1.48 instead of 1.645) for concretes with higher compressive strengths increases in reality, as we have shown in this publication using the Weibull distribution according to the actual slope (skewness) of the concrete strengths.
4. Evaluation of the concrete compressive strength results with the lower Weibull distribution in the concrete standard EN 206:2013+A2:2021 would serve the safety and durability of our concrete and reinforced concrete structures. Our antecedents who used the k, skewness factor depending on the average compressive strength in the k×t_n×s product (expressing the acceptance distance) as it was discribed in the withdrawn MSZ 4720-2:1980 Hungarian standard valid until August 2004. This factor k served an approximate consideration of skewness.

7. REFERENCES

Federighi, E. T. (1959), „Extended tables of the percentage points of Student's *t*-distribution", Journal of the American Statistical Association, Vol. 54. pp. 683-688.

Hartung, J. – Elpelt, B. – Klösener, K.-H. (2009), „Statistik. Lehr- und Handbuch der angewandten Statistik", Oldenbourg Wissenschaftsverlag GmbH. München

Kausay, T. – Simon, T. K. (2007), „Acceptance of concrete compressive strength", Concrete Structures (Journal of the Hungarian Group of *fib*), Vol. 8. No. 4., pp. 54-63.

Mistéth, E. (1974), „Erőtani méretezés valószínűségelméleti alapon (Strength sizing on the basis of probability theory)", series of publications of the Institute Építésügyi Minőségellenőrző Intézet. No. 23., Építésügyi Tájékoztatási Központ. Budapest

Misténth, E. (1977), „Építőanyagok küszöbszilárdságának valószínűségi sűrűségfüggvénye (Probability density function of threshold strength of building materials)", Manuscript. Építéstudományi Intézet. Budapest

Misténth, E. (2000), „A keresztmetszeti mennyiség valószínűségelméleti alapon való meghatározása (Determination of the cross-sectional quantity on the basis of probability theory)", Vasbetonépítés (Journal of the Hungarian Group of *fib*), Vol. 2. No. 4., pp. 106-111.

Misténth, E. (2001), „Méretezéselmélet (Sizing theory)", Akadémiai Kiadó. Budapest

Palotás, L. (1979), „Mérnöki szerkezetek anyagtana 1. Általános anyagismeret (Materials Science of Engineering Structures 1. General material knowledge)", Akadémiai Kiadó. Budapest

Rinne, H. (2009), „The Weibull Distribution. A Handbook", CRC Press. Boca Raton (Florida). London, New York

Stange, K. – Henning, H.-J. (1966), „Graf/Henning/Stange. ormeln und Tabellen der mathematischen Statistik", Springer-Verlag. Berlin/Heidelberg/New York

Ujhelyi, J. (1978), „A betonok szilárdsági szórásának és a szilárdság valószínű eloszlásának a vizsgálata (Investigation of the standard deviation of strength and the probable distribution of strength of concretes)", Manuscript. Építéstudományi Intézet. Budapest

Ujhelyi, J. (1985), „Betontechnológia I. (Concrete Technology I.)", Hydraulic engineering aids. Vízdok. Budapest

Weibull, E. H. W. (1939), „The Phenomenon of Rupture in Solids", Ingeniars Vetenskaps Akademiens Handligar. No. 153. Royal Swedish Institute for Engineering Research. Stockholm

8. REFERRED STANDARDS

EN 206:2013+A2:2021 „Concrete. Specification, performance, production and conformity"

EN 1990:2002+A1:2005 "Eurocode. Basis of structural design"

EN 1992-1-1:2004+A1:2014 „Eurocode 2: Design of concrete structures. Part 1-1: General rules and rules for buildings"

EN 1992-2:2005 „Eurocode 2: Design of concrete strucutres. Part 2: Concrete bridges. Design and detailing rules"

EN 1992-3:2006 „Eurocode 2: Design of concrete strucrures. Part 3: Liquid retaining and containment structures"

MSZ 4798:2016 „Concrete. Specification, performance, production, conformity, and rules of application of EN 206 in Hungary"

MSZ 4720-2:1980 „Quality control of concrete. Control of general characteristics" Withdrawn Hungarian standard

Hon. Prof. Tibor KAUSAY (1934), bachelor of civil engineering (1961), reinforced concrete engineer (1967), PhD (1969), candidate of Technical Sciences (1978), Ph.D. (1997), associate professor (1985), honorary professor at the Budapest University of Technology Department of Civil Engineering (2003), member of the Hungarian Section of the fib (2000), commemorative medal of Count Menyhért Lónyay of the Hungarian Academy of Sciences (2003), holder of the László Palotás Prize (Hungarian Section of the fib, 2015). Its activities cover research, development, expertise, education and standardization in the concrete technology and stone and gravel industries. The number of his publications is about 220.

SOLIDIFICATION OF RADIOACTIVE EVAPORATOR RESIDUES WITH HIGH BORATE CONTENT





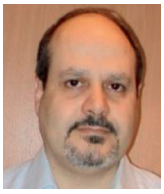

Josef Süssmilch – Lukáš Gric – Petr Fabián – Edit Tóth-Bodrogi – Salem Nehme – Attila Baranyi – Katalin Kopecskó

Keywords: cementation, radioactive waste treatment, mix design development

https://doi.org/10.32970/CS.2022.1.4

1. INTRODUCTION

The Paks Nuclear Power Plant established a new cementation technology to solidify its untreatable liquid radioactive waste; therefore, CHEMCOMEX Praha a.s. company was entrusted with the task. The work involved the development of the mix design and the installation and turn operation of the technology. Using cementation technology, cement paste made using liquid radioactive waste is poured onto solid radioactive waste stored in steel barrels placed in a reinforced steel container. The qualified so-called compact waste package (CWP) will be disposed of in the National Radioactive Waste Repository in Bátaapáti (Hungary), replacing the currently used concrete container solution. These regulations are consistent with International Atomic Energy Agency (IAEA) standards (IAEA, 1990; IAEA, 1996) and the international practice (Spence et al., 2005, Ojovan et al., 2011; Bart et al. 2013; Abdel Rahman et al., 2015).

During the mix design development, the contractual conditions imposed on the cement paste, the Waste Acceptance Criteria (WAC, Radioaktív Hulladékokat Kezelő Kft., 2018), and the technological conditions had to be taken into account. During the optimisation of the mix proportions, the economic aspects had to be kept in mind, i.e. the liquid radioactive waste content of the cement paste had to be maximised while strictly adhering to the requirements.

2. THE REQUIREMENTS FOR THE CEMENT PASTE

During the mix design of cement paste development, primary attention had to be paid to safety aspects, which primarily meant reducing the leaching properties of the various radionuclides. These must also comply with the WAC of the National Radioactive Waste Repository (NRWR).

The further requirements of the mix design development are the following:

- the cement paste must be made of Hungarian cement,
- the mix must be as simple as it can be with the least number of supplementary cementing materials (SCMs) and admixtures,
- with the selected cement type, it must be processed in a wide concentration range of the characteristic composition of the given waste type,
- the mix design must allow all liquid radioactive waste type procession with the planned technological equipment.

3. THE WASTE ACCEPTANCE CRITERIA (WAC)

The final disposal conception of radioactive waste is based on the multi-barrier approach, a combination of technical barriers and protection provided by the geological environment. The technological barrier system aims to allow only a small amount of radioisotopes over a long period. This purpose can be achieved with low leachable waste form (hardened cement paste) waste isolation by its durable container and infilling any free space around the packages. The space-filling restricts the movement of water and other solutions and can provide appropriate chemical conditions and have adsorption properties for leached radioactive isotopes (Chapman, 2003; Nős et al., 2010; Ojovan, 2011).

The WAC prescribes detailed physico-chemical requirements for depositable waste:

- organic matter content and gas formulation (max. 0.5 bar),
- waste with gas content (max. 1,5 bar at 20 ºC),
- heat evaluation (max. 2 kW/m^3),
- dust content (max. 1 %m/m),
- cavity volume (max. 5 cm, max.10 %V/V)
- free liquid content (max. 1 %V/V)
- content of corrosive substances and complexing agent (max. 1 %m/m)
- hazardous material (it must not contain flammable, explosive, oxidising, infectious and corrosive substances)
- flammability (combustible, compressible waste must be compacted with a compression force of 500 kN. The empty space around combustible, uncompacted waste must be cast with cement paste or cement mortar.),
- compressive strength (min. 10 MPa),
- chemical stability and homogeneity,
- the value of diffusion coefficient (max. 10^{-7} cm^2/s)
- radioactive isotope and nuclear material content

Cementation technology meets both the free liquid content and the cavity volume requirement for waste. However, the criteria for the compressive strength and leaching properties of cement paste, which a testing laboratory will control, must also be met (Baranyi and Kopecskó, 2021).

4. TECHNOLOGY REQUIREMENTS

One of the most important requirements for cementation technology is to ensure the highest space-filling of the compact waste package with the highest water/binder (w/b) ratio and, at the same time, provide that the waste package complies with the WAC. However, the high water content causes porosity to increase due to the growth of capillaries (Lian et al., 2011; Chen et al., 2013; Kondraivendhan et al., 2016). Multiple capillaries cause a larger surface area, and water penetrates more easily into the open pores, making it easier for radioactive isotopes to leach out (Carde et al., 1999). A high w/b ratio can also cause sedimentation and bleeding of cement paste. For bleeding, the requirement is max. 1 %V/ V. About 35 - 40 %m/m of water can be incorporated into the hardened cement paste; this corresponds to a w/c ratio of 0.35 to 0.40. If the concrete is made with more water, the water will evaporate from the surface of the cement paste even in its plastic state. As a result, it begins to shrink (early or plastic shrinkage), and capillary pores of the cement stone will form (Powers, 1958; Nehme, 2004). In addition to the above, cement stone may contain air bubbles from mixing and casting. The strength of the solidified cement paste depends on the strength and porosity assumed to be non-porous cement paste.

The strength function according to Powers:

$$R_{c,\square} = R_{c,max}\left(1 - \frac{p}{100}\right)^{n},$$

where $R_{c, max}$ is the cube strength of assumed to be non-porous cement paste (cc. 200 MPa), p is the porosity, and n is an exponent (kb. 4,7) (Balázs, 1994). The leaching properties of hardened cement paste can also be deduced by measuring the compressive strength.

The thermal stress due to the high hydration heat can create cracks in the compact waste package. The requirement can reduce this if the heat of hydration of the cement paste should not reach 80 ºC in the middle of the container (Amin et al., 2009; Batog et al. 2017).

The mix design must also ensure the proper consistency of the cement pastes, which allows the free cavity volume between the solid waste in the barrels to be filled. At the same time, it must meet that requirement to minimise the amount of cement paste remaining in the mixer. For cement paste to meet these criteria, the Suttard consistency must be in the range of 150 to 200 mm. It is an essential technological requirement that the value of the consistency does not fluctuate significantly during mixing and draining.

The expected time of container filling is approx. 3 - 5 hours depending on the empty cavity of the barrels. It is undesirable for the cement paste prepared at the beginning of the filling process to begin to solidify before the last batch of cement paste is drained, as the bonding of the cement paste during the vibration of the container will be damaged. Therefore, the initial set of the cement paste should not be less than 3 hours, but the too-long setting time prevents the waste package from being moved. Particular attention should be paid to this phenomenon, as the borates in the solution retard the hydration of the cement (Cseténi and Glasser, 1995; Coumes, 2003; Davraz, 2010; Han et al., 2010; Sun et al., 2011; Kratochvíl et al., 2014; Li et al., 2019).

5. PROPERTIES OF RADIOACTIVE EVAPORATOR RESIDUES (CONCENTRATES)

The wastewater generated in the Paks NPP is evaporated to be stored in a smaller volume. The pH of the evaporated solution was adjusted at 12 with sodium hydroxide (NaOH) to increase the solubility of the borates. The resulting evaporation residues (concentrates) contain boric acid (borates) in a concentration of 180 – 200 g/dm^3; mainly, this causes the high (200 – 400 g/dm^3) dry matter content of the solution, which must be taken into account when embedding waste in cement.

The evaporator residues are stored in 17 TW-labelled tanks containing significant amounts of nitrates in addition to borates (*Table 1*). The bottom of the tanks also contains different amounts of sludge, which may consist of unknown amounts of undissolved borate crystals in addition to the insoluble phase. The molar ratio of Na:B ≈ 1 in the solutions indicates that boric acid is present in the form of sodium metaborate ($NaBO_2$) in the evaporator residues (Blansdae, 1939; Pungor, 1987).

Concerning the composition of the evaporator, residues differ in each storage tank and may even vary in the different parts of the given tank (400 – 500 m^3), so the concentrates must be homogenised in the first step. Therefore, the pre-homogenisation step takes place already in the storage tank, and after the liquid waste transportation, it is mixed in the homogeniser tank of the cementation plant.

Table 1. Composition of the various evaporator residues (MVM Paks NPP, 2019)

pH	Nitrate [g/dm^3]	Boric acid [g/dm^3]	Molar ratio ($NaOH/H_3BO_3$)
12	5 - 72	110 - 203	0.95 – 1.21
Oxidizable [g/dm^3]		Density [kg/dm^3]	Dry matter [g/dm^3]
1.3 – 52.1		1.15 –1.27	206 - 435

The cementation mix design thus had to cover the evaporation residues for approx. 230 g/dm^3 dry matter and ca. 90 g/dm^3 boric acid concentration difference. During the experiments, the mixtures were designed to its water/cement ratio (w/c) of 0.5.

6. MIX DESIGN DEVELOPMENT

The followed logic was applied during the process of the mix design development:

1. laboratory experiment with model (surrogate) solutions,
2. determination of the composition of liquid radioactive waste,
3. laboratory cementation experiments with model solutions,
4. investigation of laboratory cementation with radioactive evaporator residues,
5. pilot cementation tests.

The basic condition for the development of a cementation mix design is the knowledge of the parameters of the liquid radioactive waste to be cemented that have a significant effect on the formulation. Hence, we determined the density, pH, free alkaline (NaOH), nitrate (NO_3^-), dry matter, and boric acid (borate) content of the concentrate. Knowing these data,

we prepared inactive model solutions to simulate the radioactive evaporator residues embedded in the cement matrix.

In the first step of the mix development, the compliance of the cement paste with the technological requirements (consistency, bleeding, initial setting time, rheological behaviour, effect of vibration, early compressive strength) was investigated. In the case of appropriate mixtures, we modified the constituens based on the experience gained during the experiments to improve the cement paste's technological parameters and the properties of the final product. The measurements that need a longer time or a particular device (e.g. heat evaluation, leach test) will only be performed on mixes that already meet the requirements in their other parameters.

6.1 Materials used for the experiments

Cement types available on the Hungarian market were used for the experiments: CEM I 52.5 N (DDC), CEM I 42.5 N (DDC), CEM I 32.5 N-LH (DDC), CEM III/B 32.5 N-S (DDC), and CEM III/B 32.5 N-LH/SR (Lafarge). Two types of metakaolin were tested during the experiments: Metakaolin KM60 (KERAMOST) and Metakaolin METAVER N (NEWCHEM), which composition can be seen in *Table 2*.

Table 2. Composition of metakaolins used

	Metakaolin KM60	Metakaolin METAVER N
SiO_2	50 - 55%	52 - 53%
Al_2O_3	min. 40%	43 - 44%
Fe_2O_3	max. 1.45%	< 1%
TiO_2	max. 0.8%	< 1%
K_2O	-	< 1%
CaO	0.05 – 0.5%	< 0.5%
MgO	0.20 – 0.45%	< 0.4%
Na_2O	-	< 1%
$K_2O + Na_2O$	max. 1.5%	-

KEMA (KEMA MORAVA) microsilica was also used for experimental purposes (*Table 3*).

Table 3. Composition of KEMA microsilica used

SiO_2	~ 90%
CaO	~ 0.8%
MgO	< 1.5%
Al_2O_3	< 1%
Na_2O	~ 0.5%

Three types of plasticiser, available in the Hungarian and European markets were used: Sika ViscoCrete 21, Sika ViscoCrete 1035, Sika ViscoCrete 4035.

6.2 Test methods for cement paste

Consistency

The consistency of the fresh cement paste was measured according to the Suttard method (Macijauskas, 2013). The Suttard type viscometer is a 50 mm internal diameter and 100 mm height stainless steel cylinder placed on a horizontal smooth, scaled base plate. The cylinder must be filled to the top with cement paste. Then lift the mould and let the cement paste flow and spread on the base plate for 15 seconds,

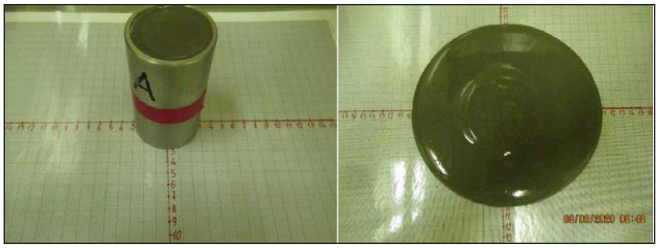

Fig. 1. Consistency measurement with Suttard method Bleeding

then measure the maximum of the cement paste spread in the two directions after 30 seconds (*Fig. 1*). The diameter of the spreading paste is calculated from the average of these two measurements.

Bleeding

Samples of cement paste of known volume are filled in a sealed sampling bottle, and the amount of water appearing on the surface is examined after 24 and 48 hours. After determining the extent of bleeding, the liquid is poured back to the surface of the sample and sealed until the subsequent measurement. The amount of bleeding is given as a %V/V of the total volume of fresh cement paste (*Fig. 2*).

Fig. 2. Bleeding and shrinkage measurement

Initial setting time (IST)

The initial setting time (IST) of the cement paste was measured with manual Vicat apparatus according to the EN 196-3 standard.

Measurement of heat evolution

The kinetics of heat of hydration was determined by pouring the cement paste into a 1 L plastic beaker and then placing it in a 300×400×300 mm polystyrene insulated box with at least 10 cm thickness. Close the calorimeter and immerse the thermocouple in the centre of the sample (*Fig. 3*), using another sensor to record the room temperature using a Comet M1200 temperature data logger (Kopecskó and Baranyi, 2022).

6.3 Test methods of hardened cement paste

Compressive strength measurement

The compressive strength of the cemented product was determined partly according to EN 196-1 and partly according to EN 12390-3 standards using a Controls DigiMax semi-au-

Fig. 3. Measurement of heat evolution

tomatic console with a compression frame with a maximum capacity of 500 kN and a 3000 kN.

Determination of rebound number

The rebound number of the solidified cement paste was measured to estimate the compressive strength of the product. The determination was performed according to EN 12504-2 with a Proceq SilverSchmidt digital Schmidt hammer.

Leaching test

The measurement method for calculating the diffusion coefficient was performed according to the ASTM C1308-08 standard. During the test, a cylindrical specimen 28 mm in diameter and 56 - 69 mm high was immersed in deionised water tempered at 20 ± 1 °C (*Fig. 4*).

The volume of the leaching water is ten times the surface of the cylinder, which must be changed to fresh (clean) water after 2, 7, 24 hours, and daily for the next 10 days by transferring the specimen. Each leaching water was sampled and examined with a gamma spectrometer. The diffusion coefficients of each component were calculated according to Fick's second law using the following equation:

$$D = \pi \left[\frac{a_n/A_0}{(\Delta t)_n}\right]^2 \left[\frac{V}{S}\right]^2 \left[\frac{1}{2}\left(\sqrt{t_n} + \sqrt{t_{n-1}}\right)\right]^2,$$

where a_n/A_0 is the cumulative leached fraction, $(Dt)_n$: $t_{n-1} - t_n$ [s] time interval, V is the volume of the specimen [cm^3], S is the surface of the specimen [cm^2].

6.4 Cementation experiments with model solutions

The first experiments were performed with CEM I 32.5 N-LH and CEM I 52.5 N cement, for which a model solution was added with a w/c ratio of 0.5. However, the cement pastes thus prepared showed a high degree of thixotropic behaviour, which would not have allowed the plant mixer to be emptied and was not suitable to fill the free space of the solid radioactive waste.

Fig. 4. The specimens stored in a climate chamber and the hanging leaching test specimen

At low salt concentrations, thixotropic behaviour of the cement paste was also observed. At high salinity, although the cement paste's consistency improved, at 0.5 w/c we experienced bleeding, initial set retardation (> 24 hours), and inappropriate compressive strength of the product made of CEM I 32.5-LH type cement.

Attempts were made to reduce the retarding effect of boric acid binding with lime hydrate ($Ca(OH)_2$), which increased the early compressive strength of the specimens by 2 to 5 MPa and minimised bleeding. Due to the early thixotropic effect of the lime hydrate and the need to solidify concentrates in a wide boric acid concentration range with only one type of cement, further experiments are required.

Mixtures made of blast furnace slag cement had better leaching properties than the Portland cement; therefore, CEM III/B 32.5 N-S cement experiments were also performed. This type of cement can be used for the solidification of evaporator residues with model solutions and lime hydrate admixture. The requirements for compressive strength, setting time and bleeding properties for these mixtures meet the specified conditions when more than 2% lime is added. Suitable consistency can only be achieved with a low boric acid content (100 g/dm^3) by using vibration. The results show that CEM III/B 32.5 N-S type cement is appropriate for solidifying the model solution with a boric acid concentration of 250 g/dm^3 at a lime hydrate addition of 1.3 - 5.4%.

Based on these results and conclusions, the effect of boric acid concentration and lime hydrate ratio on the properties and technological parameters of the solidified product was investigated. We performed the experiments with three model solutions of different boric acid concentration (80, 140, 200 g/dm^3) with a nitrate content of 42.5 g/dm^3 and a constant w/c ratio of 0.5.

Table 4. Influence of boric acid and lime hydrate on the technological parameters of the cement paste

Boric acid conc. [g/dm^3]	Suttard [mm]	IST [h]	Compressive strength[2] [MPa]
80 (0.5 – 2.5%)[1]	60 – 95	50 - 60	33 - 37
140 (0.9 – 4.6%)[1]	50	0.3 – 0.6	20 - 26
200 (1.4 – 6.9%)[1]	110 – 175	0.4 – 0.7	29 - 34

[1] Lime hydrate concentration given in cement %m/m, [2]at 28 days of age.

It can be seen from the results of *Table 4* the technological parameters studied depend on the boric acid concentration. Still, the addition of lime hydrate has practically no effect on them. All tested parameters reach the minimum expected value at medium (140 g/dm^3) boric acid concentration; therefore, further studies were performed to investigate the effect of $Ca(OH)_2$ concentration with lime hydrate-free mixtures.

Table 5. Properties of the mixtures without lime hydrate

Boric acid [g/dm^3]	Suttard [mm]	IST [h]	Compressive strength [MPa]	
			7 days	28 days
80	85	48	28.39	38.09
140	50	< 15	21.31	24.20
200	195	< 15	22.37	30.15

Our studies confirmed that the addition of lime hydrate has a negligible effect on the final properties of the solidified evaporation residue (*Table 5*). These parameters depend mainly on the concentration of boric acid in the evaporation residue.

6.5 Investigation of the kinetics of hydration heat

The kinetics of the hydration heat evolution of a cement paste prepared using a model solution with a boric acid concentration of 150 g/dm^3 can be seen in *Fig. 5*. It can state that the maximum temperature (62 °C) of CEM I 52.5 N cement paste does not exceed the limit of 80 °C.

6.6 Solidification possibilities of evaporator residues with CEM III/B 32,5 N-LH/SR type cement

The leaching properties of the hardened cement paste can be improved by reducing the porosity, which can be achieved mainly by using materials with pozzolanic properties (e.g. slag, microsilica, metakaolin) and by reducing the w/c ratio (Poon et al., 2001). By decreasing the w/c, the cement paste's viscosity is increased; at the same time, the porosity and the

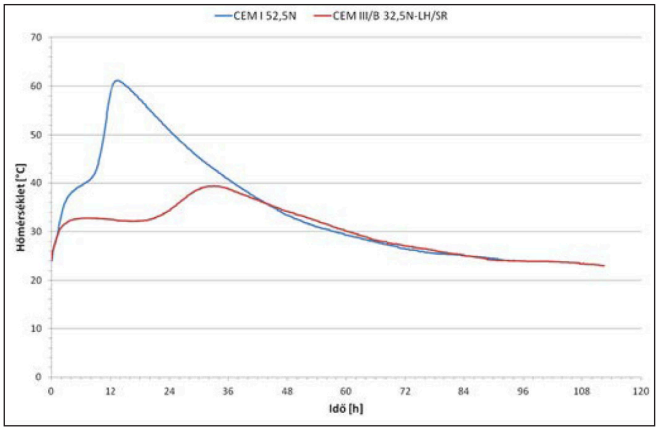

Fig. 5. Heat of hydration comparison of cement paste by using the model solution with CEM I 52.5 N and CEM III/B 32.5 N-LH/SR type cement

diffusivity are also reduced, as well as the bleeding of the cement paste but, which means a higher consistency. Therefore, in addition to the change of cement type, we also examined the effect of w/c factors on technological parameters. At the same time, we studied whether the conditions for the preparation of cement paste and the results of the experiments with pure CEM I 42.5 N Portland cement can be used to apply CEM III/B 32.5 N LH/SR cement. These experiments were also performed with evaporation residue model solutions containing 120 g/dm^3, and 210 g/dm^3 boric acid in the presence of 1.25 %V/V nitric acid (HNO_3). The rheological properties (densifying) of the cement paste can be affected by the decrease in pH, thus the optimal volume of the nitric acid was determined in previous examinations.

Based on the results shown in *Table 6*, the w/c ratio should be reduced below 0.54 to achieve better bleeding and compressive strength values.

Table 6. Parameters of mixtures made using 120 g/dm^3 boric acid concentration model solution and CEM III/B 32.5N LH/SR type cement

w/c		0.54	0.56	0.58
IST [h]		18	24 – 48	24 – 48
Suttard consistency [mm]		128	143	150
Bleeding after 24 hours [%]		0.7	0.9	1.1
Compressive strength [MPa]	7 days	4.92	4.05	3.45
	14 days	9.03	8.06	7.78
	28 days	19.96	20.55	18.24

Table 7. Parameters of mixtures made using 210 g/dm^3 boric acid concentration model solution and CEM III/B 32.5N LH/SR type cement

w/c		0.46	0.48	0.50
IST [h]		< 15	< 15	< 15
Suttard consistency [mm]		120	135	140
Bleeding after 24 hours [%]		0	0.90	0.88
Compressive strength [MPa]	7 days	8.87	8.28	8.32
	14 days	14.23	12.88	13.95
	28 days	26.67	22.66	20.09

The best parameters were shown in the sample with a boric acid concentration of 210 g/dm^3 and a w/c ratio of 0.46 (*Table 7*), but early thixotropic behaviour was also observed in this case. Increasing the w/c ratio to 0.47 could improve these properties but would increase the certainty of cement paste bleeding.

6.7 Cement pastes with the addition of metakaolin and microsilica

Henceforth, experiments were performed to improve the properties of the mixture using CEM I 42.5 N using metakaolin and microsilica at a constant nitric acid content of 1.43 %V/V (*Table 8 – 11*).

Table 8. *The main properties of cement paste made using 120 g/dm³ boric acid and metakaolin KM60 (w/c = 0.50)*

Metakaolin KM60 [%]		0	5	10
Suttard [mm]		170	150	125
IST [h]		3 – 4.5	2.5 – 3	2.5 – 3
Bleeding after 24 hours [%]		0.4	0.3	0
Bleeding after 48 hours [%]		0	0	0
Compressive strength [MPa]	7 days	24.81	18.07	27,47
	14 days	28.95	27.27	37.95
	28 days	35.78	30.70	39.49

Table 9. *The main properties of cement paste made using 210 g/dm³ boric acid and metakaolin KM60 (w/c = 0.48)*

Metakaolin KM60 [%]		0	5	10
Suttard [mm]		170	150	125
IST [h]		3 – 4.5	2.5 – 3	2.5 – 3
Bleeding after 24 hours [%]		0.4	0.3	0
Bleeding after 48 hours [%]		0	0	0
Compressive strength [MPa]	7 days	24.81	18.07	27.47
	14 days	28.95	27.27	37,95
	28 days	35.78	30.70	39.49

Table 10. *The main properties of cement paste made using 120 g/dm³ boric acid and KEMA microsilica (w/c = 0.50)*

Microsilica [%]		0	5	10
Suttard [mm]		170	145	113
IST [h]		3 – 4.5	1.42	2
Bleeding after 24 hours [%]		0.4	0	0
Bleeding after 48 hours [%]		0	0	0
Compressive strength [MPa]	7 days	24.81	22.17	19.68
	14 days	28.95	24.14	28.26
	28 days	35.78	32.07	31.47

Table 11. *The main properties of cement paste made using 210 g/dm³ boric acid and KEMA microsilica (w/c = 0.48)*

Microsilica [%]		0	5	10
Suttard [mm]		180	155	120
IST [h]		1.5	2 – 3	2 – 3
Bleeding after 24 hours [%]		0.50	0	0
Bleeding after 48 hours [%]		0.37	0	0
Compressive strength [MPa]	7 days	24.76	19.02	17.01
	14 days	31.30	26.14	24.45
	28 days	36.14	30.57	35.40

It can be seen from the data in Table 11 that the addition of microsilica and metakaolin increase the consistency of the cement paste, while these SCMs reduce the bleeding tendency. There is a slight decrease in compressive strength for both materials; however, even at 7 days of age, these values exceed the required 10 MPa.

6.8 Leaching tests of cement paste made of model solution containing ^{137}Cs tracer

The cementation experiments were performed with ^{137}Cs-labelled model solutions, which showed the efficiency of replacing part of PC with SCMs to improve the leaching properties of the final cemented product. The experiments were implemented at Nuclear Research Institute (Ústav jaderného výzkumu Řež u Prahy). The leaching test was performed according to standard ASTM C1308-08. During the specimen preparation CEM I 42.5 N, CEM III/B 32.5 N-LH/SR type cement, metakaolin, and microsilica were used with ^{137}Cs-labelled, 120 and 210 g/dm³ boric acid concentration model solution. The results showed that the diffusion coefficient of ^{137}Cs corresponded with the defined value in the WAC (10^{-7} cm²/s) even without SCMs; but using these materials, the diffusion coefficient can be reduced by an order of magnitude.

6.9 Experiments with evaporator residues

Based on observations of cementation experiments with model solutions, test mixtures were performed using different evaporation residues, which showed similar results to the inactive model solutions; therefore, further optimisation experiments were performed using CEM I 52.5 N and supplementary cementing materials (SCMs).

Table 13 shows that we achieved better results for all technological parameters using CEM 42.5 N cement.

Table 12. *The main properties of cement paste made using type CEM I 42.5 N cement and evaporation residue from the tank 02TW10B003*

w/c	0.43	0.49
pH (concentrate)	11.5	11.7
Suttard [mm]	125	160
IST [h]	25.5 - 40	28 - 40
Bleeding after 24 hours [%]	0	0.4
Compressive strength [MPa]	26.75	24.82

Table 13. *The main properties of cement paste made using two types of cement and evaporation residue from the tank 02TW10B003 (w/c = 0.49, pH = 11.8)*

Cement type	CEM I 52.5 N	CEM 42.5 N
Suttard [mm]	125	160
Suttard after 30 min. [mm]	118	155
IST [h]	48	28 - 40
Bleeding after 24 hours [%]	0	0.4

6.10 Experiences with cementation of evaporation residues from tank 02TW80B003

The concentrate to be processed for the first time with the current cementation technology is located in tank 02TW80B003, which contains a high-salt, alpha-emitting (trans-uranium-containing) solution generated during a malfunction at the Paks Nuclear Power Plant in 2003 (*Table 14*).

Table 14. Composition of evaporator residue in tank 02TW80B003 (550 m³) (MVM Paks NPP, 2019)

Molar ratio ($NaOH/H_3BO_3$)	Density [kg/dm³]	Dry matter [g/dm³]
1.08	1.232	362.60
pH	**Nitrate [g/dm³]**	**Boric acid [g/dm³]**
12	22.59	184.54

During the further mix design development, we tried to increase the waste content, so the concentrate/bonding ratio of the cement paste also ruled out the importance of using other admixtures such as superplasticiser or nitric acid. Finally, the cementation results have shown that the optimal mix proportions of the evaporator residue from the 02TW80B003 tank was achieved using 0.61 w/b (w/c = 0.44) and 25% KM60 type metakaolin. Thus the desired mixing ratio was as follows: concentrate : cement (CEM I 42.5 N) : metakaolin (Keramost KM 60) = 1 : 1.32 : 0.33. During the laboratory experiments, compressive strength tests were performed on 40×40×40 mm specimens, and then during the pilot tests, we also performed on standard specimens with an edge length of 150 mm. The results are summarised in *Table 15*, which are the averages of three parallel measurements.

Table 15. Compressive strength results of solidified cement paste made using evaporation residue from tank 02TW80B003

Exp.	Specimen type	KM60 [%]	Compressive strength [MPa]		
			7 days	14 days	28 days
Lab.	40 mm	11	6.30	38.65	48.16
	40 mm	25	22.96	50.80	55.38
Pilot	40 mm	25	1.47	18.56	40.28
	150 mm	25	n.a.	n.a.	36.96

It should be noted that the 7-day demoulding of the specimens was problematic in some cases, on the one hand, due to the slow setting of the cement paste; on the other hand, due to the adhesion of the cement paste to the mould. Another critical parameter for a cemented product is the leaching property of each isotope, i.e. the value of the diffusion coefficient. Measurements were performed according to ASTM C1308-08, previously described in *Chapter 6.2*. In our experience, the ^{60}Co isotope is only slightly, while the ^{137}Cs isotope is more soluble from the specimens. However, its diffusion coefficient is still two orders of magnitude lower ($4 \cdot 10^9$ cm²/s) than the 10^{-7} cm²/s as prescribed in the WAC.

7. CONCLUSIONS

In this study we summarised the inactive and radioactive laboratory experiments of the cementation mix design of different types of liquid radioactive waste; we presented the used materials and test methods.

The first step of the mix design development was to determine the composition of the evaporator residues, which followed by the cementation of inactive model (surrogate) solutions with CEM I 32.5 N-LH, CEM I 52.5 N, CEM III/B 32.5 N-S and CEM III/B 32.5 N-LH/SR types of cement. Henceforth, attempts were performed to reduce the set retardation effect of boric acid with lime hydrate. The measurements show that the lime hydrate has a negligible impact on the final parameters of the hardened cement paste, but the boric acid content has a great effect on it. During the further experiments, supplementary cementing materials (SCMs) were added to the cement paste to decrease the porosity and improve the leaching properties. For this purpose microsilica and metakaolin were used, but in order to decrease of diffusion coefficient, the w/c ratio of the cement paste must be reduced. During these measurements, the effect of nitric acid (1.25 – 1.43 %V/V) on the rheological properties were observed. Since the most important property of the cement paste is the low diffusion coefficient, thus the w/c and porosity must be reduced. Finally, CEM I 42.5 N type Portland cement and 20 %m/m Keramost KM60 type metakaolin was used, and with this mix design all technological parameter of the cement paste was provided.

In the case of evaporation residues, the composition can vary from tank to tank, a protocol for the development of proper and applicable mix design was also determined. As a result of the inactive laboratory experiments, all studied radioactive evaporator residues can be solidified, and the properties of the fresh and hardened cement paste meets the WAC and all technological requirements.

9. REFERENCES

Abdel Rahman R. O.; Rakhimov, R. Z.; Rakhimova, R. N.; Ojovan, M. I. (2015), „Cementitious Materials for Nuclear Waste Immobilization", *Wiley*, ISBN: 9781118512005, https://doi.org/10.1002/9781118511992

Amin, M. N.; Kim, J.-S.; Lee, Y.; Kim, J.-K. (2009), „Simulation of the thermal stress in mass concrete using a thermal stress measuring device", *Cement and Concrete Research* 39, 154–164, https://doi.org/10.1016/j.cemconres.2008.12.008

Balázs, Gy. (1994), "Építőanyagok és kémia", *Műegyetemi Kiadó*, Budapest

Baranyi A., Kopecskó K., Feil F., Grič, L. (2021), "A Paksi Atomerőmű hulladékainak cementbe ágyazása, és a technológiához tartozó vizsgáló laboratórium kialakítása", *Vasbetonépítés* 2021/2 31-40, https://doi.org/10.32969/VB.2021.2.2

Bart, F.; Cau-dit-Coumes, C.; Frizon, F.; Lorente, S. (2013), "Cement-Based Material for Nuclear Waste Storage", *Springer*, ISBN 978-1-4614-3445-0

Batog, M.; Giergiczny, Z. (2017), „Influence of mass concrete constituents on its properties", *Construction and Building Materials* 146, 221–230, https://doi.org/10.1016/j.conbuildmat.2017.04.085

Blasdalae, W. C.; Slansky, C. M. (1939), "The Solubility Curves of Boric Acid and the Borates of Sodium*", Chemical Laboratory of the University of California*, April

Carde, C.; Raoul Frarqois, R. (1999), "Modelling the loss of strength and porosity increase due to the leaching of cement pastes", *Cement & Concrete Composites* 21, 181-188, https://doi.org/10.1016/S0958-9465(98)00046-8

Chapman, N.; McCombie, C. (2003), „Principles and Standards for the Disposal of Long-Lived Radioactive Wastes", *Waste Management Series 3*, Academic Press, Elsevier, ISBN: 978-0-08-044192-4

Chen, X, Wu, S., Zhou, J. (2013), „Influence of porosity on compressive and tensile strength of cement mortar", *Construction and Building Materials* 40, 869–874, https://doi.org/10.1016/j.conbuildmat.2012.11.072

Coumes, C.C.D. (2003), "Cementation of a low-level radioactive waste of complex chemistry Investigation of the combined action of borate, chloride, sulfate and phosphate on cement hydration using response surface methodology", Cement and Concrete Research 33, 305–316, https://doi.org/10.1016/S0008-8846(02)00943-2

Csetényi, L. J.; Glasser, F. P. (1995), "Borate retardation of cement set and phase relations in the system Na_2O-CaO-B_2O_3-H_2O, *Advances in Cement Research* 7(25), 13-19, https://doi.org/10.1680/adcr.1995.7.25.13

Davraz, M. (2010), "The effects of boron compounds on the properties of cementitious composites", *Science and Engineering of Composite Materials* 17(01), 1-18, https://doi.org/10.1515/SECM.2010.17.1.1

Ding, J.; Li, Z. (2002), "Effects of metakaolin and silica fume on properties of concrete" *ACI Materials Journal* 4(99), 393-398

IAEA (1990), "Qualitative acceptance criteria for radioactive wastes to be disposed of in deep geological formations", *TECDOC-560*, IAEA: Vienna, Austria

IAEA (1996), "Processing of Nuclear Power Plant Waste Streams Containing Boric Acid", TRS No. 911, IAEA: Vienna, Austria.

Kratochvíl, J.; Opravil, T.; Pavel, D. (2014), "The effect of boron and its compounds on setting of portland cement", *Advanced Materials Research* 1000, 16-19, https://doi.org/10.4028/www.scientific.net/AMR.1000.16

Kondraivendhan, B; Bhattacharjee, B. (2016), "Strength and w/c ratio relationship of cement based materials through pore features", *Materials Characterization* 122, 124-129, https://doi.org/10.1016/j.matchar.2016.10.036

Kopecskó, K., Baranyi, A. (2022), „Comparative study of setting time and heat of hydration development of Portland cement according to EN 196-3", *Calorimetry*, IntechOpen, https://doi.org/10.5772/intechopen.101912

Li, B.; Ling, X.; Liu, X.; Li, Q.; Chen, W. (2019), "Hydration of Portland cements in solutions containing high concentration of borate ions: Effects of LiOH", *Cement and Concrete Composites* 102, 94–104, https://doi.org/10.1016/j.cemconcomp.2019.04.010

Lian, C.; Y. Zhuge, Y.; Beecham S. (2011), "The relationship between porosity and strength for porous concrete", *Construction and Building Material* 25, 4294–4298, https://doi.org/10.1016/j.conbuildmat.2011.05.005

Macijauskas, M.; Gailius A. (2013), "Influence of cement type and admixtures on rheological properties of cement paste", *Engineering Structures and Technologies* 5(4), 175-181, https://doi.org/10.3846/2029882X.2014.912431

MVM Paks NPP (2019), „Az MVM Paksi Atomerőmű Zrt. Radioaktív hulladékainak kezelése, tárolása és elhelyezése", Éves jelentés 2019, In English: "Treatment, Storage and Deposition of Radioactive Waste Generated in Paks Nuclear Power Plant", *Annual Report 2019*

Nehme, S. G. (2004), „A beton porozitása", *PhD értekezés*, In English: "Porosity of concrete", *PhD Thesis*

Nős, B.; Ormai, P.; Fritz, A.; Bérci, K.; Feil, F. (2010), „A Bátaapáti NRHT hulladék átvételi rendszere, és ennek alkalmazása egy jellemző hulladéktípusra", In English: „Waste acceptance system and its application for a typical waste type of PURAM in Bátaapáti" *Nukleon* 03/2010,

Ojovan, M. I. (2011), „Handbook of Advanced Radioactive Waste Conditioning Technologies", *Woodhead Publishing Limited*, ISBN 978-0-85709-095-9

Pungor E. (1987), „Analitikusok kézikönyve", In English: "Analytics Handbook", *Műszaki Könyvkiadó*, Budapest, ISBN: 9631070530

Poon, C.-S; Lam, L.; Kou, S.C; Wong, Y.-L.; Wong, Ron (2013), „Rate of pozzolanic reaction of metakaolin in high-performance cement pastes", *Cement and Concrete Research* 31, 1301–1306

Powers, T.C. (1958), "Structure and physical properties of hardened Portland cement paste", *Journal of the American Ceramic Society*, 41(1), 1-6

Radioaktív Hulladékokat Kezelő Kft. (2018), „Hulladék átvételi követelmények (HÁK)", *NRHT üzemeltetést megalapozó biztonsági jelentés (RHK-K-076B/16)*, 11. fejezet: Üzemeltetési feltételek és korlátok, In English: „Waste acceptance criteria (WAC), *Basic operational safety report of requirements and limits of the PURAM"*, Chapter 11:Operational conditions and limits

Sun, Q.; Li, J.; Wang, J. (2011), "Effect of borate concentration on solidification of radioactive wastes by different cements", *Nuclear Engineering and Design* 241, 4341–4345, https://doi.org/10.1016/j.nucengdes.2011.08.040

Spence, R. D.; Shi, C. (2005), "Stabilisation and Solidification of Hazardous, Radioactive, and Mixed Wastes", *CRC Press*, New York, NY, USA, 2005, ISBN 1-56670-444-8

10. LIST OF REFERRED STANDARDS

EN 196-1: 2005 Methods of testing cement. Part 1: Determination of strength

EN 196-3: 2009 Methods of testing cement. Part 3: Determination of setting time and soundness

EN 12390-3: 2009 Testing hardened concrete. Part 3: Compressive strength of test specimens

EN 12504-2: 2009 Non-destructive testing. Determination of rebound number

ASTM C1308-08 Standard Test Method for Accelerated Leach Test for Diffusive Releases from Solidified Waste and a Computer Program to Model Diffusive, Fractional Leaching from Cylindrical Waste Forms, ASTM International, West Conshohocken, PA, 2008, www.astm.org, https://doi.org/10.1520/C1308-08

Jozef Süssmilch: He graduated from the University of Chemical Technology, Prague with a degree in inorganic chemistry (1978), then became a candidate for chemical sciences at Charles University (1993). In the beginning, he worked in the vitrification of intermediate-level radioactive waste. He was the Head of the Department of Radioactive Waste Solidification for 9 years then the Head of the Research and Development Centre. He designed and implemented development projects and technological improvement and operation of geopolymer matrices at Chemcomex, a.s. for 18 years. He was a member of the Nuclear Research Institute for 34 years.

Lukás Grič: Chemical Engineer, he works as a researcher in the Department of Development of Chemcomex, a.s. in the Czech Republic. His main field of interest in radioactive waste management and fly ash treatment from hazardous waste incinerators.

Petr Fabián: Researcher-developer Engineer at Chemcomex, a.s. in the Czech Republic. Earlier he worked on the development and optimisation of the properties and colors of enamels for the production of jewelry and semi-finished products. Then he dealt with the development of methods for applying platinum coatings to ceramic components of glass aggregates at Safina, a.s. Nowadays he works on the design and implementation of research projects in the field of technology development and application of geopolymer matrices. His special field of interest is the research and application of geopolymeric materials for the embedding of hazardous and radioactive waste.

Edit Tóth-Bodrogi: Associate professor at University of Pannonia. She is graduated as an Environmental Engineer (2002) at the University of Veszprém and got a PhD degree (2005) in the field of Material sciences and technologies. She teaches in the Department of Radiochemistry and Radioecology, Faculty of Engineering (BSc, MSc, postgraduate and PhD courses). Her research field is the nuclear measurements, radiological characterisation (alpha-, beta-, gamma-spectrometry) of different environmental matrices, investigation the leachability of radioisotopes from different matrices, human exposure assessment in case of NORM activities and radiation exposures and radiation protection planning.

Salem Nehme: Civil Engineer, PhD, Associate Professor, Head of the Department of Construction Materials and Technologies, BME. His main areas of interest are the porosity of concrete, the relationship between the durability of concretes and self-compacting concretes and porosity, the use of self-compacting concretes and steel fiber self-compacting concretes in the reinforced concrete, the elimination of the application issues of self-compacting concretes as a mass concrete. He is a member of the Hungarian Chamber of Engineers (T1-01-9159), the Hungarian Group of the ***fib*** and the Hungarian Silicate Industry Scientific Association.

Attila Baranyi: Chief Technologist at MVM Paks NPP in Hungary. He graduated in chemistry (2003) and chemistry teacher (2006) from the University of Veszprém, and then graduated in concrete technology (2021) from Budapest University of Technology and Economics. He previously worked on radioanalysis and then on the development of liquid radioactive waste treatment technologies: testing of ultrafiltration membranes, selective sorbents, and developing Advanced Oxidation Processes (AOPs). He currently works on the establishment of a new testing laboratory related to the radioactive waste cementation technology under construction at the Paks Nuclear Power Plant, the development of testing method and equipment.

Katalin Kopecskó: Associate Professor at the BME. Graduated in Chemical Engineering (1990) and has postgraduate studies in Concrete Technology (2004). She has PhD degree since 2006. She teaches in the Civil Engineering Faculty, BME (BSc, MSc, postgraduate and PhD courses). Her research fields are deterioration processes of construction materials, durability of construction materials, durability of concrete, cement hydration, diagnostics, mineralogical and microstructural analysis, X-ray diffraction (XRD), thermal analyses (TG/DTG/DTA), scanning electron microscopy (SEM). She is a member of the ***fib***, Hungarian Group of *fib*, RILEM TC CNC, TC MSZT/MB 102 (Cement and Lime), and Hungarian Silicate Industry Scientific Association. E-mail: kopecsko.katalin@emk.bme.hu

STRENGTHENING AND SHM SYSTEM INSTALLATION ON RC SLAB USING NON-LINEAR FE ANALYSIS

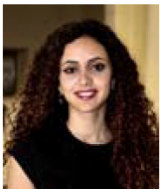


Asseel Al-Hijazeen - Muhammad Fawad - Kálmán Koris - Marek Salamak

https://doi.org/10.32970/CS.2022.1.5

Re-life of aged load-bearing structures may be more efficient and economical than complete re-building. Nowadays, the strengthening of an RC structure can be designed using non-linear FE analysis, taking a realistic structural behaviour into account. Within the current article, this process is demonstrated in connection with the strengthening of a monolithic RC slab. The slab must be strengthened due to a change of function which increases live load. To ensure satisfactory operation in SLS for increased load, the flexural strengthening of the slab by CFRP strips and bonded steel plates was considered. Static verification of the slab for original and increased loads is performed by linear FE analysis. The load-bearing capacities of the original and the strengthened slabs are also determined by non-linear FE calculation. A comparative analysis of the results highlights the effectiveness of different strengthening methods in increasing the stiffness and SLS capacity of the slab. To perform real-time monitoring of the slab in question, an SHM system is also suggested with the installation of three different types of sensors. This system increases the safety of operation and reduces future maintenance and strengthening costs.

Keywords: monolithic concrete slab, damage diagnostics, 3D nonlinear FE analysis, CFRP strengthening, steel plate strengthening, monitoring, SHM installation.

1. INTRODUCTION

Reinforced concrete slabs are essential structural elements in buildings and bridges. Nevertheless, they might encounter damages under different loadings such as fatigue, aging, overloading, earthquakes, and further natural disasters during their service life (Ahmed, 2016)such as permanent, sustained and transient during their lifetime. Reinforced concrete slabs are one of the most fundamental structural elements in buildings and bridges, which might be exposed to unfavourable conditions such as, impaired quality control, lack of maintenance, adverse environmental effects, and inadequate initial design. Therefore, the resistant capacity of the affected elements would dramatically be reduced which most likely leads to the partial or whole collapse of the structure. Non-destructive testing (NDT. Excessive cracking is one of the most common damages in reinforced concrete slabs, in addition to deflections at midspan (Nejadi, 2022). Therefore, damage detection is vital to guarantee the integrity and safety of civil structures (Fujino, 2002). The conventional procedure is based on human visual inspection, which cannot locate any hidden or minor damages (Kot et al., 2021) which involves inspection, monitoring, and maintenance to support economics, quality of life and sustainability in civil engineering. Currently, research has been con-ducted in order to develop non-destructive techniques for SHM to extend the lifespan of monitored structures. This paper will review and summarize the recent advancements in non-destructive testing techniques, namely, sweep frequency approach, ground penetrating radar, infrared technique, fiber optics sensors, camera-based methods, laser scanner techniques, acoustic emission and ultrasonic techniques. Although some of the techniques are widely and successfully utilized in civil en-gineering, there are still challenges that researchers are addressing. One of the common challenges within the techniques is interpretation, analysis and automation of obtained data, which requires highly skilled and specialized experts. Therefore, researchers are investigating and applying artificial intelligence, namely machine learning algorithms to address the challenges. In addition, researchers have combined multiple techniques in order to improve accuracy and acquire additional parameters to enhance the measurement processes. This study mainly focuses on the scope and recent advancements of the Non-destructive Testing (NDT. Therefore, other non-destructive techniques are necessary to complement visual inspection and can be used to inspect for defects without further damaging the tested component and provide methods for detecting hidden damages (Triantafillou, 1998)such as permanent, sustained and transient during their lifetime. Reinforced concrete slabs are one of the most fundamental structural elements in buildings and bridges, which might be exposed to unfavourable conditions such as, impaired quality control, lack of maintenance, adverse environmental effects, and inadequate initial design. Therefore, the resistant capacity of the affected elements would dramatically be reduced which most likely leads to the partial or whole collapse of the structure. Non-destructive testing (NDT.

In this manner, static linear and non-linear finite element

(FE) models have been extensively applied for structural analysis (Ding et al., 2022)the instantaneous characteristics of the mono-components are firstly extracted from the structural dynamic response and applied to the calculation of likelihood function. Then, the posterior probability density function associated with Bayesian theorem is derived under the assumption of Gaussian prior distribution by using instantaneous characteristics. Afterwards, to calculate the posterior probability density function and improve the sampling efficiency, the delayed rejection adaptive Metropolis-Hastings (DRAM, where FE modelling can perform a global damage detection, and can even predict the possible damages that can appear, for example after a function change that increases the imposed loads on the structure (Durmazgezer et al., 2018). FE analysis is also essential as it verifies the structural elements by examining their load-bearing capacity to withstand the applied dead and live loads; for example, an FE model can predict residual deflection (Zhao & Ye, 2022). For instant, Scamardoa non-standard finite element (FE et al. (Scamardo et al., 2022)a non-standard finite element (FE used FE models to approximate the directions of in-plane tensile cracks, and Foti (Foti, 2014) Italy developed a 3D FE model of Normand tower town of Craco (Matera, Italy) to evaluate the structural behaviour of the tower.

With the decreasing life of existing structures, research and industry are continuously striving to find innovative and cost-effective methods that can increase the life span of these structures to satisfy the needs of owners and users (Khalifa et al., 1999). Strengthening could be achieved by section enlargement, external post-tensioning, externally bonded steel elements, advanced fibre-reinforced polymer (FRP) composites, textile reinforced concrete (TRC), and near-surface mounted (NSM) system, or a combination of these techniques (Heiza et al., 2014).

External bonding of steel plates to damaged RC structures is an important method. It has proved to be efficient and a well-known strengthening technique similar to composite materials like carbon fibre reinforced polymers which can be an alternative to steel plates (David et al., 1998). Steel plates have been used for many years due to their simplicity in managing and applying and their effectiveness for strengthening (Brosens & Van Gemert, 2014).. Externally bonded steel plates to rehabilitate reinforced concrete members were first reported in 1964 in Durban, South Africa (McKenna & Erki, 1994). In 1972, externally bonded steel plates were employed on the tension face of a concrete T-beam bridge in France to correct a permanent deflection of 80 mm due to creep (Merter & Ucar, 2013). The bonding of the steel plates or steel flat bars to the surface of concrete members is ensured by epoxy adhesives, and, in some cases, extra fastening is provided using dowels or bolts glued to the holes drilled in the concrete members (Garg et al., 2020). In the case of RC slabs strengthening, steel plates are used to enhance the bending resistance of structural members. They can be applied to flexural zones of the slab to improve its positive flexural capacity (Pryl et al., 2015).

In recent years, the strengthening and retrofitting of structural members using externally bonded carbon fibre reinforced polymer (CFRP) materials has achieved much attention (Lima et al., 2016). Initial developments of the FRP-strengthening technique took place in Germany and Switzerland (Triantafillou, 1998); besides, it revolutionized the strengthening field and appears to be a superb solution for the retrofitting and strengthening of reinforced concrete elements because of its unique properties, including high strength-to-weight ratio, high fatigue endurance, environmental degradation, and corrosion resistance and user-friendliness (Lima et al., 2016). CFRP has proved to increase the flexural stiffness of the studied samples and increase the axial, flexural, or shear capacities (Azizi et al., 2019), ductility, remaining fatigue life, and durability against harsh environments (Lima et al., 2016). Moreover, Piątek and Siwowski noticed a 22–33% increase in RC beams‘ ultimate load-bearing capacity strengthened by CFRP (Piątek & Siwowski, 2022). Several vital contributions involving the design of RC elements with externally bonded FRP laminates are present in the literature (Pryl et al., 2015, Khalifa et al., 1999, Szabó & Balázs, 2007).

The installation of wireless sensors as Smart Health Monitoring (SHM) tools for buildings is getting boom day by day. The applications of these sensory systems can be visualized by their implementation as an SHM system in the world's famous San Pedro Apostol Church in Peru (Macwilliam & Nunes, 2019). The effects of specific parameters like temperature, strain, acceleration, and wind, were monitored and analysed in an ancient building of the ottoman empire (Urla, Izmir) by installing different sensors constituting the SHM system (Kilic, 2015). Large-scale SHM application can be observed on China's 600 m tall canon tower, where the existing condition and associated damages were examined based on SHM data (Sivasuriyan et al., 2021). SHM system helps carry out real-time monitoring of multi-story buildings subjected to dynamic loading close to coastal areas where structures can be subjected to hydrodynamic forces produced due to tsunami (López et al., 2017). The application of 3D linear and non-linear FE techniques for stress and deformation analysis of buildings was utilized for hospital buildings where piezoelectric sensors were used for proper SHM of buildings (Roghaei & Zabihollah, 2014)the building may suddenly goes to failure, requiring a reliable yet efficient health monitoring system. An array of piezoelectric sensors is mounted at desired location to measure the deformation and stress at critical points. The voltage generated by piezoelectric sensors is sent to computer via a data acquisition system. Measuring and monitoring the trend of changing sensors voltages indicate the probability of existing damages and the rate of propagation. The performance-based seismic is reported based on the nonlinear static analysis (pushover. Similarly, the same sensors have already been used for damage evaluation of a building based on impedance measurement (Park & Inman, 2007) and measure the impedance of structures by monitoring the current and voltage applied to the piezoelectric transducers. Changes in impedance indicate changes in the structure, which in turn can indicate that damage has occurred. An experimental study is presented to demonstrate how this technique can be used to detect structural damage in real time. Signal processing methods that address damage classifications and data compression issues associated with the use of the impedance methods are also summarized. Finally, a modified frequency-domain autoregressive model with exogenous inputs (ARX. In case of multi-story buildings, the primary consideration is given to the vibration response mode of buildings that affects the period of building and produces severe stress concentrations at different floor levels, which ultimately produces severe cracks in the slabs of different floors. These vibration response modes provide installing various sensors at the prescribed locations (Hasan et al., 2002).

FEM modelling and simulation are currently used for long-term monitoring of buildings where the dynamic behaviour of the building is observed by executing the operational ambient survey (Pierdicca et al., 2017)it has been possible to follow the dynamic evolution of the structure, using Finite Element Method (FEM. Nowadays, online damage monitoring tools are also available to observe cracks and deflections of structures without the application of measurable input. These tools use the Operational Model Analysis technique for monitoring (Pierdicca et al., 2016). Rainieri and Fabbrocino used model-based damage detection algorithms to identify civil structures' modal parameters based on the data observed from the SHM system (C. Rainieri & Fabbrocino, 2011a), (Rainieri & Fabbrocino, 2011c), (Rainieri & Fabbrocino, 2011b), (Rainieri & Fabbrocino, 2015), (Wierzbicki et al., 2020). The significance of SHM monitoring of buildings can be easily visualized because 102 papers were presented in an international workshop held at Stanford University in September 1997 (Fawad et el., 2019). The technical presentations highlighted the advancements in sensing technology, modelling, and diagnostic methods, system integration, and applications.

Considering the importance of monitoring systems, three different sensors were used in this research to monitor the deflection, strain, temperature, and cracks on different floors in a concrete building, especially on the 2nd-floor slab. The applied sensors include Inclinometers for deflection monitoring, optical Fibre Bragg Grating (FBG) sensors for strain and temperature monitoring, and crack monitoring smart film for monitoring of cracks. The applications of these sensors can be found in the existing buildings highlighted in many research works (Avci et al., 2021), (Zhang et al., 2014), (Zhang & Xiong, 2018)as an important component of buildings and structures, require inspection for the purposes of crack detection which is an important part of structural health monitoring. Now existing crack detection methods usually use a single technology and can only detect internal or external cracks. In this paper, the authors propose a new sensing system combining BOFDA (Brillouin optical frequency-domain analysis, (Juraszek, 2019).

2. DESCRIPTION OF THE ANALYSED BUILDING

The analysed structure resembles a 7-story monolithic reinforced concrete office building located in Hungary. The building height is approximately 20.75 m above the ground and its overall floor plan dimensions are 25.13×51.96 m. The building sits on an 800 mm thick slab foundation. Floors 2-7 denote 30 cm thick reinforced concrete slabs and 3.10 m height and 20 cm thick shear walls with openings. The ground floor is 3.5 m high and includes a green roof of 30 cm thickness. The authors examined the monolithic RC slab on the 2nd floor *(Figure 1)* Within the above structure due to reclassification from category B to category E, which increased the imposed load from 3 kN/m² to 7 kN/m² at the customer's request.

3. LINEAR FE ANALYSIS

There are some methods for the analysis of structures. These methods may be linearly elastic or non-linear as well as static or dynamic (Merter & Ucar, 2013). In the context of condition control and damage assessment of civil engineering

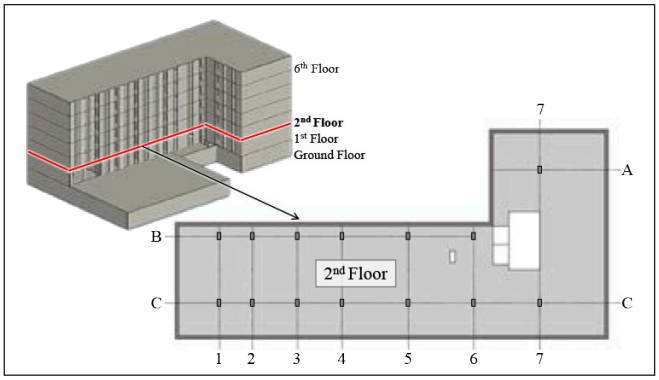

Fig. 1: General view of the building and the location of the examined slab

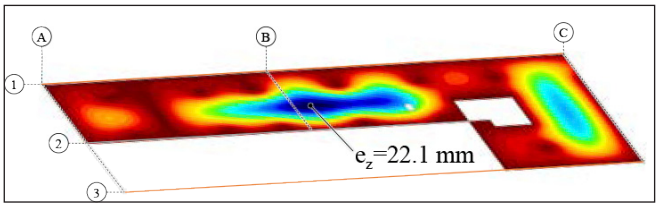

Fig. 2: Deflection of the slab in case of increased live load

structures, static load tests are widespread (Mahowald et al., 2010); they can also be used for research studies to explore the progressive collapse behaviour of structural members and sub-structural structures under severe deformations (Garg et al., 2020b).

In the first part of the research, the authors carried out a 3D linear static FE analysis for the whole building using AxisVM software to obtain the examined slab's internal forces, vertical deflections, and load-bearing capacity before and after function change. In the numerical model, the slab is supported by load-bearing concrete walls and columns. The structural elements were modelled as shells or line elements. Table 1 shows some details about applied materials and loads. The 3D model was also exposed to wind loads according to Eurocode.

Table 1: Material grades and characteristic loads used in the linear numerical model

Concrete grade	C25/30
Steel grade	S500B
Concrete density (self-weight)	25 kN/m³
Permanent load	2,00 kN/m²
Live load *before* function change	3,00 kN/m²
Live load *after* function change	7,00 kN/m²
Live load on stairs	3,00 kN/m²
Live load on green roof	5,00 kN/m²
Snow load	1,00 kN/m²

Based on the calculated internal forces, the applied reinforcement of the slab was satisfactory for bending, torsion, and shear also after increasing the live load. Deflections were determined on the cracked slab, considering the actual reinforcement, as well as the shrinkage and creep of concrete. The maximum calculated deflection was 18.4 mm and 22.1 mm in case of original and increased live loads, respectively. Both values were less than the limit value (span/250 = 32 mm) from EC2. Calculated deflections are illustrated in *(Figure 2)* in case of the increased live load level. The maximum

crack width was 0.35 mm for the original live load, but after increasing the load it increased to 0.43 mm, exceeding the 0.4 mm limit value from EC2. Based on this, we concluded that the slab was not satisfactory for SLS after increasing the live load, which necessitated the strengthening, for which we have analysed two different solutions.

4. NON-LINEAR FE ANALYSIS

Linear elastic analysis can only give a vague idea about the distribution of internal forces, whereas 3D non-linear FE analysis helps learn the plastic moment redistribution (Pryl et al., 2015) and the collapse load of the slab. Since geometric nonlinearity and behaviour of materials beyond the linear elastic limit are considered, it can provide an effective way to determine and evaluate the realistic behaviour of RC structures by civil engineers (Merter & Ucar, 2013). The non-linear behaviour deals mainly with changes in the bending stiffness caused by cracks (Mahowald et al., 2010). The non-linear analysis is either force-controlled or deformation-controlled.

In our research, force-controlled analysis was used, where the load was applied step by step until the maximum load was attained or the collapse of the slab was reached (Dasgupta et al., 2020). In this context, ATENA 3D non-linear analysis software was used to model the examined slab, first in its original state, then after strengthening.

One can benefit from the symmetricity feature in ATENA 3D, so given this, only a portion of the slab was modelled (S2) instead of the whole second-floor slab *(Figure 3)*. Analysed slab portion is 300 mm thick and has 4.00×14.4 m floor plan dimensions. The columns were implemented as surface supports for the slab, acting on 30 mm thick steel plates; this gives more realistic results than applying the supports directly to the concrete. Shear walls were also modelled as fixed surface support acting upward on 30 mm thick steel plates with dimensions identical to the cross-section of the corresponding wall.

According to the actual slab reinforcement, top and bottom rebar mesh of Ø10/200 mm were used in both directions in the slab. In addition to a top reinforcement of Ø25/200 mm was also applied around the column heads in both directions. The top and bottom basic meshes of steel grade S500B were modelled as 'smeared' reinforcement; this method assigns the reinforcement in an average sense to the element by specifying an appropriate reinforcement ratio P [%] which can be calculated: .

ATENA 3D offers a variety of material models that can be used. Based on the experiences of Roszevák and Haris (Roszevák & Haris, 2021), the concrete was modelled as *3D Non-linear Cementitious2* material using f_{cu} = 30 N/mm² concrete cube strength, E = 31 kN/mm² elastic modulus, f_t = 2.6 N/mm² tensile strength, and G_f = 5.5×10^{-5} MN/m specific fracture energy (Roszevák & Haris, 2021). For the modelling of supporting steel plates, the *3D elastic isotropic* material was selected, with an elastic modulus of E_s = 210 kN/mm² and a Poisson's ratio of μ = 0.3. The modelling was done using a 0.2 m average mesh size; thus, 19480 finite elements were created altogether. *Table 2* demonstrates the boundary conditions employed for the examined slab segment (S2).

In the strengthened slab, the applied CFRP strips and high yield strength steel plates were introduced as *3D elastic isotropic* material with their specific properties.

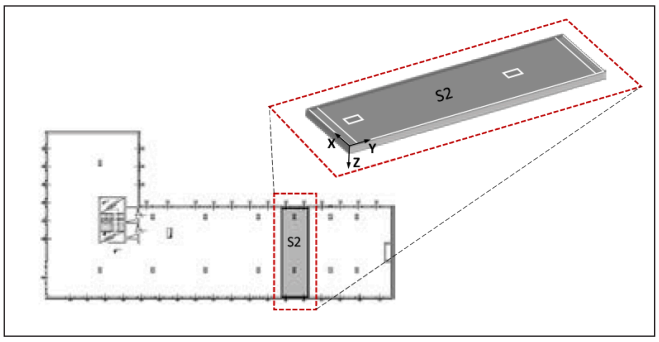

Fig. 3: Location and bottom view of the analysed slab segment (S2)

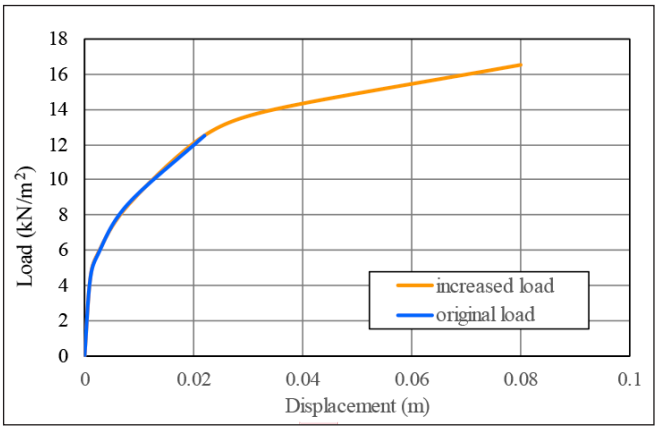

Fig. 4: Load-displacement curves of the slab for original (grey) and increased load (red)

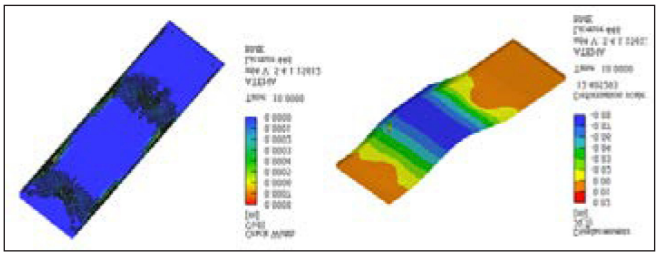

Fig. 5: Calculated crack width and deflection of un-strengthened slab S2 after increasing the load

Due to the applied advanced material models and finite element types, the results of the non-linear analysis may be more accurate than the linear analysis mentioned before. To make the two methods comparable, the original slab was also modelled for the original and increased live load in ATENA and confirmed that the load-bearing capacity of the slab is satisfactory in both cases. However, ATENA calculation also indicated some problems in SLS for the case of increased load *(Table 3)*.

Table 2: Support conditions for the analysed slab segment (S2)

Macro-element/Surface	Support direction		
	x	y	z
1/6	Fixed	Free	Free
1/4	Fixed	Free	Free
2/6	Fixed	Fixed	Fixed
3/6	Fixed	Fixed	Fixed
4/6	Fixed	Fixed	Fixed
5/6	Fixed	Fixed	Fixed

Table 3: Differences between AxisVM and ATENA results in SLS

Criteria	AxisVM	ATENA
Original load		
Max. deflection [mm]	18.4	22.0
Max. crack width [mm]	0.35	0.31
Increased load		
Max. deflection [mm]	22.1	80.0
Max. crack width [mm]	0.43	0.80

As described before, the total load acting on the slab increased from 12.36 kN/m^2 to 16.36 kN/m^2 due to the change in the function of the second floor; this caused a serious increase in deflections and cracks appeared. Nevertheless, the slab maintained its load-bearing capacity since the load-displacement curves *(Figure 4)* show no failure at the maximum load levels. The maximum deflection and crack width values calculated by ATENA for the case of increased load (*Figure 5*) are significantly higher than the AxisVM values. This is mainly because ATENA is able to consider the yielding of steel bars and plastic behaviour of the RC material, while AxisVM is always taking elastic material behaviour into account, regardless of the level of internal forces. Calculated maximum deflection and crack width values imply that limit values according to EC2 were exceeded, again indicating the need for strengthening the slab to maintain its safety and reduce the possibility of crack and deflection occurrence.

5. ANALYSIS OF THE STRENGTHENED SLAB

5.1. Strengthening by CFRP strips

The need to strengthen the concrete slab in question was revealed previously; therefore, the authors considered two different strengthening solutions. The first one was the application of bonded, pre-impregnated Carbon Fibre Reinforced Polymer (CFRP) strips. The second one was bonded, high-strength steel plates, both applied parallel to the main load-bearing (*y*) direction as additional external flexural reinforcement. Two separate numerical models were prepared in ATENA software for these two solutions, taking advantage of non-linear calculation into account.

HM-3.0T carbon fibre laminate strips fixed by HM-120CP adhesive were used in the first model. The applied strips are 3 mm thick and 100 mm wide, and they were modelled as a group of 26 strips of length 4.00 m and 50 mm spacing. CFRP strips were applied to the bottom surface of the slab at the position where the maximum deflections occurred *(Figure 6)*. CFRP material was modelled as *3D elastic isoelastic* material with a mean tensile strength of 3100 N/mm^2, a modulus of elasticity of 65 kN/mm^2, an ultimate strain of 1.7%, and a density of 1.6 g/cm^3. A perfect connection was assumed between the concrete and the CFRP strips, but the maximal contact stresses were manually verified and found to be less than the stress-causing delamination.

The construction stages were modelled to obtain more realistic internal force distribution for the strengthened slab. In the first load step only the self-weight of the slab was applied to the un-strengthened structure. After that, the CFRP strip macro-elements *(figure 6)* were activated, and the rest of the loads were applied in several steps. During the analysis,

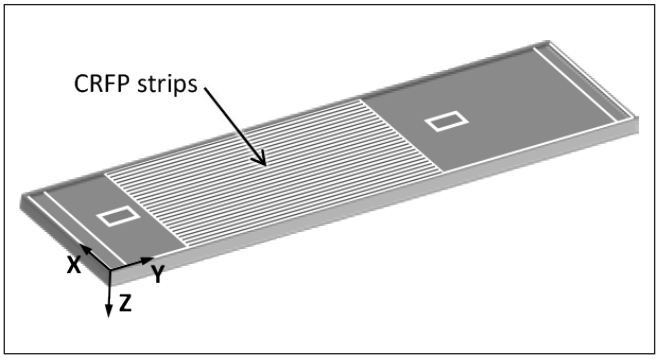

Fig. 6: View of the applied CFRP strip macro-elements

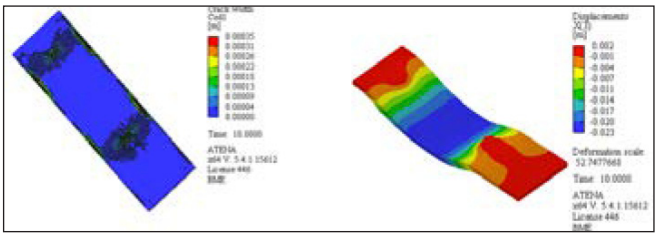

Fig. 7: Calculated crack width and deflection of slab S2 after applying strengthening by CFRP strips

it was assumed that any existing cracks inside the slab are injected before strengthening to restore the original stiffness of the slab. Considering the CFRP strengthening the maximum deflection and crack width values were significantly decreased. *(Figure 7)* shows that deflection decreased to 23 mm and crack width to 0.35 mm, which are below the corresponding limit values.

(Figure 8) illustrates the load-displacement curves for the un-strengthened and CFRP strengthened slab. Thanks to the CFRP material's linear elastic behaviour, the strengthened slab maintained most of its initial stiffness at higher load levels resulting in smaller deflection and crack width. Curves in *(Figure 8)* are plotted only until the maximum load was applied to the slab but increasing the load until failure revealed that the strengthened slab possessed significantly higher load-bearing capacity too. Although the first cracks appeared at the same load level in both cases, internal steel bars started to yield much later, and the post-cracking stiffness was much higher in case of the strengthened slab.

5.2. Strengthening by steel plates

Another numerical model was created to analyse the effect of bonded steel plates as additional external flexural reinforcement at the bottom of the slab. For this purpose, S690QL high yield strength steel plates were used, with a minimum yield strength of 690 N/mm^2, a tensile strength of 770 N/mm^2, and 14% minimum elongation before fracture. Steel plates were used as a group of 8 strips of 500 mm width and 6 mm thickness *(Figure 9)*. In ATENA, *3D elastic isotropic* material was assigned to steel material with an elastic modulus of E_s = 210 kN/mm^2 and a Poisson's ratio of μ = 0.3. Between the concrete and the steel plates, a 3D interface contact surface was used to represent the epoxy resin layer. The connection was assumed to be perfect, but again it was manually verified that no delamination of the steel plate would occur. Construction stages were modelled the same way as described for CFRP strengthening.

Compared to the un-strengthened slab, the maximum deflection was significantly reduced by applying external steel plate reinforcement to 24 mm. In contrast, the maximum

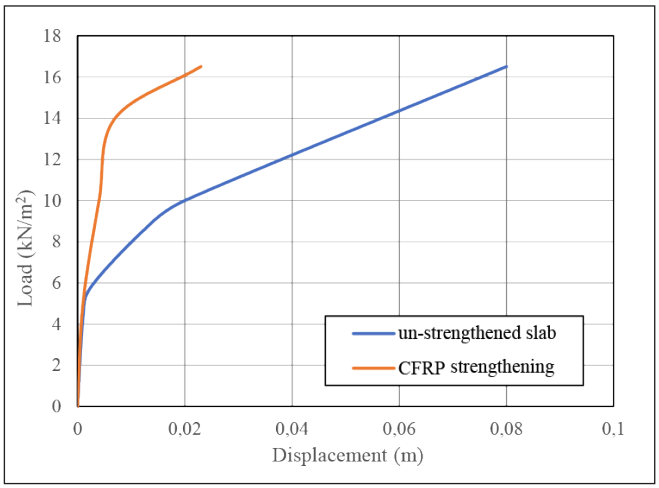

Fig. 8: Load-displacement curves of the un-strengthened and CFRP strengthened slab for increased load

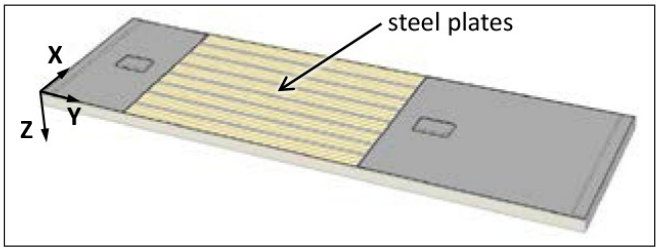

Fig. 9: Load-displacement curves of the un-strengthened and CFRP strengthened slab for increased load

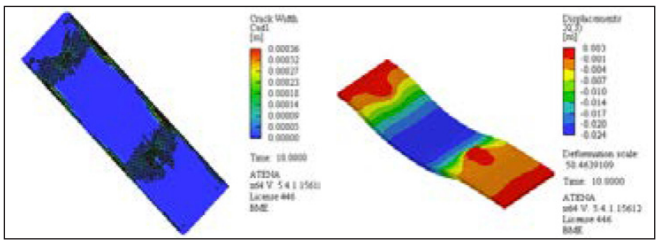

Fig. 10: Calculated crack width and deflection of slab S2 after applying strengthening by steel plates

crack width reached 0.36 mm, meaning that SLS requirements are fulfilled. Calculated cracks and deflections are presented in *(Figure 10)*.

(Figure 11) illustrates the load-displacement curves for the un-strengthened and steel plate strengthened slab. In case of the strengthened slab, the initial stiffness was mainly maintained after cracking of concrete. The first jump in the load-displacement curve of the strengthened slab was related to the yielding of internal steel reinforcement, which was later followed by the yielding of external steel plates. Regardless of these, the stiffness of the strengthened slab remained much higher than the original slab, resulting in smaller deflections and crack width. Again, the curves in *(Figure 11)* were plotted only until the maximum load was applied to the slab. But increasing the load until failure revealed that the strengthened slab possesses significantly higher load-bearing capacity.

5.3. Comparison of the proposed strengthening methods

The previous analyses showed similar improvements in deflection and crack width for the slab in case of both strengthening methods. *Table 4* illustrates that CFRP strengthening gave slightly better results in decreasing the deflection and crack width, but the difference was small. CFRP material is more expensive than steel, but on the other hand, the construction is faster and easier in CFRP, resulting in lower labour and machinery costs. Yooprasertchai found that FRP materials are competitive compared to steel materials (Yooprasertchai et al., 2022). Ibach Bridge in the county of Lucerne, Switzerland, was also strengthened by CFRP sheets instead of steel because it suffered accidental damage due to a prestressing tendon in the outer web with some of its wires completely severed by an oxygen lance, and, as a result, the load capacity of the bridge decreased. It was estimated that 175 kg of steel plates would have been required to strengthen the bridge to its original design load. However, only 6.2 kg of CFRP sheets were used instead (McKenna & Erki, 1994).

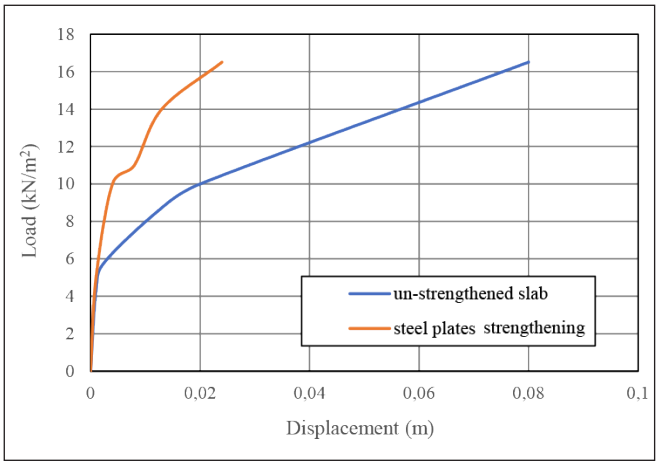

Fig. 11: Load-displacement curves of the un-strengthened and steel plate strengthened slab for increased load

(Figure 12) compare the load-displacement curves of CFRP strengthened and steel plate strengthened slabs. Because of the linear elastic behaviour of CFRP material, the stiffness of the CFRP strengthened slab remains higher as the load was increasing. The capacity of the slab in SLS was similar in case of both strengthening methods. However, after reaching the maximal load and un-loading the slab again, we had less residual deformation left using CFRP strengthening because of the linear elastic behaviour of CFRP material.

Based on the above considerations, the application of CFRP strengthening was proposed, as it was feasible in terms of price and was better in terms of overall structural performance.

Table 4: Calculated deflections and crack widths in case of slab strengthened by steel plates and CFRP strips in case of increased load

Criteria	Original slab	Slab strengthened by CFRP strips	Slab strengthened by steel plates
Max. deflection [mm]	80.0	23.0	24.0
Max. crack width [mm]	0.80	0.35	0.36

6. PROPOSAL OF THE SHM SYSTEM

The changing trend of the construction industry and the boom of the building monitoring system is urging the owners of this building to install the proper monitoring system for the whole building. As the building is quite young, the owners are not planning dismantling or complete reconstruction in the near future and want to monitor the performance of the building for at least the next 15 years. Therefore, the installation of the

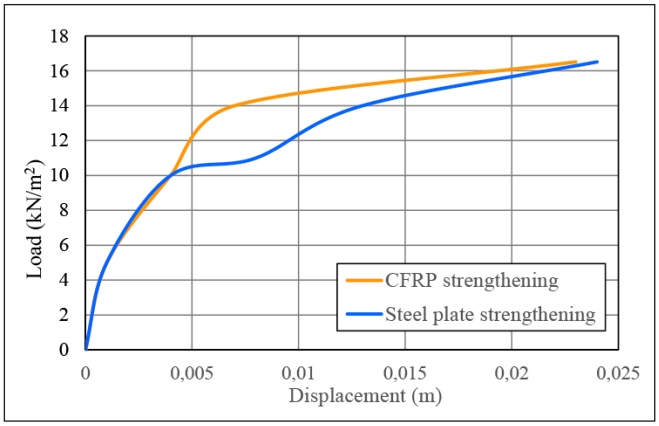

Fig. 12: Comparison of load-displacement curves of the CFRP strengthened, and steel plate strengthened slabs for increased load

SHM system is not only fulfilling the needs of the owners but also provides a cost-effective and user-friendly solution for monitoring the building during its entire life cycle.

Before going for the full-scale monitoring of the whole building, owners are interested in carrying out a study by just installing an SHM system to the problematic areas of the building, which are highlighted on the second floor in this study. Considering the scenario, the authors decided to design the SHM system for the second floor of the building initially, and upon the satisfaction of the owners', results could be projected to the whole building with minor modifications.

In order to install the SHM system, critical zones of structure in terms of deflection and crack width are identified. These identified locations are considered the installation points of sensors. Damage detection data is usually used to establish a new SHM system, but in this research, numerical analysis data will be used to model this system. For this task, linear analysis done by AxisVM software provides the locations of critical points where the parameters mentioned above have the maximum values. These locations are marked for the installations of different sensors, identified as the sensory system for SHM of the building that is capable enough to highlight the main causes of the damages and warn the concerned authorities of any preventive measures well before time.

6.1. Location identification of deflection sensors

Deflection is calculated as per the real loading and support conditions, considering the actual reinforcement inside the slab, as along with the shrinkage and creep of concrete.

Measurement of span displacements usually requires a fixed point of reference. Although displacements without contact (laser, radar) can be measured, but certainly not at many points at the same time. In addition, some places (especially near the beam-column joints) will show such small displacements that will not be measurable. Alternatively, the authors suggest an indirect measurement with inclinometers. The angles of rotation of a bending span can be measured relatively easily and accurately. In this way, it can be assessed whether the span has lost its stiffness. This may be due to repeated cracks, progressive corrosion, or deterioration of the concrete's mechanical properties.

For the whole floor level, two sets of sensors are recommended, one set at the centre locations of grid B and C, where six sensors will cover the maximum deflections of each of the grids 1-6, and a second set along the grid A, where two sensors

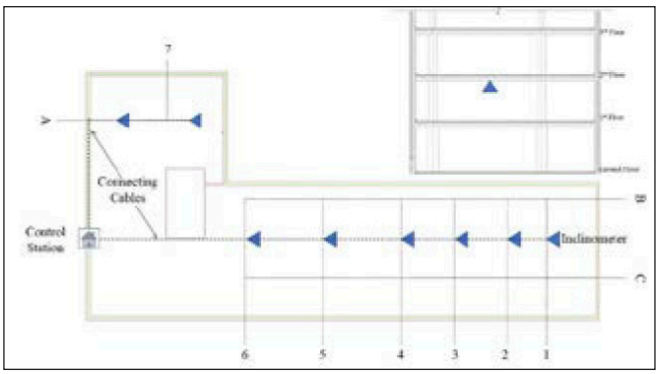

Fig. 13: Planned location of inclinometers along the second floor

will calculate the deflection along the centreline of the grid. *(Figure 13)* shows the locations of these sensors. In the cross-section, sensors are located along the slab's length. Sensors of each set are connected by a single cable to the central data acquisition system. In this way, the measured angle of rotations will be giving the deflected shape to each section along with the whole floor level. So, a total of eight sensors are recommended for the entire floor.

6.2. Location identification of strain and temperature sensors

In such a condition where excessive loads might cause problems for the floor slab, strain (axial and bending), and temperature sensors are certainly of significant importance. In the case of this building static and transient strains, and temperature gradient at the height of each floor level are critical factors that need attention. The traditional method of strain measurement involves a dense network of strain gauges which not only increases the size of the test set-up but also produces a very complex electric wiring network. Moreover, strain gauge installation is not favourable in case of the existing conditions of the subject slab, so authors suggest the installation of optical Fibre Bragg Grating (FBG) optical wire. Their installation is very easy as they can be inserted directly into structural elements. Considering their ability to measure strain and temperature using a single wire, their noise tolerance, and their efficiency, these sensors are highly recommended in this case. The location of this wire is suggested along with the points of maximum stress concentrations as the maximum stresses are observed at each of the connections of the beams between the columns, so, this is why these locations require monitoring of the strain values. So, the optical fiber wire will run along the length between the columns, connecting it to the central control unit of the slab. Locations of FBG optical wires are shown in *(Figure 14)*. These optical fiber wires will be connected directly to the reinforcement inside of the concrete.

Fig. 14: Planned locations of FBG fiber optical wires

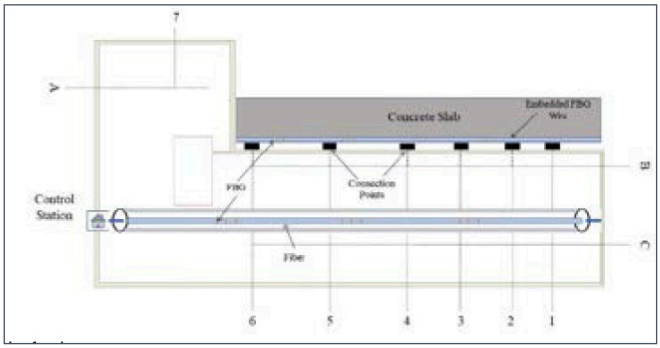

6.3. Crack width monitoring sensors

From the results of linear and 3D non-linear analyses, it can be observed that some damages like concrete cracks may occur to the slab (regardless the level of maximum applied load). Not to mention other possible future problems like corrosion of the reinforcement. The most important thing here is to monitor the progression of existing cracks and the formation of new ones. This can be done in various ways, but the most advanced approach is to use the smart film method. This smart film contains a group of insulated enamel copper wires. It forms the shape of an optical fiber that sends the electrical signal among different terminals of the film that are connected to a secondary processor at different intervals along the film where the signals are simultaneously detected. Initiation of a crack will break the wires carrying these signals and instantaneously results in the failure of signal detection at the other end. The width of the crack in this system is calculated by the diameter of copper wires used for crack detection using the relation shown in the following equation:

$$R_m = \rho \frac{l - \Delta l}{A} + \rho \frac{\Delta l}{A'}$$

Where A is the area of wire before the crack opening, A' is the area after the crack opening, is the resistivity of the bar which is taken as 1. 7x10^{-8}Ω.m, l is the length of the section before fracture and Dl is the length of the fractured section. Using the diameter of the wire before and after the crack opening, crack width can be calculated. The benefit of using this film is its efficiency for the short-term and long-term crack monitoring of buildings without disrupting its regular usage. Further, specific dynamic properties of the material can also be monitored in real-time with this film.

An important task is to identify the location of the installation of smart film. From the results of linear analysis, it is evident that the stress concentrations are producing severe cracks at the beam-column joints. So, the film will be glued externally at the bottom of the slab surrounding these joints throughout the floor. The film will emerge from the central control station and will pass through each of the secondary processors, and after collecting the data from each of the secondary processors, it will end at the other end of the control station. The film will be glued, protected by the plastic coverings, and covered by the false ceiling. The control station will then yield the results about the length, width, and propagation of the cracks. The installation plan of the smart film can be seen in *(Figure 15)*.

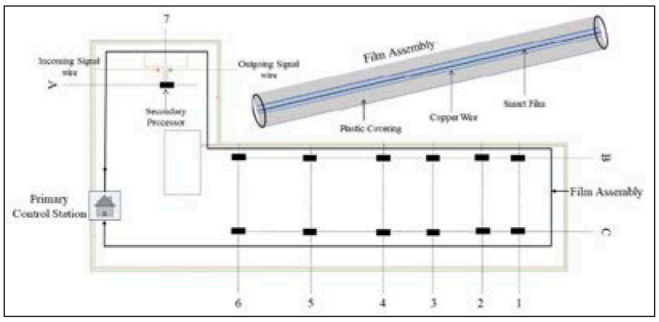

Fig. 15: *Planned locations of smart crack monitoring films*

7. CONCLUSIONS

The main topic of this article was to analyse the condition of a monolithic RC slab in connection to function change that increases live load. The slab in question was, on one hand, calculated using AxisVM linear FE analysis software, and, on the other hand, 3D non-linear FE analysis was also performed using ATENA 3D software. Both calculations showed sufficient load-bearing capacity also in case of increased loads. However, linear and non-linear analysis also highlighted some problems in the serviceability limit state, the maximum deflection and crack width were beyond the corresponding limit values given by EC2 standard.

Considering the above problems, two different strengthening methods (application of bonded CFRP strips and bonded steel plates as additional external reinforcement) were suggested and analysed using 3D non-linear FE analysis. Based on the analysis results, both strengthening solutions gave similar and acceptable results, as not only load-bearing capacity was increased, but maximum deflection and crack width were also decreased to a satisfactory level. Because of the linear elastic behaviour of CFRP material, the stiffness of CFRP strengthened slab was slightly higher in general, and the residual deformations were smaller in case of repeated loads. Taking the better corrosion resistance also into account, the application of CFRP strengthening provides better overall structural performance. Therefore, it was suggested as suitable strengthening solution.

Considering the expected future damages to the analysed concrete slab, and SHM system was also suggested in this study. The suggested system aims to provide real-time monitoring of the slab using three different types of sensors. The locations of these devices have been extracted from the results of linear FE analysis. To properly monitor the deflection of the whole slab, eight inclinometers are suggested to be installed. Further, monitoring of strain and temperature is planned by using the FBG optical wire that will run through the structural grids of the slab. Besides this, monitoring of existing cracks and the formation of new ones is planned to be done using the smart crack monitoring film that uses the primary and secondary processors to send and receive signals through the concrete, which helps to quantify the size and shape of cracks. Installation of the suggested sensor will give rise to the proper SHM system of the slab. That will provide the safe operation for the next 15 years and save financial resources for the owners.

8. REFERENCES

Avci, O., Abdeljaber, O., Kiranyaz, S., Hussein, M., Gabbouj, M., & Inman, D. J. (2021). A review of vibration-based damage detection in civil structures: From traditional methods to Machine Learning and Deep Learning applications. *Mechanical Systems and Signal Processing*, *147*, 107077, DOI: 10.1016/j.ymssp.2020.107077

Azizi, R., Sayed, ·, & Talaeitaba, B. (2019). Punching shear strengthening of flat slabs with CFRP on grooves (EBROG) and external rebars sticking in grooves. *International Journal of Advanced Structural Engineering*, *11*(3), 79–95. DOI: 10.1007/s40091-019-0218-4

Brosens, K., & Van Gemert, D. (2014). Strengthening of Concrete Structures with Externally Bonded Steel Plates or CFRP Laminates - Part I: Specific Design Concepts / Verstärken von Betontragwerken durch aussen aufgeklebte Stahlplatten oder Kohlenstofffaser verstärkte Kunststofflamellen - Teil. *Restoration of Buildings and Monuments*, *7*(3–4), 367–402, DOI: 10.1515/rbm-2001-5578

Dasgupta, K., Sudheesh, T. K., Praseeda, K. I., Kartha, G. U., & ... (2020). *Proceedings of SECON 2020: Structural Engineering and Construction Management*, DOI: 10.1007/978-3-030-55115-5

David, E., Djelal, C., & Buyle-Bodin, F. (1998). Repair and strengthening

of reinforced concrete beams using composite materials. *Proceedings - 2nd International PhD Symposium in Civil Engineering*, 382–389.
Ding, Y. J., Wang, Z. C., Chen, G., Ren, W. X., & Xin, Y. (2022). Markov Chain Monte Carlo-based Bayesian method for nonlinear stochastic model updating. *Journal of Sound and Vibration*, *520*(May 2021), 116595, DOI: 10.1016/j.jsv.2021.116595
Durmazgezer, E., Yucel, U., & Ozcelik, O. (2018). *Damage Identification Studies of a Reinforced Concrete Portal Frame by Sensitivity-Based Finite Element Model Updating Method*. *September*, 12–14.
Foti, D. (2014). Non-destructive techniques and monitoring for the evolutive damage detection of an ancient masonry structure. *Key Engineering Materials*, *628*, 168–177. KEM.628.168
Fujino, Y. (2002). Vibration, control and monitoring of long-span bridges - Recent research, developments and practice in Japan. *Journal of Constructional Steel Research*, *58*(1), 71–97, DOI: 10.1016/S0143--974X(01)00049-9
Garg, S., Agrawal, V., & Nagar, R. (2020a). Progressive collapse behaviour of reinforced concrete flat slab buildings subject to column failures in different storeys. *Materials Today: Proceedings*, *43*(xxxx), 1031–1037, DOI: 10.1016/S0143-974X(01)00049-9
Garg, S., Agrawal, V., & Nagar, R. (2020b). Progressive collapse behaviour of reinforced concrete flat slab buildings subject to column failures in different storeys. *Materials Today: Proceedings*, *43*, 1031–1037, DOI: 10.1016/j.matpr.2020.07.692
Hasan, R., Xu, L., & Grierson, D. E. (2002). Push-over analysis for performance-based seismic design. *Computers and Structures*, *80*(31), 2483–2493, DOI: 10.1016/S0045-7949(02)00212-2
Heiza, K., Nabil, A., Meleka, N., & Tayel, M. (2014). State-of-the Art Review: Strengthening of Reinforced Concrete Structures–Different Strengthening Techniques. *International Conference on NANO-TECHNOLOGY IN CONSTRUCTION*, *1*(March), 1–24.
Juraszek, J. (2019). Application of fiber optic FBG techniques in analysis of strain in engineering machines. *New Trends in Production Engineering*, *2*(1), 480–485, DOI: 10.2478/ntpe-2019-0051
Khalifa, A., Tumialan, G., Nanni, A., & Belarbi, A. (1999). Shear Strengthening of Continuous RC Beams Using Externally Bonded CFRP Sheets. *Proceedings of the 4th International Symposium on FRP for Reinforcement of Concrete Structures*, 995–1008.
Kilic, G. (2015). Using advanced NDT for historic buildings: Towards an integrated multidisciplinary health assessment strategy. *Journal of Cultural Heritage*, *16*(4), 526–535, DOI: 10.1016/j.culher.2014.09.010
Kot, P., Muradov, M., Gkantou, M., Kamaris, G. S., Hashim, K., & Yeboah, D. (2021). Recent advancements in non-destructive testing techniques for structural health monitoring. *Applied Sciences (Switzerland)*, *11*(6), DOI: 10.3390/app11062750
Lima, M. M., Doh, J. H., Hadi, M. N. S., & Miller, D. (2016). The effects of CFRP orientation on the strengthening of reinforced concrete structures. *Structural Design of Tall and Special Buildings*, *25*(15), 759–784, DOI: 10.1002/tal.1282
López, J. J. O., Reyes, L. V., & Vera, C. O. (2017). Structural health assessment of a R/C building in the coastal area of Concepción, Chile. *Procedia Engineering*, *199*(September), 2214–2219, DOI: 10.1016/j.proeng.2017.09.185
Macwilliam, K., & Nunes, C. (2019). *Structural Analysis of Historical Constructions*. *18*, 1949–1958, DOI: 10.1007/978-3-319-99441-3
Mahowald, J., Bungard, V., Maas, S., Waldmann, D., Zuerbes, A., & De Roeck, G. (2010). Comparison of linear and nonlinear static and dynamic behaviour of prestressed and non-prestressed concrete slab elements. *Proceedings of ISMA 2010 - International Conference on Noise and Vibration Engineering, Including USD 2010*, 717–728.
McKenna, J. K., & Erki, M. A. (1994). Strengthening of reinforced concrete flexural members using externally applied steel plates and fibre composite sheets - a survey. *Canadian Journal of Civil Engineering*, *21*(1), 16–24, DOI: 10.1139/l94-002
Merter, O., & Ucar, T. (2013). A comparative study on nonlinear static and dynamic analysis of RC frame structures. *Journal of Civil Engineering and Science*, *2*(3), 155–162.
Nejadi, S. (n.d.). *An experimental study of flexural cracking in reinforced concrete members under short term loads*. Retrieved January 19, 2022, from 267386473
Park, G., & Inman, D. J. (2007). Structural health monitoring using piezoelectric impedance measurements. *Philosophical Transactions of the Royal Society A: Mathematical, Physical and Engineering Sciences*, *365*(1851), 373–392, DOI: 10.1098/rsta.2006.1934
Piątek, B., & Siwowski, T. (2022). Experimental study on flexural behaviour of reinforced concrete beams strengthened with passive and active CFRP strips using a novel anchorage system. *Archives of Civil and Mechanical Engineering*, *22*(1), 1–17, DOI: 10.1007/s43452-021-00364-7
Pierdicca, A., Clementi, F., Maracci, D., Isidori, D., & Lenci, S. (2016). Damage detection in a precast structure subjected to an earthquake: A numerical approach. *Engineering Structures*, *127*, 447–458, DOI: 10.1016/j.engstruct.2016.08.058
Pierdicca, A., Clementi, F., Mezzapelle, P., Fortunati, A., & Lenci, S. (2017). One-year monitoring of a reinforced concrete school building: Evolution of dynamic behavior during retrofitting works. *Procedia Engineering*, *199*(April 2018), 2238–2243, DOI: 10.1016/j.proeng.2017.09.206
Pryl, D., Janda, Z., Cervenka, J., & Cervenka, V. (2015). *ATENA Program Documentation Part 8 User 's Manual for ATENA-GiD Interface*. *June*.
Rainieri, C., & Fabbrocino, G. (2011a). A hybrid automated modal identification algorithm for structural health monitoring applications. *4th International Operational Modal Analysis Conference, IOMAC 2011*, *February 2016*, 569–576.
Rainieri, C., & Fabbrocino, G. (2011b). A hybrid automated modal identification algorithm for structural health monitoring applications. *4th International Operational Modal Analysis Conference, IOMAC 2011*, 569–576.
Rainieri, C., & Fabbrocino, G. (2011c). Validation of a hybrid automated modal identification algorithm for structural health monitoring applications. *Structural Health Monitoring 2011: Condition-Based Maintenance and Intelligent Structures - Proceedings of the 8th International Workshop on Structural Health Monitoring*, *1*(June 2015), 135–142.
Rainieri, Carlo, & Fabbrocino, G. (2015). Development and validation of an automated operational modal analysis algorithm for vibration-based monitoring and tensile load estimation. *Mechanical Systems and Signal Processing*, *60*, 512–534, DOI: 10.1016/j.ymssp.2015.01.019
Roghaei, M., & Zabihollah, A. (2014). An Efficient and Reliable Structural Health Monitoring System for Buildings after Earthquake. *APCBEE Procedia*, *9*, 309–316. https://doi.org/10.1016/j.apcbee.2014.01.055
Roszevák, Z., & Haris, I. (2021). *MODERN NUMERICAL MODELING*. 13–20, DOI: 10.32970/CS.2021.1.1.3
Scamardo, M., Franchi, A., & Crespi, P. (2022). A non-standard numerical method for finite element modelling of tensile cracks in quasi-brittle material. *Computers and Structures*, *258*, 106664, DOI: 10.1016/j.compstruc.2021.106664
Sisen Ahmed, M. (2016). *Damage Detection in Reinforced Concrete Square Slabs Using Modal Analysis and Artificial Neural Network Dedication*. *March*.
Sivasuriyan, A., Vijayan, D. S., Górski, W., Wodzyń, Ł., Vaverková, M. D., & Koda, E. (2021). Practical implementation of structural health monitoring in multi-story buildings. *Buildings*, *11*(6), DOI: 10.3390/buildings11060263
Szabó, Z. K., & Balázs, G. L. (2007). Near surface mounted FRP reinforcement for strengthening of concrete structures. *Periodica Polytechnica Civil Engineering*, *51*(1), 33–38, DOI: 10.3311/pp.ci.2007-1.05
Triantafillou, T. C. (1998). Shear strengthening of reinforced concrete beams using epoxy-bonded FRP composites. *ACI Structural Journal*, *95*(2), 107–115, DOI: 10.14359/531
Wierzbicki, S., Pióro, Z., Osiniak, M., & Antoszkiewicz, E. (2020). Inclinometer method of displacement measurements as an alternative to optical measurements in structural health monitoring - On site tests. *Archives of Civil Engineering*, *66*(3), 109–124. journals.pan.pl/dlibra/publication/134387/edition/117454/
Yooprasertchai, E., Piamkulvanit, M., Srithong, C., Sukcharoen, T., & Sahamitmongkol, R. (2022). A comparison of punching shear strengthening of RC flat plates with FRP bars and steel bolts. *Case Studies in Construction Materials*, *16*, e00828, DOI: 10.1016/j.cscm.2021.e00828
Zhang, B., Wang, S., Li, X., Zhang, X., Yang, G., & Qiu, M. (2014). Crack width monitoring of concrete structures based on smart film. *Smart Materials and Structures*, *23*(4), DOI: 10.1088/0964-1726/23/4/045031
Zhang, Q., & Xiong, Z. (2018). Crack Detection of Reinforced Concrete Structures Based on BOFDA and FBG Sensors. *Shock and Vibration*, *2018*, DOI: 10.1155/2018/6563537
Zhao, W., & Ye, J. (2022). Dynamic behavior and damage assessment of RC columns subjected to lateral soft impact. *Engineering Structures*, *251*, DOI: 10.1016/j.engstruct.2021.113476
Fawad, M., Koris. K, Khushnood. R. A, Usman. M., Retrofitting of a damaged Rc bridge structure. Procedia structural integrity, 18, 189-197, 2019, DOI: 10.1016/j.prostr.2019.08.153

Asseel Al-Hijazeen (1994) MSc structural engineer at Budapest University of Technology and Economics. currently pursuing her PhD studies at Department of Structural Engineering, Budapest University of Technology and Economics. Research fields: Smart health monitoring of bridges, including Digital Twin models, machine learning applications, and automation of damage identification process of bridges. A member of the Hungarian group of fib association and Jordan Engineers Association.

Kálmán Koris (1970) civil engineer, graduated in 1993 at the Budapest University of Technology and Economics, PhD, Associate Professor at the Department of Structural Engineering, Budapest University of Technology and Economics. Research fields: safety of reinforced concrete structures, analysis of prefabricated, prestressed concrete structures, strengthening of structures, timber structures. Member of the standardization subcommittee "NAD MSZ ENV 1992 Eurocode 2, Design of concrete structures" and the Hungarian Chamber of Engineers. Member of the Hungarian Group of ***fib*** and the public body of the Hungarian Academy of Sciences. Presidential member of the Construction Board of the Hungarian Chamber of Engineers.

Muhammad Fawad (1995) MSc Structural Engineering from Budapest University of Technology and Economics, Hungary. Member of Pakistan Engineering council since 2015. Pursuing joint doctorate from Budapest University of Technology and Economics, Hungary, and Silesian University of Technology Poland. Currently engaged in PhD research work involving the use of BIM technology and Cyber-Physical devices for the Structural Health Monitoring (SHM) of bridges. Currently working on the use of Virtual Reality (VR) and Mixed Reality (MR) devices like Microsoft HoloLens. Site Vision and Oculus Quest, supplemented with wireless sensors for bridge health monitoring.

Marek SALAMAK (1965) Dr. Hab. Inz, Assoc. Prof. at the Silesian University of Technology. PhD from Silesian University of Technology Poland. Bridge engineer, expert in CAD, BIM and digitization of construction. Creator of an accredited research laboratory for bridge structures. Author or co-author of over 150 publications, including the book "BIM in the life cycle of bridges".

STRUCTURAL ASPECTS OF TOPOLOGY OPTIMIZATION IN 3D PRINTING OF CONCRETE



Naser S. Alimrani - Marwah M. Thajeel - György L. Balázs

https://doi.org/10.32970/CS.2022.1.6

The 3D printing technologies have been initially developed in the 1980s. Currently, these technologies have become an integral part of modern product development and have been successfully applied in a wide range of industries including automotive manufacturing, biomedical, consumer, food, and construction. Since material efficiency is becoming a critical design driver in the construction industry, many strategies for improving material efficiency have been developed such as recycling materials, reusing components, reducing waste, extending life spans, etc. Furthermore, in the design phases, there are different design models that reduce the use of materials such as hollow-core and pre-stressing construction systems, or by applying concept of Topological Optimization. Topology optimization is a design method used in 3D printing technologies to reduce material without affecting the functionality of an object.

Keywords: 3D printing, topological optimization, structural aspects

1. INTRODUCTION

Material efficiency is becoming a critical design driver in the construction industry. While many strategies for improving material efficiency focus on the end of a building's lifecycle (recycling materials, reusing components, reducing waste, extending life spans, etc.), there is also great potential for reducing material use in the early design phases especially for materials that are difficult to recycle, such as concrete (Allwood et al., 2011). The usual means for achieving material reduction with concrete are hollow-core construction systems, pre-stressing, and the use of lightweight concrete. Computational methods, such as the optimization of size, shape, and topology, can also be used to ensure the efficient distribution of concrete for a given part. While significant material reduction can be achieved with these methods, the resulting geometries are often so intricate that fabrication becomes problematic (Dombernowsky and Søndergaard, 2011). Topology optimization is a powerful design tool aiming to maximize the performance of a structure by optimizing its material layout within certain conditions (Rong et al., 2022). This result is obtained by applying the concept that lies in the fact that no specified initial structural topology needs to be presumed a priori (Zhu et al., 2016). Several topology optimization techniques have been recently developed such as the homogenization method (Bendsøe and Kikuchi, 1988), the solid isotropic material with penalization (SIMP) (Zhou and Rozvany, 1991; Sigmund and Maute, 2013), the level set (Allaire et al., 2002; Wang et al., 2003), the bi-directional evolutionary structural optimization (BESO) (Xie and Steven, 1993; Huang and Xie, 2009), and the moving morphable components (MMC) (Guo et al., 2014). These techniques have been considerably applied in different fields such as mechanical engineering, advanced manufacturing, architectural design, and aerospace engineering. Finally, advanced manufacturing techniques such as 3D printing can be used to fabricate free-form designs generated by structural topology optimization (Rong et al., 2022).

The American Society for Testing and Materials (ASTM) International Committee F42 on AM technologies defines 3D printing as "the process of joining materials to make objects from 3D model data, usually layer upon layer" (ASTM F42, 2015). Topology optimization can be used as a design method to reduce material without affecting the functionality of an object. It is a process that promises almost no fabrication constraints, potentially enabling the production of topologically optimized complex geometries. Despite being one of the most demanding economic sectors in terms of material consumption, the construction industry has not yet adopted such design methods. This is generally because computational optimization algorithms produce solutions that are difficult to fabricate, especially at a large scale (Jipa et al., 2016). Furthermore, the conventional approach of casting concrete into a formwork limits geometrical freedom for the architects to build in various geometries, unless high costs are paid for bespoke formworks. Rectilinear forms not only limit creativity of the architects, but they are also structurally weaker than curvilinear forms owing to stress concentration (Nematollahi et al., 2017).

Regarding the environmental aspects, the current construction industry has serious issues with sustainability. In general, the current construction methods and materials are not environmentally friendly. The entire construction process, including off-site manufacturing, transportation of materials, installation and assembly, and on-site construction, emits huge amounts of greenhouse gases and consumes large quantities of energy (Yan et al., 2010). In addition, conventional concrete made by ordinary Portland cement (OPC) is not sustainable. Manufacture of OPC is highly energy and carbon intensive (Nematollahi et al., 2015). From another hand, astonishing data presented in Llatas's paper (Llatas, 2011) showed that the construction industry is responsible for generating approximately 80% of the total waste in the world. Application of three-dimensional (3D) printing techniques in concrete construction could solve the challenges stated in the literature. 3D printing technology

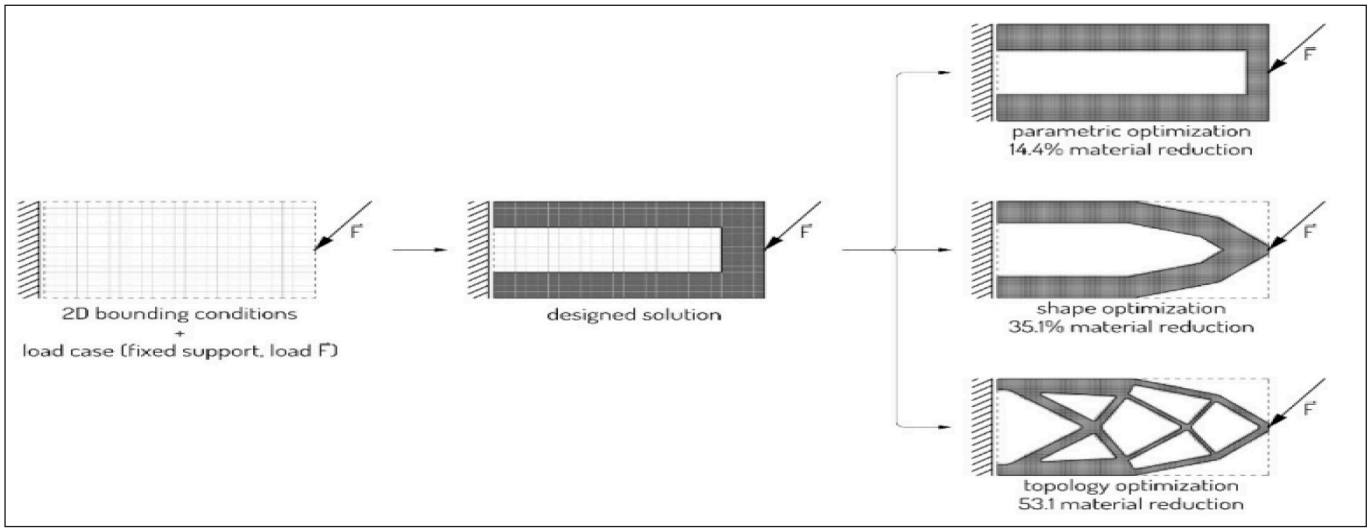

Figure 1: *Different computational optimization processes: size, shape, and topology (Perrot et al., 2019)*

is recently gaining popularity in construction industry. In the last few years, different 3D concrete printing (3DCP) technologies have been explored (Nematollahi et al., 2017).

2. TOPOLOGY OPTIMIZATION (TO)

Designing for efficient material distribution can be achieved through size, shape, or topology optimization processes. Size optimizations are contained within a fixed shape, while shape optimizations are constrained by a fixed topology (*Figure 1*).

Topology optimization processes are the most versatile and most broadly applicable of improving material distribution in terms of size, shape, and topology (Mijar et al., 1998).

Topology optimization is an iterative computational process that works within a confined, discretized space. For given loads and supports, the algorithm will refine material distribution to meet a prescribed set of performance targets. There are a number of different topology optimization algorithms, including Solid Isotropic Microstructure with Penalization (SIMP), Evolutionary Structural Optimization (ESO), and Topological Derivatives (Rozvany, 2009; Aremu, 2010). Despite the computational differences between these algorithms, they all produce a family of typical geometric features: interconnected networks of thin ribs and narrow tubular structures with dynamic changes in porosity (Jipa etl., 2016).

3. IMPORTANT DEVELOPMENTS OF TO

Three important developments of TO might directly influence the manufacturing and design process of 3D printed concrete structures, as follow (Vantyghem et al., 2018).

3.1 Compliance-Based Topology Optimization

The minimum compliance problem is one of the most well-known TO problems in literature. In this problem, the strain energy (also called compliance) is a global measure of the displacements. By minimizing the strain energy, the stiffness of the structure is maximized. Additionally, a volume constraint is added to act as an opposing restriction, and is comparable to a cost factor in reality. Mathematically, this material distribution problem is solved very efficiently using gradient-based optimizers coupled with adjoint sensitivity analysis (Vantyghem et al., 2018). In the example presented in Fig. 1, a benchmark problem and its optimal shape are presented.

3.2 Stress-Based Topology Optimization

In the previous section, an optimal printing path and the positioning of the steel (chain) reinforcements was extracted from TO results. However, the use of steel reinforcements is today not commonly seen in 3D concrete printing processes. This lack of use of embedded tensile reinforcements hampers the fabrication of "functional" large-scale building components. A viable solution to this problem is studied, where carbon, glass and basalt fibers are being added to the cement mix before (or during) extrusion. Study showed that using reinforcing short fibers can result in materials that exhibit much higher flexural (up to 30 MPa) and compressive strength (up to 80 MPa). Additionally, "an alignment of the fibers, caused by the 3D printing extrusion process is observed, opening up the possibility to use the print path direction as a means to control fiber orientation within the printed structures" (Wu et al., 2016). The use of ultrahigh performance fiber-reinforced concrete was reviewed in some studies, and their superiority in comparison to conventional FRC structures proven (Yoo and Yoon, 2016).

The optimized structures are in fact oversized in the compression zones and would crack or break rather easily in the tensile zones. By introducing stress constraints in the topology optimization algorithm, optimal shapes can be generated which are optimized and take into account this strength asymmetry. Figure 2 illustrates this concept and presents a small concrete specimen which was optimized using Drucker–Prager yield criterion. For this case study, the maximum compressive strength was 60 MPa and the maximum tensile strength 15 MPa. The mathematical formulation was based on a study by (Bruggi and Duysinx, 2012) and optimized using special globally convergent version of MMA (Svanberg, 2002). In post-production, the resulting topology was reverse engineered in Fusion 360, and using Abaqus, a few manual design iterations were performed to further improve the model.

3.3 Multi-physics Topology Optimization

In this last example, traditional structural TO techniques are extended to include multi-physical requirements. By using

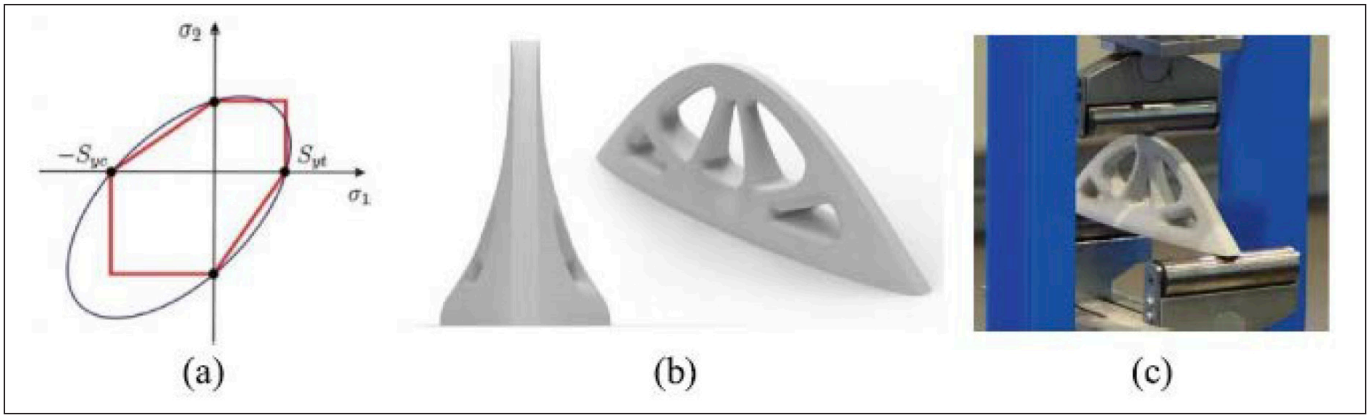

Figure 2: *(a) Mohr-Coulomb (red), Drucker-Prager (blue), (b) yield criterion optimized concrete specimen using stress-based TO, and (c) 3-point-bending test (Vantyghem et al., 2018)*

such multi-physics approach, an optimal design can be found which not only meets structural requirements, but where also the heat transfer characteristics of the structure are optimized (Bruggi and Taliercio, 2013; Vantyghem et al., 2017). In the case that is presented here, the thermal transmittance through the dome wall is minimized, the weight or volume of the structure is restricted, and the domain is subjected to gravity and surface loads. Similar to previous examples, the Young's modulus of each element depends on the density. However, in this example, the element's thermal conductivity is also calculated from this density. In contrast to previous studies, the design variables (element densities) have three optimal states. One state symbolizes the surrounding air (where, $x_e = 0$), another state represents the solid structure ($x_e = 1$), and finally, a third optimal state is created ($x_e = 0.5$) which symbolizes a thermally efficient mesostructure made from an intermediate density (Fig. 3). Originally, this idea was inspired by the infill pattern used in plastic 3D printing. However, the principle can be applied to concrete 3D printing as well, where one extrusion nozzle uses plain or fiber-reinforced concrete, and another nozzle could use a thermally efficient substitute such as "Foamcrete" (Othuman, 2013).

4. COMPUTATIONAL MODELING AND OPTIMIZATION

Computational modeling and topology optimization techniques provide for the possibility to design and optimize the 3 D printed cement-based element on a multitude of scales and materials and to achieve more sustainable and cost-effective designs. Topology optimization consists of the discretization of an object or structure into small elements and optimization of the material composition, volume fractions, and spatial distribution within each element to achieve functionally graded objects or structures with desired properties and/or functional performance. New computational frameworks for topology optimization with microstructures that supports design spaces of multiple dimensions are emerging and are being combined with 3 D printing in many fields (Zhu et al., 2017; Liu et al., 2019; Martens, et al., 2018; Kazakis et al., 2017; Nguyen et al., 2019). Another application of topology optimization techniques for concrete concerns the optimization of the cement binder itself by tuning the internal topology at different scales. Advances and challenges in this area are discussed in (Martens, et al., 2018).

Despite the remarkable achievements in the field of structural topology optimization, there still remain many challenging issues which require further research. For example, an interesting issue is how to make the design domain automatically and intelligently evolve during the form-finding process. In case that the resolution is specified, the larger the design space, the higher the computational cost. The design space cannot be excessively large due to the limit of computing resources. In the conventional topology optimization, the predefined design space keeps fixed. However, it is desirable to update or reshape the design space due to the following reasons. First, in many optimization problems, the designer cannot predefine an optimized design space that guarantees a satisfactory

Figure 3: *Multi-physics topology optimization of a dome structure where the element density variable has three optimal states. xe = 0 (void), xe = 0.5 (mesostructured), and xe=1 (solid) (Vantyghem et al., 2018)*

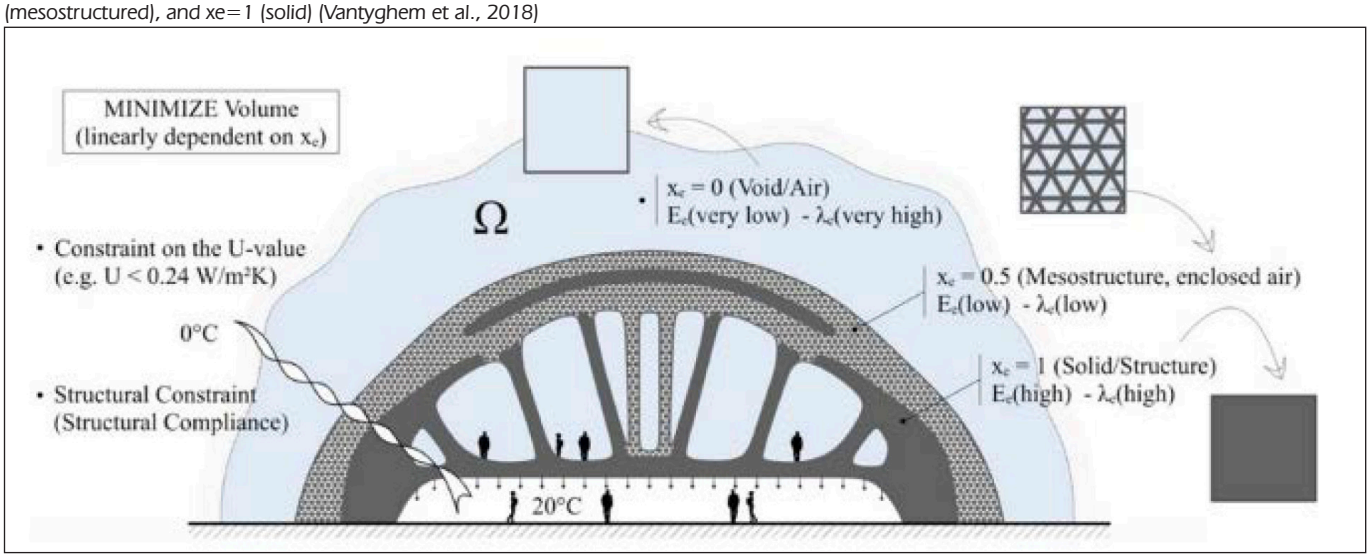

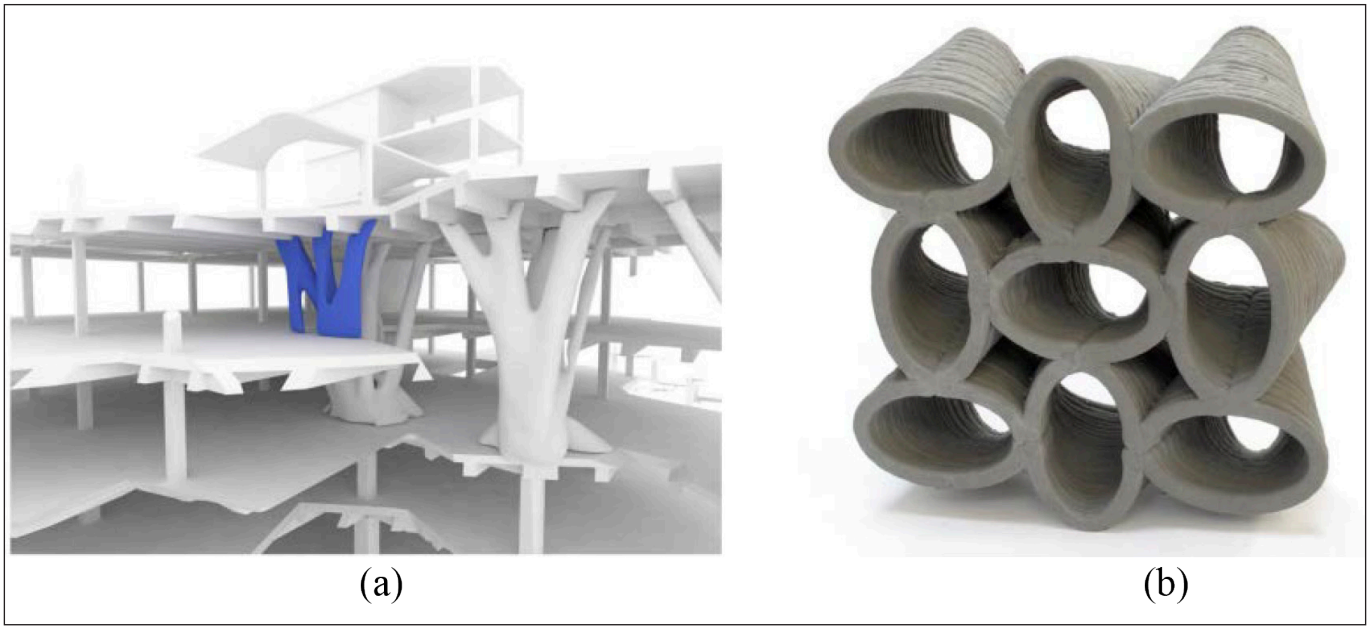

Figure 4: *Examples for large-scale application, a) Architectural context for the multifunctional wall element, and b) Concrete 3D printed acoustic damping wall element (Gosselin et al., 2016)*

solution. Second, in transdisciplinary form-finding problems such as biomechanical morphogenesis, the evolution of the design space is necessary to mimic the real biological growth in nature. A grid-based method was proposed to adjust the design space layer by layer (Kim and Ewak, 2002; Jang and Ewak, 2006). However, the grid is predefined and fixed, and the expansion of the design space features low efficiency.

There is a lack of an adequate method for updating the design domain during the form-finding process. Such a method should help broaden the application of structural topology optimization in many disciplines. Rong et al. (2022) proposed a subdomain-based method that performs topology optimization in an adaptive design domain (ADD). A subdomain based parallel processing strategy that can vastly improve the computational efficiency is implemented. In the ADD method, the loading and boundary conditions can be easily changed in concert with the evolution of the design space. Through the automatic, flexible, and intelligent adaptation of the design space, this method is capable of generating diverse high-performance designs with distinctly different topologies. Finally, this approach might help broaden the applications of structural topology optimization (Rong et al., 2022).

5. APPLICATIONS OF TO

3D printing is a disruptive technology which offers novel solutions that reconciliate non-standard shapes, and low costs. Targeting unprecedented efficiency and/or multifunctionality through geometry can push the boundaries of the design space available for engineers, architects, and designers. Additional functions can be embedded in the structural parts, i.e., not only mechanical properties but also thermal insulation, soundproofing, etc. Two examples for large-scale application are presented in this paper. Both cases are relevant examples for demonstrating feasibility of the technology developed for application in architecture and construction (Gosselin et al., 2016).

5.1 Multifunctional wall element

This element was designed within a context of structural rehabilitation, starting from the damaged structure, i.e., one floor and its upper level without any structural support. The element was designed with the aim of optimizing what would become the external supporting wall, as shown on Fig. 4 a. The element consists in an absorptive formwork to be filled either with ultra-high performance fibre-reinforced concrete on structural parts or with an insulating material such as foam for thermal insulation. Some parts are also left intentionally empty to be able to host pipes or electrical wires. The formwork has two column-like parts, linked to two straight plates in-between which waves a bi-sinusoidal shell (Gosselin et al., 2016).

5.2 Acoustic damping wall element

Another example is the following element which was designed as a generic element both structural and acoustic performance, to be assembled alongside with others in order to form a complete wall. The different hole geometries could provide enhanced soundproofing properties to the element, by damping the acoustic waves passing through depending on the geometry of the wall cells and material properties. The produced element sizes roughly 650 mm × 650 mm × 300 mm and is shown in Fig. 4 b. It was printed in 2 h (26 layers), orthogonally to the plan of the wall in order to allow lace support (Gosselin et al., 2016).

6. CONCLUSIONS

Topology optimization is a powerful design tool aiming to maximize the performance of a structure by optimizing its material layout by applying an approach that no specified initial structural topology needs to be presumed a priori. Several topology optimization techniques have been recently developed and considerably applied in different fields such as mechanical engineering, advanced manufacturing, architectural design, and aerospace engineering. Finally, advanced manufacturing techniques such as 3D printing can be used to fabricate free-form designs generated by structural topology optimization.

Despite being one of the most demanding economic sectors in terms of material consumption, the construction industry has not yet adopted such design methods. This is

generally because computational optimization algorithms produce solutions that are difficult to fabricate, especially at a large scale. The conventional approach of casting concrete into a formwork limits geometrical freedom for the architects to build in various geometries unless high costs are paid for bespoke formworks. Rectilinear forms not only limit creativity of the architects, but they are also structurally weaker than curvilinear forms owing to stress concentration.

At the current study, the authors review the aspects of topology optimizations in concrete alongside with its potential structural, economic, and environmental impacts.

ACKNOWLEDGEMENT

The authors would like to acknowledge support of the Hungarian Project VKE 2018-1-3 1_0003 "Development of concrete products supported by techniques of material science".

REFERENCES

Allaire, G. Jouve, F. Toader, A.M. (2002), "A level-set method for shape optimization", *C. R. Math*. 334 (12) 1125–1130. https://doi.org/10.1016/s1631-073x(02)02412-3

Allwood, J.M. Michael F.A. Timothy G.G. and Ernst W. (2011), "Material efficiency: A white paper." *Resources, Conservation and Recycling* 55, (2011), no. 3 362–381. https://doi.org/10.1016/j.resconrec.2010.11.002

Aremu, A. Ashcroft, I. Hague, R. Wildman, R. and Tuck, C. (2010), "Suitability of SIMP and BESO topology optimization algorithms for additive manufacture." *In Twenty First Annual International Solid Freeform Fabrication Symposium*, Austin, pp. 679– 692. 2010.

ASTM F42. (2015), "Standard Terminology for Additive Manufacturing Technologies". West Conshohocken: ASTM International, 2015.

Bendsøe, M.P. Kikuchi, N. (1988), "Generating optimal topologies in structural design using a homogenization method, *Computer Methods in Applied Mechanics and Engineering*. 71 (2) 197–224. https://doi.org/10.1016/0045-7825(88)90086-2

Bruggi, M. Duysinx, P. (2012), "Topology optimization for minimum weight with compliance and stress constraints". *Struct. Multidiscip. Optim*. 46(3), 369–384 (2012). https://doi.org/10.1007/s00158-012-0759-7

Bruggi, M. Taliercio, A. (2013), "Design of masonry blocks with enhanced thermomechanical performances by topology optimization". *Constr. Build. Mater*. 48, 424–433. https://doi.org/10.1016/j.conbuildmat.2013.07.023

Gosselin, C. Duballet, R. Roux, P. Gaudillière, N. Dirrenberger, J. and Morel, P. (2016), "Large-scale 3D printing of ultra-high-performance concrete–a new processing route for architects and builders". *Materials and Design*, 100, pp.102-109. https://doi.org/10.1016/j.matdes.2016.03.097

Guo, X. Zhang, W. Zhong, W. (2014), "Doing topology optimization explicitly and geometrically—a new moving morphable components-based framework", J. *Appl. Mech.* 81 (8) 081009. https://doi.org/10.1115/1.4027609

Huang, X. Xie, Y.M. (2009), "Bi-directional evolutionary topology optimization of continuum structures with one or multiple materials", *Comput. Mech*. 43 (3) 393–401. https://doi.org/10.1007/s00466-008-0312-0

Jang, I.G. Kwak, B.M. (2006), Evolutionary topology optimization using design space adjustment based on fixed grid, *Internat. J. Numer. Methods Engrg*. 66 (11) (2006) 1817–1840. https://doi.org/10.1002/nme.1607

Jipa, A. Bernhard, M. Meibodi, M. and Dillenburger, B. (2016), "3D-printed stay-in-place formwork for topologically optimized concrete slabs". *In Proceedings of the 2016 TxA Emerging Design+ Technology Conference*, pp. 97-107.

Kazakis, G. Kanellopoulos, I. Sotiropoulos, S. Lagaros, N. (2017), "Topology optimization aided structural design: interpretation, computational aspects and 3D printing", Heliyon 3, e00431. https://doi.org/10.1016/j.heliyon.2017.e00431

Kim, I.Y. Kwak, B.M. (2002), "Design space optimization using a numerical design continuation method", Internat. *J. Numer. Methods Engrg.* 53 (8) (2002) 1979–2002. https://doi.org/10.1002/nme.369

Liu, H. Du, T. Krishnan, N. Li, H. Bauchy, M. (2019), "Topological optimization of cementitious binders: advances and challenges". *Cem. Concr. Compos*. 101 (2019) 5–14. https://doi.org/10.1016/j.cemconcomp.2018.08.002

Llatas C. (2011), "A model for quantifying construction waste in projects according to the European waste list". *Waste Management*, 6(31):1261–1276. https://doi.org/10.1016/j.wasman.2011.01.023

Martens, P. Mathot, M. Bos, F. Coenders, J. (2018), "Optimizing 3D Printed Concrete Structures Using Topology Optimization, Springer International Publishing," *Cham*, 2018, pp. 301–309. https://doi.org/10.1007/978-3-319-59471-2_37

Mijar, A.R. Colby C.S, Jasbir S.A. and Iku K. (1998), "Continuum topology optimization for concept design of frame bracing systems." *Journal of Structural Engineering* 124, no. 5 (1998): 541–550. https://doi.org/10.1061/(asce)0733-9445(1998)124:5(541)

Nematollahi B. Sanjayan J. and Shaikh F.U.A. (2015), "Synthesis of heat and ambient cured one-part geopolymer mixes with different grades of sodium silicate. Ceramics International". 41(4): 5696–5704. https://doi.org/10.1016/j.ceramint.2014.12.154

Nematollahi, B. Xia, M. and Sanjayan, J. (2017), "Current progress of 3D concrete printing technologies". In ISARC. *Proceedings of the International Symposium on Automation and Robotics in Construction* Vol. 34. IAARC Publications. https://doi.org/10.22260/isarc2017/0035

Nguyen, K.C. Tran, P. Nguyen, H. (2019), "Multi-material topology optimization for additive manufacturing using polytree-based adaptive polygonal finite elements", Autom. Constr. 99 (2019) 79–90. https://doi.org/10.1016/j.autcon.2018.12.005

Othuman M.M. (2013), "An experimental investigation on thermal conductivity of lightweight Foamcrete for thermal insulation". *Jurnal Teknologi* 63(1). https://doi.org/10.11113/jt.v63.1368

Perrot, A. ed. (2019), "3D printing of concrete: state of the art and challenges of the digital construction revolution". https://doi.org/10.1002/9781119610755

Rong, Y., Zhao, Z.L., Feng, X.Q. and Xie, Y.M. (2022), "Structural topology optimization with an adaptive design domain". *Computer Methods in Applied Mechanics and Engineering*, 389, p.114382. https://doi.org/10.1016/j.cma.2021.114382

Rozvany, G. (2009), "A critical review of established methods of structural topology optimization." *Structural and Multidisciplinary Optimization* 37, no. 3 (2009): 217–237. https://doi.org/10.1007/s00158-007-0217-0

Sigmund, O. Maute, K. (2013), "Topology optimization approaches", *Structural and Multidisciplinary Optimization.* 48 (6) 1031–1055. https://doi.org/10.1007/s00158-013-0978-6

Søndergaard, A. and Dombernowsky, P. (2016), "Unikabeton Prototype." In Fabricate: Making Digital Architecture, eds. Ruairi Glynn and Bob Sheil. *Cambridge, Ontario: Riverside Architectural Press.* 2011. https://doi.org/10.2307/j.ctt1tp3c6d.14

Svanberg, K. (2002), "A class of globally convergent optimization methods based on conservative convex separable approximations". *SIAM J. Optim*. 12(2), 555–573 (2002). https://doi.org/10.1137/s1052623499362822

Vantyghem G. Boel V. De Corte W. et al. (2018), "Compliance, Stress-based and Multi-physics topology optimization for 3D-Printed concrete structures", in *RILEM International Conference on Concrete and Digital Fabrication,* pp. 323–332, 2018. https://doi.org/10.1007/978-3-319-99519-9_30

Vantyghem, G. Steeman, M. De Corte, W. Boel, V. (2017), "Design of Cellular materials and mesostructures with improved structural and thermal performances". In: *Advances in Structural and Multidisciplinary Optimization*, pp. 1983–1996. https://doi.org/10.1007/978-3-319-67988-4_147

Wang, M.Y. Wang, X. Guo, D. (2003), "A level set method for structural topology optimization", *Computer Methods in Applied Mechanics and Engineering*. 192 (1–2) 227–246. https://doi.org/10.1016/s0045-7825(02)00559-5

Wu, P. Wang, J. Wang, X. (2016), "A critical review of the use of 3-D printing in the construction industry". *Autom. Constr*. 68, 21–31 (2016). https://doi.org/10.1016/j.autcon.2016.04.005

Xie, Y.M. Steven, G.P. (1993), "A simple evolutionary procedure for structural optimization", *Comput. Struct*. 49 (5) 885–896. https://doi.org/10.1016/0045-7949(93)90035-c

Yan H. Shen Q. Fan L.C. Wang Y. and Zhang, L. (2010), "Greenhouse gas emissions in building construction: A case study of One Peking in Hong Kong". *Building and Environment*, 45(4):949–55. https://doi.org/10.1016/j.buildenv.2009.09.014

Yoo, D. Yoon, Y. (2016), "A review on structural behavior, design, and application of ultra-high-performance fiber-reinforced concrete". *Int. J. Concr. Struct. Mater*. 10(2), 125–142 (2016). https://doi.org/10.1007/s40069-016-0143-x

Zhou, M. Rozvany, G. (1991), "The COC algorithm, Part II: topological, geometrical and generalized shape optimization", *Computer Methods in Applied Mechanics and Engineering*. 89 (1–3) 309–336. https://doi.org/10.1016/0045-7825(91)90046-9

Zhu, B. Skouras, M. Chen, D. Matusik W. (2017), "Two-scale topology optimization with microstructures", *ACM Trans*. Graph. 36, (4) 1 (2017). https://doi.org/10.1145/3072959.3126835

Zhu, J., Zhang, W. and Beckers, P., 2009. Integrated layout design of multi-component system. *International journal for numerical methods in engineering*, 78(6), pp.631-651. https://doi.org/10.1002/nme.2499

Zhu, J.H., Zhang, W.H. and Xia, L. (2016), "Topology optimization in aircraft and aerospace structures design". *Archives of Computational Methods in Engineering,* 23(4), pp.595-622. https://doi.org/10.1007/s11831-015-9151-2

Naser S. Alimrani (1989), PhD Candidate at the Department of Construction Materials and Technologies, Budapest University of Technology and Economics. His main fields of research interest are fire design, behaviour of concrete, shear performance, failure modes of concrete at high temperatures, hollow core slabs, bond properties, bond stress-slip relationships, 3D printing concrete, sustainability, and construction management. Member of the Hungarian Group of ***fib***, and member of the YMG in the ***fib.***

Marwah M. Thajeel (1991), *PhD* student at the Department of Construction Materials and Technologies, Budapest University of Technology and Economics. Finished her bachelor (2012) in Civil Engineering at College of Engineering, Al-Muthanna University in Iraq and finished her master studies (2020) Master of Science in Structural Engineering at College of Engineering, Al-Qadisiyah University in Iraq. Research areas: Reinforced Concrete, Shear Strengthening, Fiber Reinforced Polymers, Fiber Reinforced Concrete. Member of the Hungarian Group of ***fib***.

György L. Balázs (1958), Civil Engineer, PhD, Dr.-habil., Professor of structural engineering at the Department of Construction Materials and Technologies of Budapest University of Technology and Economics (BME). His main fields of activities are experimental investigation and modeling of RC, PC, FRC, FRP, HSC, HPC, LWC, fire resistance and fire design, durability, sustainability, bond and cracking. He is chairman of several commissions and task groups of ***fib***. He is president of Hungarian Group of ***fib***, Editor-in-chief of the Journal "Concrete Structures". He was elected as President of ***fib*** for the period of 2011-2012. Since then, he is Honorary President of ***fib***. Chairman of ***fib*** Com 9 Dissemination of knowledge.

3D CONCRETE PRINTING STRUCTURAL AND NON-STRUCTURAL SOLUTIONS



Marwah M. Thajeel - Naser S. Alimrani - György L. Balázs

https://doi.org/10.32970/CS.2022.1.7

Digital production has been applied in many branches of the industry; however, the construction industry was an exception. Applying this new technology could help to reshape the construction world as we know it today. Using 3D printing technologies in construction offers significant potential to increase efficiency in terms of speed construction, waste reduction, design freedom, reduce human error as well as green building construction materials. In the current research, the authors review the structural and non-structural applications of the 3D concrete printing, as well as the potential applications, challenges, and possible solutions, respectively.

Keywords: 3D concrete printing, digital manufacturing, structural application, non-structural application

1 INTRODUCTION

1.1 3D concrete printing geometry

3D concrete printing or cementitious 3D construction printing (3DCP) is a form of additive manufacturing used to fabricate buildings or construction components in completely new shapes not previously possible with traditional technologies. Concrete is extruded, using this new technology, through a nozzle to build structural components layer-by-layer without the use of formwork or any subsequent vibration. Extrusion/deposition method of 3D printing is one of the most studied techniques where material has three planes, with perpendicular symmetry between these planes producing an orthotropic material (*Fig. 1*). Hence, its mechanical behaviour differs based on the three axes as defined by the direction of the deposition, the layer width and the structure height to be printed. In addition, the interfacing between layers conjectural appears to be a critical zone, which can have a large effect on the overall mechanical characteristics of the printed material (Perrot, 2019).

1.2 Functionality of 3D printed materials

Specific requirements must be taken into a count at the phase of designing a structure. Structural requirement is one of the important requirements that deal with safety, ability of the structure to support all loads, and to completely understand the mechanical properties of printed structures. In addition, the degree of orthotropy should be taken into considerations. This could be possible by contrasting its mechanical behaviour in different directions of loads, as shown in *Fig. 2*, or by comparing the properties of a 3D printed material with the same conventional cast material. Several studies measured the perpendicular and parallel compressive strength and compared to the cast concrete, in which all results were higher than the conventionally cast samples. The compressive strength in the parallel direction is slightly lower than the cast samples while the perpendicular is the same (Lim et al., 2012). Moreover, they concluded that anisotropy in terms of compressive strength is due to defects at the interface of the layers whereas the flexural strength in all direction is higher than the cast concrete. As a result, the printed materials have a better bending strength than conventional poured concrete (Malaeb et. al., 2015, Nerella et. al., 2017).

Furthermore, several authors have proposed combinations that contain natural fibres, silica fume and fly ash to improve the mechanical propertied particularly tensile characteristics to the printed cementitious materials (Ogura et. al., 2018, Sonebi et. al., 2018). The studies have concluded that it is possible to print concrete or mortars with obtained mechanical characteristics that can be qualified as high or very high performance by choosing the best methods of printing (Xia and Sanjayan, 2016, Weger et. al., 2016, Shakor et. al., 2017, Weger et. al., 2018, Pierre et. al., 2018 and Gaudillière et al., 2019). In addition, it is suggested to reduce time intervals between layers to improve the bonding between the layers and prevent cold joints to be formed (Wangler et. al., 2016). Finally, spraying the water on the layer before the print of a new layer increases the compressive strength compared to the sample printed without wetting (Sanjayan et. al., 2018).

2 STRUCTURAL APPLICATION

2.1 Formwork freedom

Architects and designers often attend to create especial structure resulting in complex structure that is a challenge to perform. Nevertheless, 3D printing concrete provides matchless freedom of form for architects and designers of concrete elements. From this point of view, this new digital production might open new fields of chances that were previously difficult for architects. In addition, it has a green impact on environment, since the production and management of forms can produce a large amount of waste, particularly in the case of forms for complex structures with assembly components that are utilized just a single time.

However, this method does not provide completely freedom

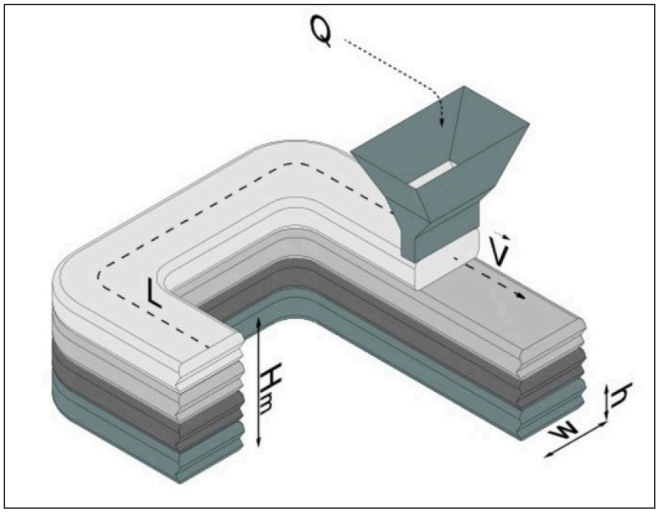

Fig. 1: Extrusion/deposition of 3D printing process (Wangler et al. 2016)

from the formwork. One of the challenges of the 3D printing is the overhanging parts of structures as shown in *Fig. 3*, because they are limited by the elastic properties of the material while it is in a fresh state (Wolfs et. al., 2018, Leventon, 2019). A common way to deal with overhangs is by generating support structures. These are towers that rise up from the ground to hold the sections that can't hold themselves up (*Fig. 4*). They can come in a variety of patterns and forms, depending on what software was used to generate them. After the print is finished, they can be ripped out to leave the model as intended (Higgs, 2018), or use printers have two nozzles that are able to print two separate materials in the same print. Special foundation materials can be used in these prints to make support structures that come cleanly off the rest of the print without hassle. Many research projects today focus on simultaneous and collaborative works performed by a team of robots with two different materials, *Fig. 5* (Duballet et. al., 2018). Although it sounds as ideal, it is also the downside to this method, in which the places where the model had support structures attached will have a rougher and less clean finish.

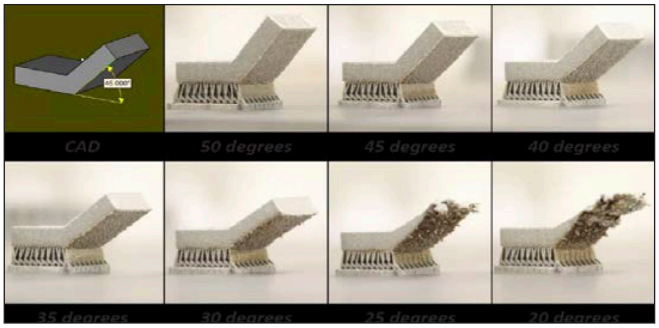

Fig. 3: A 3D-printed overhang of less than 45 degrees generally needs support structures to prevent it from crumbling (Leventon, 2019)

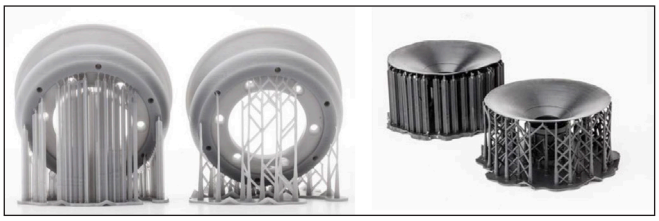

Fig. 4: Different software have different algorithms for support structures (Baptiste, 2018)

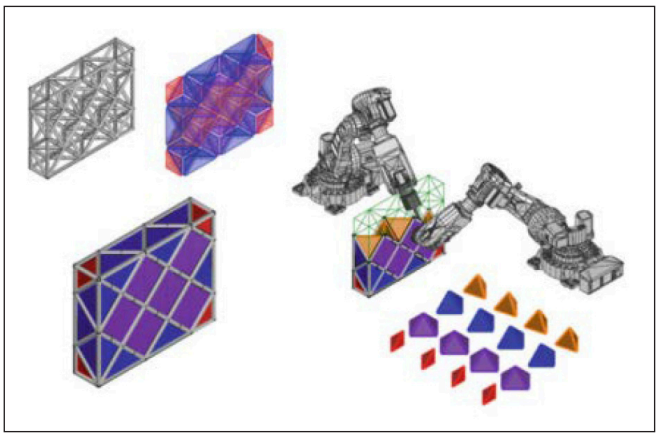

Fig. 5: Production of concrete walls with two robots working together (Duballet et. al., 2018)

2.2 Structures with shape optimization

2.2.1 Topological optimization

Digital manufacturing can also help to optimize the amounts of materials installed since the materials are only placed where they are important for the structural stability. Thus, the building design and structural construction can be done using the concept of topological optimization. In many areas of application, digital manufacturing is related to a design using this topological optimization (Hollister, 2005, Brackett et. al., 2011). Topological optimization is a design tool that uses mathematical methods that allow the amounts of materials to be minimized in each volume subjected to mechanical stress (Bendsoe, 2001). Figure 6 (a) shows the application of topological optimization on simply supported beam subjected to concentrated load at the mid-span (Vantyghem et. al., 2018), while *Figure 6 (b)* shows the reduction in quantities of materials using topological optimization during the design phase (Tripathy, 2016).

2.2.2 Inspired by nature

It is also possible to print designs from the living world and inspired by nature through a slow process of natural selection. This process has ultimately been able to produce structures that

Fig. 2: Testing direction (a) compressive strength and (b)flexural strength (Marchent, 2017)

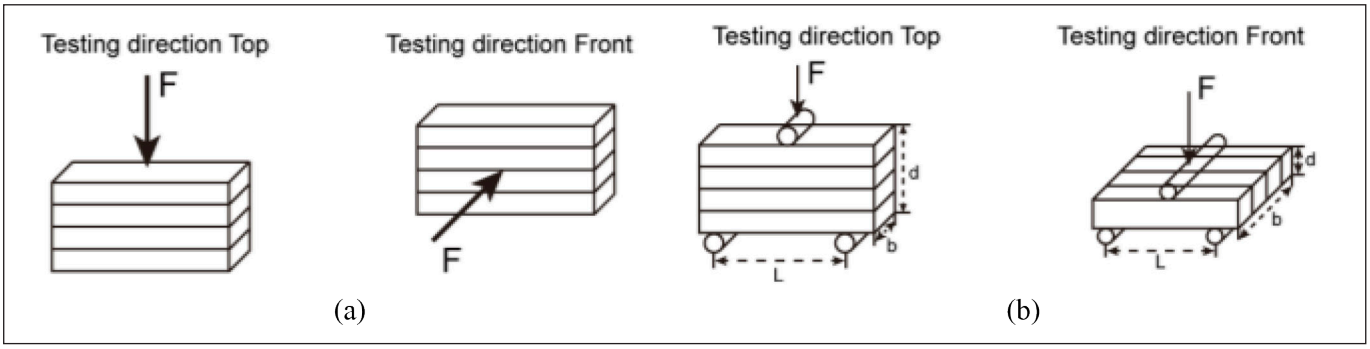

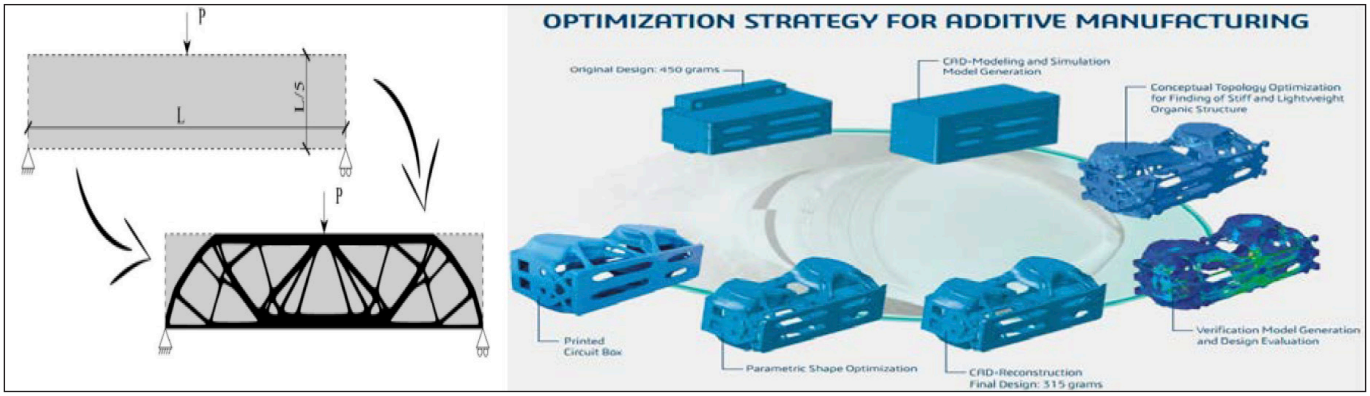

Fig. 6: *Topological optimization concept, (a) simply supported beam subjected to load (Vantyghem et. al., 2018), and (b) reduced amounts of materials during the design phase (Tripathy, 2016)*

Fig. 7: *Column inspired from human bones, (a) initial sketch, and (b) printed (Nadja et. al., 2019)*

optimize the use of materials to design load bearing elements that can decrease the volume of the material. From this point of view, a porous structure inspired by human bones is shown in *Fig. 7*. The structure was printed in segments at the factory and then assembled on site. The finished piece stands 4 meters tall and blends seamlessly with the concrete of the preschool building (Nadja et. al., 2019).

The concept of optimization offers the advantage of a potential reduction in the supplies of raw materials, especially aggregates, which have become increasingly scarce. However, it is important to note that the formulas of cement-based materials tested in the literature often use reduced maximum grain sizes, which significantly increases the cement dosage. Similarly, a significant use of chemical admixtures has also been reported in many cases. As a result, the environmental impact of the printable material is greater than that of conventional concrete. Thus, for the printed concrete to have less of an impact, the design must be optimized at least to compensate for the higher environmental cost of the formulas used for printing. Therefore, this technology encourages us to reconsider the way in which buildings are designed, in order to have structures that optimize the forms and the quantities of materials used (Martens et al., 2017).

2.3 Possibility to print shell elements

One more component of 3D concrete manufacturing is to print structures that are only subjected to compression loads, like masonry structures in the form of a dome or an arch. Since the concrete tensile strength is low, this method allows to overcome on the natural tensile fragility of the concrete. This technique has been especially utilized by the set of Pr. Block at ETH University, Zurich, Switzerland (Rippmann and Block, 2013).

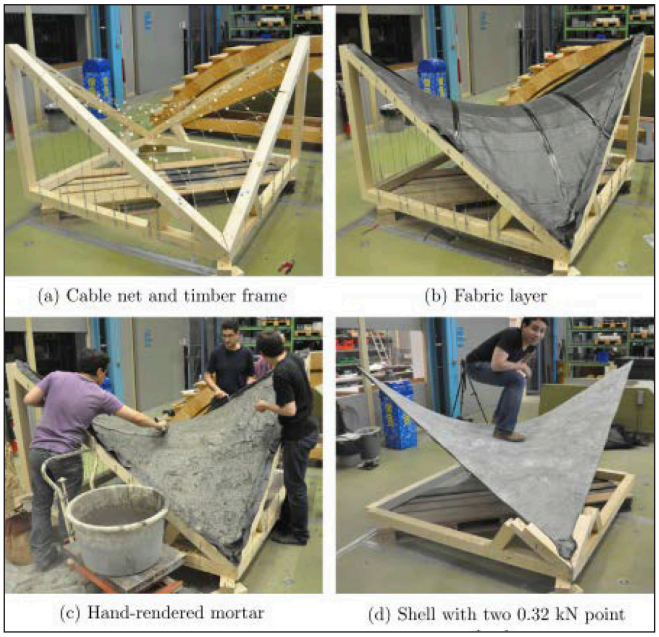

Fig. 8: *Shell construction by reducing the tensile forces (Veenendaal and Block, 2014)*

The thought is to utilize the strategies of the digital production of forms dependent on reinforcing cables and fabrics as a help for the projection of a thin strata of concrete to be utilized in compression (*Fig. 8*). Other digital production methods using concrete (injection into particle beds or by extrusion/deposition) may be utilized in the future in a trail to reprinting traditional structural forms, active in compression, as in cathedrals, like arches and keystones without steel reinforcing (Veenendaal and Block, 2014).

2.4 Prominent 3D printed construction models

2.4.1 The highest 3D printed building across the globe, in China

The world's highest 3D printed building was built in 2015 in China. The apartment building was consisted of five-story (*Fig. 9*). The method of construction was off-site, elements such as walls, doors and windows were fabricated, transported and assembled on-site. Finishing works were carried out using traditional methods (Winsun, 2015).

2.4.2 The world largest 3D printed office, in Dubai

The first largest 3D printed office building was opened in 2016 in Dubai, UAE, known as the "office of the future" (Augur, 2016). The office was designed by an Emirati Architecture Firm and 3D printed in Shanghai. Once all parts were ready, they were shipped to Dubai, where the components were assembled. The construction process took only 17 days to print 240-square-meter, which were followed by an on-site installation that took an additional two days. According to Gensler, using 3D printing technology instead of conventional methods has saved labour cost by 50-80%, and reduced construction waste by 30-60% (Ferro, 2016). This 3D printed office is a fully functional building featuring electricity, water, telecommunications, and even air-conditioning systems, *(Fig. 10).*

Fig. 9: 3D printed five story apartment building in China (Hossain et al., 2020)

Fig. 11: 3D printed villa in China (Hossain et al., 2020)

2.4.3 3D printed two-story villa, in China

The two-story villa as shown in *Fig. 11* was completely printed on site in Beijing, China, in 2016. The entire construction process of 400-square-meter villa took only 45 days. However, a same building with traditional construction would take up to 7 months. In contrast with other 3D printed construction, the construction process was first carried out by installation the frame of the villa with steel reinforcement, then the C30 class concrete was printed by a huge 3D printer on site. Seismic testing estimates found that this 3D printed villa could be able to withstand an 8.0 earthquake on the Richter scale (Scott, 2016).

2.4.4 The first 3D printed footbridge, in Spain

The world's first 3D printed footbridge was inaugurated in 2016 in Madrid, Spain. The building was designed with a total length of 12 m and width of 1.75 m (*Fig. 12.b*), taking a total process to complete, of one year and a half. The 3D printed footbridge shows difficulties of the forms of nature, it was developed through parametric and computational designs that allows optimizing the distribution of materials and maximizing the structural performance. This enables the engineers to use the material only where it is needed, with total freedom of forms (Valencia, 2017).

Fig. 10: World's largest 3D printed office in Dubai (Ferro, 2016)

Fig. 12: 3D printed bridges, (a) bike bridge in Netherlands (Saunders, 2017), and (b) footbridge in Spain (Valencia, 2017)

2.4.5 3D printed bike bridge in Netherlands

The process of designing and printing the bike bridge was started in the Netherlands in 2017, with a total length of 8 m and width of 3.5 m (Fig. 12 a). The goal of the project was announced to "connect the future, to look for a newer, smarter approach to addressing infrastructure issues and thus making a significant contribution to improving the mobility and sustainability of society," (Saunders, 2017).

3 NON-STRUCTURAL APPLICATION

Current 3D concrete printing technology limits its applications to non-structural applications such as stamped concrete, outdoor living area, fountains, pool areas. Visual arts are perhaps the most obvious non-structural application of 3D printing technology. Art installations, sculptures, and other 3D printed objects can be found almost anywhere. 3D printing gives these artists more freedom to create complex structures that would otherwise be almost impossible to make, or extremely time-consuming and difficult. It also gives artists more creative freedom because they don't require specialist abilities to manufacture the 3D printed objects; all they need is basic CAD design knowledge and a 3D printer (Asherian, 2019).

Fig. 13 shows 3D printed sculpture introduced by an American digital artist Joshua Harker. The declaration of the piece of art was to push the limits of form and dimensions to share vision and exploration into what can be made and how to accomplish it in effort to tell a story or create an experience. Digital tools, software, and technology as well as traditional mediums were incorporated to create art that is unique and engaging. Bolstered by the advent of organic modeling software, visions are now able to be realized sculpturally in archival materials. Never have forms of this organic complexity been able to be created. This boon of technology is a revolutionary time for the arts and one which will be boldly marked in history.

3D printing has spread across many different areas, and the furniture industry is no exception. Furniture is still mass-produced using traditional manufacturing methods, but 3D printing has come in handy for designers who want to bring innovation into the market. However, 3D printing still is not the most appropriate tool for furniture. 3D printing offers a great tool for producing high-end furniture, often developed by famous designers who want to explore new shapes and ideas. Such furniture is produced in rather limited quantities and often features complex geometries, which is easier to produce using 3D printing. This often results in extraordinary designs, which are hard or impossible to produce with molds. *Fig. 14 (a)* shows 3D printed concrete furniture piece (Aduatz, 2020). *Fig. 14 (b)* shows intricacy of the shapes and surfaces (artificial reefs) that can be made through the digital manufacturing methods of 3D concrete printing. The servals air holes produced by the concrete encourage sea animals to settle in the region (Xtree, 2018).

Fig. 13: 3D printed sculpture (Harker, 2014)

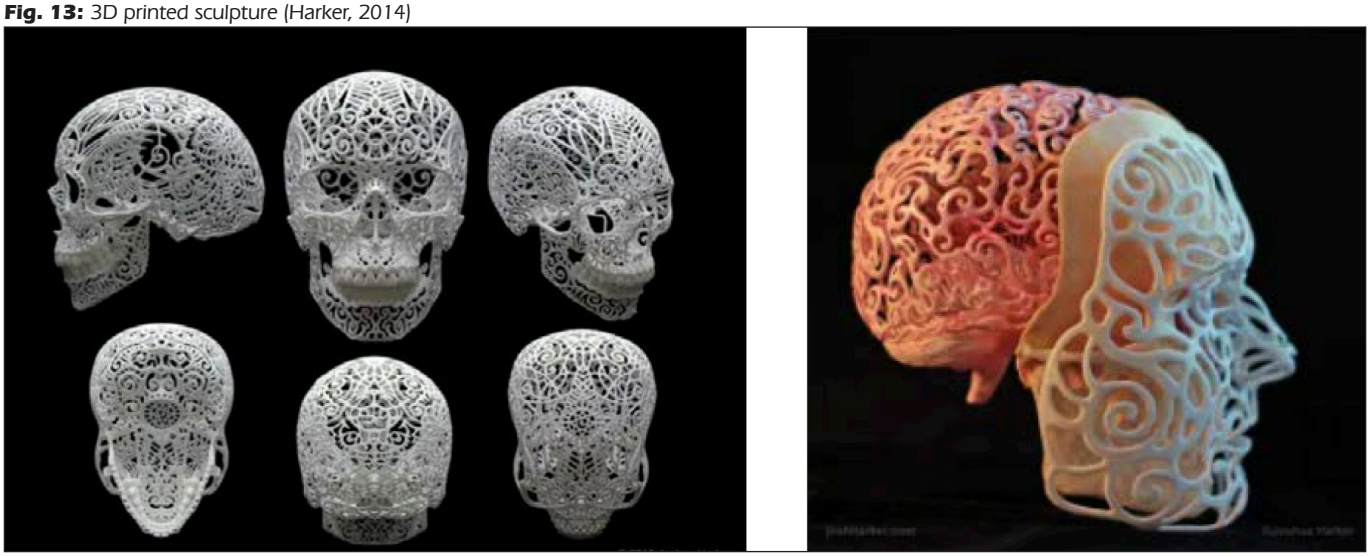

Fig. 14: Non-structural 3D printing concrete, (a) furniture (Aduatz, 2020), and (b) artificial underwater reefs (Xtree 2018)

4 CONCLUSIONS

3D concrete printing is an innovative construction method that promises to be highly advantageous in the field of construction in terms of optimizing construction cost, time, error reduction, design flexibility and environmental effect. It can be utilized to build the affordable housing in low-income countries, constructs military bunker in the wild, build in Mars or Lunar using in site material, and print the complex structure when the form is difficult to production, manufacture, restore or repair.

However, the behaviour of 3D printed concrete is orthotropic, changing the conventional concrete behaviour which exhibits as isotropic material. Thus, the utilization of the principles and test techniques utilized for traditional concrete may not be suitable for printed materials and structures. It is important to modify the standards and the new regulations to measure and assess the mechanical exhibition of the 3D concrete printing, as well as to develop new theoretical models to evaluate their structural behaviour. New standards design is very crucial to make sure the 3D printed elements able to carry all loads. At present, many constructions have been printed successfully and even put into practice, but it still needs a lot of work to do to encourage the growth of 3D concrete printed technology.

Non-structural applications of 3D concrete printing are still limited. The most used of this technology is sculptures, art installations and interior decorations. However, one of the extraordinary applications of this technology is 3D concrete printing artificial reefs with various air hols that helped underwater animals to settle in it.

ACKNOWLEDGMENT

Authors acknowledge the support by the Hungarian Research Grant VKE 2018-1-3-1_0003

"Development of advanced concrete elements".

5 REFERENCES

Aduatz, P. (2020), *"philipp aduatz creates 3D printed concrete outdoor furniture"* available at https://www.designboom.com/design/philipp-aduatz-3d-printed-outdoor-concrete-furniture-07-27-2020/, July 27, 2020, (Accessed on 20 October 2021)

Asherian, N. (2019), *"3D Printed Art: How 3D Printing Makes its Way into Creativity"*, July 17, 2019, Available online at: https://all3dp.com/, (Accessed on 19 October 2021)

Augur H. (2016), *"3D Printed Office Building Unveiled in Dubai"*, published May 27, 2016, Available online at, https://all3dp.com/3d-printed-office-building/ , (Accessed on 19 October 2021)

Bendsoe, M.P. (2001), "Topology optimization", in Encyclopedia of Optimization, Springer, pp. 2636–2638, 2001. https://doi.org/10.1007/0-306-48332-7_527

Brackett, D., Ashcroft, I., Hague, R. (2011), *"Topology optimization for additive manufacturing"*, in Proceedings of the Solid Freeform Fabrication Symposium, Austin, TX, vol. 1, pp. 348–362, 2011.

Dfab house (2018), "Building with robots and 3D printers", Available at: http://dfabhouse.ch/, 2018, (Accessed on 15 October 2021)

Dubai building (2019), *" World's largest 3D-printed building completes in Dubai"*, available at: https://www.dezeen.com/2019/12/22/apis-cor-worlds-largest-3d-printed-building-dubai/, 2019, (Accessed on 15 October 2021)

Duballet, R., Baverel, O., Dirrenberger, J. (2018), *"Design of Space Truss Based Insulating Walls for Robotic Fabrication in Concrete"*, Humanizing Digital Reality, pp. 453-461, 2018. https://doi.org/10.1007/978-981-10-6611-5_39

Ferro, S. (2016), *"The World's First Fully 3D-Printed Office Building Is Opening in Dubai"*. Published May 30, 2016. Available online at: http://mentalfloss.com/article/80738/worldsfirst-fully-3d-printed-office-building , (Accessed on 15 October 2021)

Gaudillière, N., Duballet, R., Bouyssou, C., Mallet, A., et al. (2019), *" Large-Scale Additive Manufacturing of Ultra-High-Performance Concrete of Integrated Formwork for Truss-Shaped Pillars"*, in Robotic Fabrication in Architecture, Art and Design, pp. 459–472, 2019. https://doi.org/10.1007/978-3-319-92294-2_35

Harker, J. (2014), "21st Century Self-Portrait", Available online at: https://www.joshharker.com/art/self-portrait/, (Accessed on 19 October 2021)

Higgs, B. (2018), *" 3D Print Overhangs and How To Deal With Them"*, available online at: https://medium.com/bravovictornovember/3d-print-overhangs-and-how-to-deal-with-them-9eed6a7bcb5d, last edit Feb 21, 2018, (Accessed on 10 October 2021)

Hollister, S.J. (2005), *"Porous scaffold design for tissue engineering"*, Nature Materials, vol. 4, no. 7, p. 518-524, 2005. https://doi.org/10.1038/nmat1421

Hossain, M.A.; Zhumabekova, A.; Paul, S.C.; Kim, J.R (2020), *"A Review of 3D Printing in Construction and its Impact on the Labor Market"*. Sustainability *2020, 12, 8492*. https://doi.org/10.3390/su12208492

Leventon, W., (2019), *"Less support is a good thing—when 3D printing"*, available online https://www.thefabricator.com/additivereport/article/additive/less-support-is-a-good-thingwhen-3d-printing, last edit October 4, 2019, (Accessed on 10 October 2021)

Lim, S., Buswell, R.A., Le, T.T. *et al*. (2012), *"Developments in construction-scale additive manufacturing processes"*, Automation in Construction, vol. 21, pp. 262–268, 2012. https://doi.org/10.1016/j.autcon.2011.06.010

Malaeb, Z., Hachem, H., Tourbah, A. *et al*. (2015), *"3D concrete printing: Machine and mix design"*, International Journal of Civil Engineering, vol. 6, pp. 14–22, 2015.

Marchent, T., Xia, M., et al. (2017), *"Effect of Delay Time on the Mechanical Properties of Extrusion-based 3D Printed Concrete"*, 34th International Symposium on Automation and Robotics in Construction (ISARC 2017). https://doi.org/10.22260/isarc2017/0032

Martens, P.A., Mathot, M., et al. (2017)," Optimising 3D printed concrete structures using topology optimization", Proceedings of the IASS Annual Symposium 2017 "Interfaces: architecture.engineering.science" 25 - 28th September, 2017, Hamburg, Germany. https://doi.org/10.1007/978-3-319-59471-2_37

Nerella, V.N., Hempel, S., Mechtcherine, V., (2017), *"Micro-and macroscopic investigations of the interface between layers on the interface of 3D-printed cementitious elements"*, International Conference on Advances in Construction Materials and Systems, 3-8. 9. 2017, Chennai.

Ogura, H., Nerella, V.N., Mechtcherine, V. (2018), *"Developing and testing of strain-hardening cement-based composites (SHCC) in the Context of 3D-Printing"*, Materials (Basel), vol. 11, no. 8, August 2018. https://doi.org/10.3390/ma11081375

Perrot, A. (2019), " *3D Printing of Concrete: State of the Art and Challenges of the Digital Construction Revolution*" First published 2019 in Great Britain and the United States by ISTE Ltd and John Wiley & Sons, Inc. https://doi.org/10.1002/9781119610755

Pierre, A., Weger, D., Perrot, A. *et al*. (2018), *"Penetration of cement pastes into sand packings during 3D printing: analytical and experimental study"*, Materials and Structures, vol. 51, no. 22, available at: https://doi.org/10.1617/s11527-018-1148-5, 2018. https://doi.org/10.1617/s11527-018-1148-5

Rippmann, M., Block P. (2013), *"Rethinking structural masonry: Unreinforced, stone-cut shells"*, Proceedings of the Institution of Civil Engineers - Construction Materials, vol. 166, no. 6, pp. 378–389, December 2013. https://doi.org/10.1680/coma.12.00033

Sanjayan, J.G., Nematollahi, B., Xia M. *et al*. (2018), *"Effect of surface moisture on inter-layer strength of 3D printed concrete"*, Construction and Building Materials, vol. 172, pp. 468–475, 2018. https://doi.org/10.1016/j.conbuildmat.2018.03.232

Saunders, S. (2017), *"3D Printed Concrete Bridge in the Netherlands Officially Open to Cyclists"*, Published October 18, 2017, Available online at: https://3dprint.com/191375/3d-printed-concrete-bridge-open/, (Accessed on 15 October 2021)

Scott, C. (2016), *"Chinese Construction Company 3D Prints an Entire Two-Story House On-Site in 45 Days"*. Published June 16, 2016, Available online at: https://3dprint.com/138664/huashang-tengda-3d-print-house/, (Accessed on 15 October 2021)

Shakor, P., Sanjayan, J., Nazari, A. *et al*. (2017), *"Modified 3D printed powder to cement-based material and mechanical properties of cement scaffold used in 3D printing"*, Construction and Building Materials, vol. 138, pp. 398–409, 2017. https://doi.org/10.1016/j.conbuildmat.2017.02.037

Sonebi, M., Rubio, M., Amziane, S. *et al*. (2018), *"Mechanical properties of 3d printing bio-based fiber cement-based materials"*, RILEM 1st International Conference on Digital Fabrication with Concrete, Extended Abstracts, pp. 50–51, September 9-12, 2018.

Tripathy, S. (2016), *" Topology Optimization for Additive Manufacturing Applications"*, available at: https://blogs.3ds.com/simulia/topology-optimization-for-additive-manufacturing-applications/, August 23, 2016, (Accessed on 10 October 2021)

USA home (2020), *"Largest 3D printed home"*, available at: https://www.sq4d.com/largest-3d-printed-home/, 2020, (Accessed on 15 October 2021)

Valencia, N. (2017), *"World's First 3D Printed Bridge Opens in Spain"*, Published February 07, 2017, Available online at: https://www.archdaily.com/804596/worlds-first-3d-printed-bridge-opens-in-spain, (Accessed on 15 October 2021)

Vantyghem, G., Boel, V., Decorte, W. *et al*. (2018), *"Compliance, Stress-based and multi-physics topology optimization for 3D-Printed concrete structures"*, in RILEM International Conference on Concrete and Digital Fabrication, pp. 323–332, 2018. https://doi.org/10.1007/978-3-319-99519-9_30

Veenendaal, D., Block, P. (2014), *"Design process for prototype concrete shells using a hybrid cable-net and fabric formwork"*, Engineering Structures, vol. 75, pp. 39–50, 2014. https://doi.org/10.1016/j.engstruct.2014.05.036

Wangler, T., Lloret, E., Reiter, L. *et al*. (2016), *"Digital concrete: Opportunities and challenges"*, RILEM Technical Letters, vol. 1, pp. 67-75, 2016. https://doi.org/10.21809/rilemtechlett.2016.16

Weger, D., Lowke, D., Gehlen, C. (2016), *"3D printing of concrete structures using the selective binding method–Effect of concrete technology on contour precision and compression strength"*, Proceedings of 11th Fib International PhD Symposium in Civil Engineering, The University of Tokyo, Tokyo, pp. 403–410, 2016.

Weger, D., Lowke, D., Gehlen, C., et al., (2018), *"Additive manufacturing of concrete elements using the selective paste intrusion – effect of layer orientation on strength and durability"*, 1 st International Conference on Concrete and Digital Fabrication Digital Concrete 2018 – Zurich, Switzerland, 10-12 September 2018

Winsun (2015), *"2015 Global Highest 3D Printing Building"*. Available online at: http://www.winsun3d.com/En/Product/pro_inner_5/id/102, (Accessed on 15 October 2021)

Wolfs, R.J.M., Bos, F.P., Salet, T.A.M. (2018), *"Early age mechanical behaviour of 3D printed concrete: Numerical modelling and experimental testing"*, Cement and Concrete Research, vol. 106, pp. 103–116, April 2018. https://doi.org/10.1016/j.cemconres.2018.02.001

Xia, M., Sanjayan, J. (2016), *"Method of formulating geopolymer for 3D printing for construction applications"*, Materials & Design, vol. 110, pp. 382–390, 2016. https://doi.org/10.1016/j.matdes.2016.07.136

Xtree, (2018), Xtree company, *"Project – Rexcor Artificial Reef | XtreeE*", available at: http:// www.xtreee.eu/, 2018, (Accessed on 20 October 2021)

Marwah M. Thajeel (1991), PhD student at the Department of Construction Materials and Technologies, Budapest University of Technology and Economics. Finished her bachelor (2012) in Civil Engineering at College of Engineering, Al-Muthanna University in Iraq and finished her master studies (2020) Master of Science in Structural Engineering at College of Engineering, Al-Qadisiyah University in Iraq. Research areas: Reinforced Concrete, Shear Strengthening, Fiber Reinforced Polymers, Fiber Reinforced Concrete. Member of the Hungarian Group of ***fib***.

Naser S. Alimrani (1989), PhD Candidate at the Department of Construction Materials and Technologies, Budapest University of Technology and Economics. His main fields of research interest are fire design, behaviour of concrete, shear performance, failure modes of concrete at high temperatures, hollow core slabs, bond properties, bond stress-slip relationships, sustainability, and construction management. Member of the Hungarian Group of ***fib***, as well as member of the YMG in the ***fib.***

György L. Balázs (1958), Civil Engineer, PhD, Dr.-habil., Professor of structural engineering at the Department of Construction Materials and Technologies of Budapest University of Technology and Economics (BME). His main fields of activities are experimental investigation and modeling of RC, PC, FRC, FRP, HSC, HPC, LWC, fire resistance and fire design, durability, sustainability, bond and cracking. He is chairman of several commissions and task groups of ***fib***. He is president of Hungarian Group of ***fib***, Editor-in-chief of the Journal "Concrete Structures". He was elected as President of ***fib*** for the period of 2011-2012. Since then, he is Honorary President of ***fib***. Chairman of ***fib*** Com 9 Dissemination of knowledge.

3D CONCRETE PRINTING: VARIETY OF AGGREGATES, ADMIXTURES AND SUPPLEMENTARY MATERIALS


Abdelmelek Nabil - György L. Balázs

https://doi.org/10.32970/CS.2022.1.8

This review paper provides a report on the up-to-date research on the 3D printing technology for the concrete in terms of materials. It reviews the required characteristics of concrete rheology, printing process and discusses the challenges for reaching compatible mix proportions using eco-friendly binders, aggregate, and chemical admixtures. The recent research on the durability behaviour of 3D printed concrete needs future research and identification.

Keywords: concrete 3D printing; extrusion; printable concrete; rheology; printing process parameters; durability

1. INTRODUCTION

3D concrete printing (3DCP) is a new emerging construction technique, and it has the capacity to revolutionize industrial building by enabling the use of construction automation. 3D printing is also known as additive manufacturing (AM), which gained its popularity in the construction field in recent years (Buswell et al., 2018; Lim et al., 2012; Mechtcherine et al., 2019). The process entails printing layers of materials product that are subsequently set up on top of each other. This technology was developed by Charles Hull in 1986 in a process known as stereolithography (SLA), then it was followed by other subsequent developments with different techniques and technology such as powder bed fusion, fused deposition modelling (FDM), inkjet printing and contour crafting (CC). 3D printing has involved various equipment, materials, and methods that gave it the ability to transform manufacturing and logistics processes. AM has been applied in different applications including construction, prototyping and biomechanical. However, the uptake of 3D printing in the field of construction industry was very slow and limited despite the advantages (Ngo et al., 2018). Compared with the existing construction methods, 3D printing can offer enormous advantages such as increased speed-related construction, architecture freedom, less work-related injuries and reduced waste material, less labour and fewer costs (Wangler et al., 2016). Therefore, such advantages have forced the construction industry to include this technique in some specific cases.

Generally, flowable cement paste contributed to increase strength particularly in the use of particle bed method. Meanwhile, it affects the shape accuracy. During the printing process, the accuracy of the printed shape relied on the size of the used particles in the bed. In which, particle with small size and layer thickness would provide high accuracy. Yet, it could also cause an increase in printing time during construction in large-scale application. Generally, the accuracy demand is not as high as in mechanical properties in the construction industry. Based on the reasons above, it is important to develop a new printing routine in order to use large particles for the expansion of the adoption of particle-bed 3DCP. Compared with other printing techniques, particle-bed printing is easier to adopt a large coarse aggregate volume.

Coarse aggregate is an important concrete part as it provides the highest strength, highest durability, less shrinkage, and cheapest cost among concrete components (Shen et al., 2010). Current research in 3DCP faced difficulty in using large aggregate size due to the requirement of extrudability. Ji et al. (2019) have made the first attempt in extrusion-based printing whereas, the design of 3DCP machine limited the size of the used coarse aggregate. In case of particle-bed printing method, coarse aggregate could be placed as the skeleton, then to be filled with cement paste.

At the moment, 3D printing technology, particularly concrete, is in its infancy. Consequently, the life-cycle behaviour is yet to be assessed. A limited number of studies on 3DCP structures have developed several methods and materials, some common of them are briefly discussed hereafter.

2. SUSTAINABILITY ADVANTAGES

Sustainability is a vast term that specifically goes beyond the decrease of the usage of raw material and decreasing environmental impact. Treatment of sustainability for environmental, economic, and societal effects has become worldwide accepted, with different procedures to quantify the impacts. The most feasible to quantify it are the economic consequences, especially in the context of construction, and the most complicated one are the societal implications. When 3DCP is compared with conventional construction, some advantages are stated such as savings in cost which is counted due to lower project durations, the non-use of formwork and labour. On the other hand, using unconventional ingredients and stricter control in 3DCP mixtures proportions may increase the cost of the concrete. The environmental impact would be decreased by the non-use of formwork and lowering in material wastage but may increase if the content of binder is high. The beneficial societal impact of using 3DCP in the construction site and prefabrication plant is predicted to be significant

because of the decrease of manual labour for pouring and compaction of concrete, the lifting of formwork, and the decrease of errors and accident probabilities due to automation.

3. RHEOLOGY

The fresh printable concrete mix process requires contradicting rheological properties. It requires high workability at the pumping stage before extrusion, whereas after extrusion, it needs low workability and high thixotropy in terms of buildability of concrete (Perrot and Rangeard, 2019; Lu et al., 2019). During the process of printing, a balance is required between the rheological properties' requirements for pumping, extrusion, and buildability phases (Wangler, 2019; Papachristoforou et al., 2018). If the printable concrete has low yield stress used for helping the pumping and extrusion phases, then the extruded concrete will negatively affect the shape retention.

Workability is an essential parameter for the printable concrete, high dosages of superplasticizer are needed because of using low water to cement (w/c) ratios (Aïtcin, 2019). Phase separation as apart from workability is also essential for pumpability and extrudability of concrete. Evaluation of phase separation has been conducted by desorptivity parameter (Rahul et al., 2020), and a decrease in w/c ratio was observed to decrease desorptivity.

4. MAIN METHODS

4.1 Inkjet printing and contour crafting

Inkjet printing is a method used for printing complex geometries and advanced ceramic structures for applications such as scaffolds for tissue engineering. A similar printing technology to inkjet method, named contour crafting, is used for large building structures. This method has the capacity for extruding concrete paste by adopting large nozzles and with high pressure. Contour crafting technology has been prototyped to be applied for construction on the moon (Nerella et al., 2020).

The fresh properties of concrete used for contour crafting are the most important aspects for successful application. The 3D printing of complex geometries demands high workability for extrusion, shape retention, or printing open time, and requires high early strength for buildability (Le et al., 2012). A mix design that can achieve the requirement of workability for extrusion before setting and at the same time have high early strength to bear successive layers without collapse needs designed materials and supported equipment. Gosselin et al. (2016) developed a printing method that could pump the accelerator and the premix mortar in different pipes and then combines it before extrusion at the printhead. The rheology properties of the premix mortar can be controlled for a longer period without losing the early strength of the printed layers to successfully retain the stability of subsequent layers. This method builds complex and larger structures by using a robotic six-axis arm and governing the behaviour of material during and after the extrusion. *Fig. 1* shows a Contour Crafting machine used for concrete processing.

4.2 Aggregate-bed 3D concrete printing

Particle-bed is one of the promised AM printing techniques, in which water-based binder is throwed pre-selected zones in order to bind the granular materials for each layer. A detailed

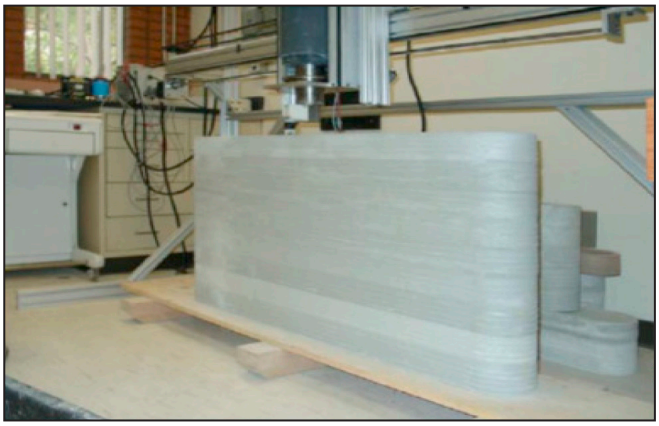

Fig. 1: Contour Crafting technology (Zareiyan and Khoshnevis, 2017)

research review of these studies was carried out by (Lowke et al., 2018). Rapid-hardening Portland cement (Gibbons et al., 2010), slag and fly ash-based geopolymer (Xia et al., 2019), a combination of OPC and calcium aluminate cement (Shakor et al., 2019) have been used to print components in ZPrinters, USA.

4.2.1 Aggregate-bed 3DCP process

A schematic of the proposed technique showed the printing process is shown in *Fig. 2*. The system contains three main key components: (1) aggregate feeder, (2) paste feeder, and (3) blade. The aggregate feeder serves to store and spread aggregate to each layer. Not similar to powder-based printers, it is impractical to govern the volume of aggregate for each layer due to the increased uncertainties of aggregate, such as particle shape, and size distribution. Therefore, an additional blade could be utilized to control the aggregate and height of each layer. The paste feeder should have the capacity to extrude the paste at a regular and accurate flowability rate. More discussion for the extrudability details can be referred to (Nerella et al., 2019).

5. INFLUENCING PARAMETERS ON 3D PRINTABLE MIXTURES

3D concrete printing process needs concrete with special properties and characteristics. Mixtures are designed based on three important material parameters, i.e., pumpability, extrudability, and buildability (Panda and Tan, 2018; Nerella et al., 2020). The pumpability and extrudability are controlled by the fresh properties such as consistency, stability, cohesiveness, and probability of separation under pressure (ACI 304.2R-96, 2008; Vanhove and Khayat, 2016). The extrudability and pumpability of concrete are further controlled by the rheological properties of the lubricating layer (Kim et al., 2017; Roussel, 2018). The main parameters governing the rheology of fresh concrete are yield stress, viscosity, and thixotropy (Roussel, 2006; Perrot et al., 2016). The buildability of the 3D printable concrete is affected by the static and dynamic shear yield stress (Kruger et al., 2020; Jeong et al., 2019), green strength and early age elastic modulus (Wolfs and Suiker, 2018; Panda et al., 2019). These properties further evolve with time as a result of hydration of cement and are affected by the conditions of curing (Diggs-McGee et al., 2019; Suiker, 2018). The other affecting parameters for the printing process of concrete are the workability open time, thixotropy open time, printability window, bond strength of layer and printing time gap (Panda, 2018; Zhang et al., 2018). The

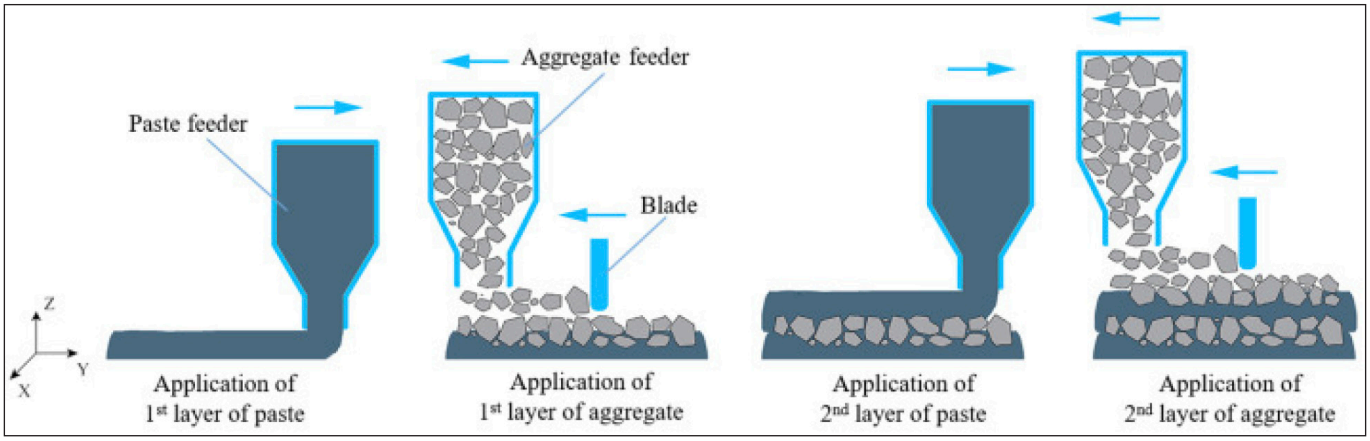

Fig. 2: *Aggregated-bed 3D concrete printing process (Yu et al., 2020)*

bond strength of layer is depended on the time gap of printing process, geometry of layer and environmental conditions affecting the properties of the surface (e.g., drying of surface) (Marchment et al., 2017; Keita et al., 2019).

Fig. 3 shows an illustrative comparison of concrete mix proportions for all of the 3D-printable concrete, self-compacting concrete (SCC), and conventional concrete. 3D printable mixes were designed with higher fine aggregate and binder content than SCC and conventional concrete mixes to increase their properties, such as yield stress and shape retention capability. Based on previous research, the design of a 3D printable mix is an iterative process.

5.1. Influence of different types of Supplementary cementitious materials (SCM)

The inclusion of SCM in 3D printable concrete could have significant consequences for its properties. For instance, the early age strength is presented to be low, whereas the usage of a low dosage of metakaolin (MK) would enhance it. In addition, the presence of SCM provide a less porous microstructure, leading to an increase in durability properties such as using fly ash (FA) and silica fume (SF) can be used to improve resistance against chloride penetration.

3D printed concrete with binary and ternary blended mixtures have the capacity of resisting phase separation under pressure, providing optimized plastic viscosity and yield strength, and therefore improve the stability of the concrete. FA is suitable material in terms of workability (Long et al., 2017), while SF is beneficial to resist phase separation, it improves yield stress and plastic viscosity (Yazici, 2008; Meng et al., 2019; Vikan and Justnes, 2007); additionally, it improves the mechanical properties and impermeability of 3D printed concrete at hardened state (Kazemian et al., 2017). The volumetric stability and robustness of fresh concrete are also improved by the incorporation of SF (Kazemian et al., 2017; Rahul et al., 2019). Adding ultra-fine FA was found to be beneficial for the workability of printing mixture in terms of reducing yield stress and viscosity at fresh mix early stage. The combination of ordinary Portland cement (OPC), SF, FA, and fine sands achieve a high packing density, better rheological behaviour, and improved the strength (Nerella and Mechtcherine, 2019; Ma and Wang, 2018).

From environmental aspects, FA or ground granulated blast-furnace slag (GGBS) are ecofriendly materials. The estimation of sustainability for printable concrete with SCM should emphasize functional parameters such as pumpability, extrudability, and buildability, which are eased by the adoption of SF and FA. From this section could be concluded that the judicious use of SCM is essential for the design of sustainable 3D printable concrete.

5.2. Influence of aggregate content and type

Researchers have studied the effect of aggregate on the behaviour of 3D printable concrete. Zhang et al. (2019) investigated the influence of increasing the aggregate content on the rheology of concrete mix with a high thixotropy. Using

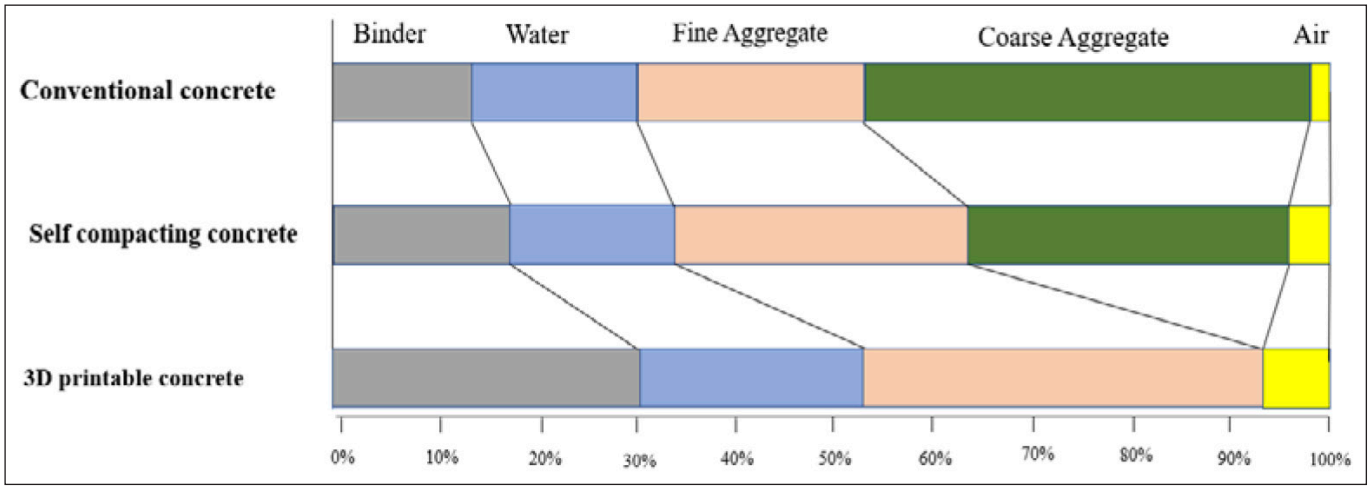

Fig. 3: *An illustrative of volumetric comparison of percentage materials used in 3D-printable concrete, self-compacting concrete, and conventional concrete (Rehman and Kim, 2021)*

different sand to binder ratio i.e., 0.6, 0.8, 1.0, 1.2, and 1.5. Results showed an increase in plastic viscosity and yield stress by 16.4% and 129.8%, where the sand to binder ratio increased from 0.6 to 1.2, while the thixotropy is reduced by 18%. Mohan et al. (2020) have noticed that increasing the sand to binder ratio from 1.0 to 1.4 increases yield stress and viscosity from 0.67 to 0.82 kPa and from 17.1 to 43.1 Pa·s, respectively.

Researchers have studied the use of recycled aggregate in 3D concrete printing, positive results have been observed in terms of buildability (Bai et al., 2021). Mine tailings residue was experimentally studied as a substitution for sand in the printable concrete (Álvarez-Fernández et al., 2021). The test results showed that using 30% of sand as mine tailings replacement produces optimum buildability and mechanical properties (Ma et al., 2018). Ding et al. (2020) investigated replacing natural sand with 25% and 50% recycled sand for printable concrete in terms of green strength and modulus of elasticity. Results showed that using recycled sand had an insignificant effect on mechanical properties up to the age of 90 min, whereas after 90 min, compressive strength and modulus of elasticity increased.

A few attempts to use printable concrete mixtures containing coarse aggregate have been reported: Rahul and Santhanam (2020) have printed mixtures containing lightweight coarse aggregate with sizes up to 8 mm (by using 30% of total aggregate content). Mechtcherine et al. (2019) used coarse aggregate up to 8 mm and printed ten layers (height of 500 mm).

While the experimental studies for 3D printing of cement-based materials generally focus on the printing process and on the mechanical properties of mortars (Roussel et al., 2020; Li et al., 2020), there are serious deficiencies such as early shrinkage cracking, long-term durability, weak interlayers, etc. Thus, this shortage of this technology seriously restrict its practical applications (Ma et al., 2020; Menna et al., 2020) and increases sustainability issues. The inclusion of coarse aggregate decreases the hydration heat and shrinkage, and it improves the volumetric stability of concrete (Shen et al., 2010). Therefore, incorporating coarse aggregate in printable mixtures is one of the important directions for researchers (Souza et al., 2020).

One of the challenges is that the use of coarse aggregate demands a nozzle with a larger cross-section to accommodate larger particles. The increase in the cross-section layer results in an increase in rate of concrete deposition, which is the product of cross-section layer and printhead speed, being a major parameter concerning productivity and thereby for economic sustainability. For instance, for a 0.4 m/s printhead speed, there is an increase of deposition rate from 0.58 m^3/h to 10.8 m^3/h for an increase of cross-section layer from 20 mm × 20 mm–150 mm × 50 mm (Storch et al., 2020). In this direction, using coarse aggregate provide additional values of static yield stress, helping obtain better shape stability and buildability for the print element.

However, Mechtcherine et al. (2019) stated that the presence of coarse aggregate in 3D-printing concrete, become more challenging compared to paste or mortar, especially at the printhead and on the rheological properties. 3D Printing of concrete having coarse aggregate requires more ambitious on the concrete conveyor in addition to the shaping tools of the printhead in terms of robustness, delivery rates, and resistance to wear (Mechtcherine et al., 2019). Yu et al. (2020) have proposed a solution for incorporating coarse aggregate by using particle bed printing method in which gravels with particle size range of 1.18–7 mm were spread over paste or mortar layers. The content of aggregate could reach 40%.

Several authors have used particle packing to minimize the binder content, to optimize the w/b ratio, and to mitigate the drying shrinkage (Kwan and Mora, 2002; Rozière et al., 2007). For a given paste volume, the increase in aggregate packing density could improve workability as a result of the increase in the paste excess thickness surrounding the particles of aggregate (Goltermann et al., 1997; Kwan and Li, 2012).

5.3 Chemical Admixtures

Concrete designed for printing purposes such as extrusion and buildability requires a high dosage of chemical admixtures. Dorn et al. (2020) studied the effect of admixtures on the setting time of printing concrete, results showed that the setting time can be controlled by accelerators such as sodium carbonate (Na_2CO_3), potassium carbonate (K_2CO_3), triethanolamine (TEA), and calcium nitrate ($Ca(NO_3)_2$). The proper use of these accelerators can judiciously regulate the setting time of printed mixtures within 5–150 min. However, the above admixtures affect the binder hydration and the crystallinity of a few hydration products. Khalil et al. (2017) investigate the effect of calcium sulfoaluminate (CSA) as a potential accelerator to control the concrete printability. A mixture containing 7% of CSA cement and 93% of OPC showed better extrudability and buildability and it improved the yield stress by 17 and 30 times compared to the reference mixture at the age of 20 and 25 min, respectively.

5.4 Nanomaterials

Researchers incorporated nanomaterials to concrete in order to modify the fresh performance in favour of 3D concrete printing (Song and Li, 2021; Sikora et al, 2021). Zhang et al. (2018) reported that cement containing 2% of nano-clay increases the concrete buildability by about 150% compared with the reference mixture. Moreover, presence of nano-clay in the concrete mix increases its shape stability (Kazemian et al., 2017). Kruger et al. (2019) concluded that using 1% nano-silica increased the concrete thixotropy. Chen et al. (2020) reported that the addition of bentonite improves the thixotropic behaviour of the printable concrete. Szostak and Golewski (2020) results showed that adding nano-calcium silicate hydrate (CSH) seeds to concrete mix reduces the setting time and shows a rapid increase in the earlier strength. Using nano-graphite platelets improve the thermal conductivity of the cementitious materials as well as provide self-sensing capability in concrete.

Incorporating nanoparticles to printable concrete increased the buildability, shape retention, mechanical properties, and interlayer bond strength. Several studies suggest that nanomaterials are beneficial for regulating concrete rheology and for optimizing the printability, but still the cost of nanomaterials is higher compared to the other ingredients of concrete.

6. DURABILITY

Several researchers have been performed different studies on the durability of 3D printed concrete. The properties of concrete constructed by layers is affected by the printing time gap and environmental conditions and therefore limit the durability. Formation of microcracks at the layer as a result

of shrinkage during the printing time gap could permit the ingress of water, chloride penetration. Meanwhile, the freeze-thaw cycling could make the interlayer joints vulnerable and weaken the bond strength (Van Der Putten et al., 2020a; Van Der Putten et al., 2020b).

7. CONCLUSIONS

This paper reviews the latest research on 3D concrete from the standpoint of materials. Rheological properties, compatible design mix, and the effect of SCM, aggregate, chemical admixtures on the 3D concrete mix are discussed to help researchers and engineers recognize the procedures for reaching their own mix. The following co points are concluded from this review work:

- SCM binders such as silica fume, metakaolin, fly ash, nanoparticles, and chemical additives are very useful for governing the rheology of printable concrete according to the requirements of the process.
- The effect of rheology, printing process, porosity, and shrinkage cracks on the durability behaviour of printed concrete require investigation.
- Special attention should be applied to the mechanical properties of 3D-printed concrete.
- Incorporating coarse aggregate into printable concrete is an important future direction for researchers. The presence of coarse aggregate decrease the hydration heat and shrinkage of concrete and improves volumetric stability, in addition to its low cost.

8. ACKNOWLEDGEMENTS

Authors acknowledge the support by the Hungarian Research Grant Project-VKE 2018-1-3-1 Developement of concrete products supported by techniques of material science.

9. REFERENCES

ACI 304.2R-96. Placing Concrete by Pumping Methods. (2008)

Aïtcin, P.C. The Influence of the Water/cement Ratio on the Sustainability of Concrete. Butterworth-Heinemann (2019), Lea's Chemistry of Cement and Concret, 4th ed.; Hewlett, PC, Liska, M., Eds, pp. 807-826. https://doi.org/10.1016/B978-0-08-100773-0.00017-4

Álvarez-Fernández, M.I., Prendes-Gero, M.B., González-Nicieza, C., Guerrero-Miguel, D.J. and Martínez-Martínez, J.E. Optimum Mix Design for 3D Concrete Printing Using Mining Tailings: A Case Study in Spain. Sustainability 13 (2021), pp. 1568. https://doi.org/10.3390/su13031568

Bai, G., Wang, L., Ma, G., Sanjayan, J. and Bai, M. 3D printing eco-friendly concrete containing under-utilised and waste solids as aggregates. Cem. Concr. Compos. 120 (2021), pp. 104037. https://doi.org/10.1016/j.cemconcomp.2021.104037

Buswell, R.A., De Silva, W.L., Jones, S.Z. and Dirrenberger, J. 3D printing using concrete extrusion: a roadmap for research. Cem. Concr. Res., 112 (2018), pp. 37-49, https://doi.org/10.1016/j.cemconres.2018.05.006

Chen, M., Liu, B., Li, L., Cao, L., Huang, Y., Wang, S., Zhao, P., Lu, L., Cheng, X. Rheological parameters, thixotropy and creep of 3D-printed calcium sulfoaluminate cement composites modified by bentonite. Compos. Pt. B-Eng., 186 (2020). https://doi.org/10.1016/j.compositesb.2020.107821

Diggs-McGee, B.N., Kreiger, E.L., Kreiger, M.A., Case, M.P. Print time vs. elapsed time: a temporal analysis of a continuous printing operation for additive constructed concrete. Addit. Manuf., 28 (2019), pp. 205-214. https://doi.org/10.1016/j.addma.2019.04.008

Ding, T., Xiao, J., Qin, F., Duan, Z. Mechanical behavior of 3D printed mortar with recycled sand at early ages. Constr. Build. Mater. 248 (2020), pp. 118654. https://doi.org/10.1016/j.conbuildmat.2020.118654

Dorn, T., Hirsch, T., Stephan, D. Study on the influence of accelerators on the hydration of portland cement and their applicability in 3D printing V. Mechtcherine, K. Khayat, E. Secrieru (Eds.), Rheology and Processing of Construction Materials, Springer International Publishing, Cham (2020), pp. 382-390. https://doi.org/10.1007/978-3-030-22566-7_44

Gibbons, G.J., Williams, R., Purnell, P. and Farahi, E. 3D printing of cement composites. Adv. Appl. Ceram., 109 (2010), pp. 287-290. https://doi.org/10.1179/174367509X12472364600878

Goltermann, P., Johansen, V., Palbøl, L. Packing of aggregate: an alternative tool to determine the optimal aggregate mix. ACI Mater. J., 94 (1997), pp. 435-443

Gosselin, C., Duballet, R., Roux, P., Gaudillière, N., Dirrenberger, J., Morel, P. Large-scale 3D printing of ultra-high performance concrete – a new processing route for architects and builders. Mater Des, 100 (2016), pp. 102-109. https://doi.org/10.1016/j.matdes.2016.03.097

Jeong, H., Han, S.J., Choi, S.H., Lee, Y.J., Yi, S.T. and Kim, K.S. Rheological property criteria for buildable 3D printing concrete. Materials, 12 (2019), pp. 1-21. https://doi.org/10.3390/ma12040657

Ji, G., Ding, T., Xiao, J., Du, S., Li, J., Duan, Z. A 3D printed ready-mixed concrete power distribution substation: materials and construction technology. Materials (Basel), 12 (2019). https://doi.org/10.3390/ma12091540

Kazemian, A., Yuan, X., Cochran, E., Khoshnevis, B. Cementitious materials for construction-scale 3D printing: laboratory testing of fresh printing mixture. Construct. Build. Mater., 145 (2017), pp. 639 647. https://doi.org/10.1016/j.conbuildmat.2017.04.015

Keita, E., Bessaies-Bey, H., Zuo, W., Belin, P. and Roussel, N. Weak bond strength between successive layers in extrusion-based additive manufacturing: measurement and physical origin. Cement Concr. Res., 123 (2019). https://doi.org/10.1016/j.cemconres.2019.105787

Khalil, N., Aouad, G., El Cheikh, K., Rémond, S. Use of calcium sulfoaluminate cements for setting control of 3D-printing mortars. Constr. Build. Mater., 157 (2017), pp. 382-391. https://doi.org/10.1016/j.conbuildmat.2017.09.109

Kim, J.H., Kwon, S.H., Kawashima, S. and Yim, H.J. Rheology of cement paste under high pressure. Cement Concr. Compos., 77 (2017), pp. 60-67. https://doi.org/10.1016/j.cemconcomp.2016.11.007

Kruger, J., Zeranka, S., van Zijl, G. A rheology-based quasi-static shape retention model for digitally fabricated concrete. Construct. Build. Mater., 254 (2020). https://doi.org/10.1016/j.conbuildmat.2020.119241

Kruger, J., Zeranka, S., van Zijl, G. An ab initio approach for thixotropy characterisation of (nanoparticle-infused) 3D printable concrete. Constr. Build Mater., 224 (2019), pp. 372-386. https://doi.org/10.1016/j.conbuildmat.2019.07.078

Kwan A., Mora, C. Effects of various, shape parameters on packing of aggregate particles. Mag. Concr. Res., 53 (2002), pp. 91-100. https://doi.org/10.1680/macr.2001.53.2.91

Kwan, A.K.H., Li, L.G. Combined effects of water film thickness and paste film thickness on rheology of mortar. Mater. Struct., 45 (2012), pp. 1359-1374. https://doi.org/10.1617/s11527-012-9837-y

Le, T.T., Austin, S.A., Lim, S., Buswell, R.A., Gibb, A.G. and Thorpe, T. Thorpe Mix design and fresh properties for high-performance printing concrete. Mater Struct, 45 (8) (2012), pp. 1221-1232. https://doi.org/10.1617/s11527-012-9828-z

Li, V.C., Bos, F.P., Yu, K., McGee, W., Ng, T.Y., Figueiredo, S.C., Nefs, K., Mechtcherine, V., Nerella, V.N., Pan, J. and van Zijl, G.P. On the emergence of 3D printable engineered, strain hardening cementitious composites (ECC/SHCC). Cement Concr. Res., 132 (2020), p. 106038. https://doi.org/10.1016/j.cemconres.2020.106038

Lim, S., Buswell, R.A., Le, T.T., Austin, S.A., Gibb, A.G.F., Thorpe, T. Developments in construction-scale additive manufacturing processes. Autom. Constr., 21 (2012), pp. 262-268. https://doi.org/10.1016/j.autcon.2011.06.010

Long, W.J., Gu, Y., Liao, J., Xing, F. Sustainable design and ecological evaluation of low binder self-compacting concrete. J. Clean. Prod., 167 (2017), pp. 317-325. https://doi.org/10.1016/j.jclepro.2017.08.192

Lowke, D., Dini, E., Perrot, A., Weger, D., Gehlen, C., Dillenburger, B. Particle-bed 3D printing in concrete construction – possibilities and challenges. Cem. Concr. Res., 112 (2018), pp. 50-65. https://doi.org/10.1016/j.cemconres.2018.05.018

Lu, B., Weng, Y., Li, M., Qian, Y., Leong, K.F., Tan, M.J., Qian, S. A systematical review of 3D printable cementitious materials. Constr. Build. Mater. 207 (2019), pp. 477–490. https://doi.org/10.1016/j.conbuildmat.2019.02.144

Ma, G., Li, Z., Wang, L. Printable properties of cementitious material containing copper tailings for extrusion based 3D printing. Construct. Build. Mater., 162 (2018), pp. 613-627. https://doi.org/10.1016/j.conbuildmat.2017.12.051

Ma, G., Salman, N.M., Wang, L. and Wang, F. A novel additive mortar leveraging internal curing for enhancing interlayer bonding of cementitious composite for 3D printing. Construct. Build. Mater., 244 (2020), p. 118305. https://doi.org/10.1016/j.conbuildmat.2020.118305

Marchment, T., Xia, M., Dodd, E., Sanjayan, J., Nematollahi, B. Effect of delay time on the mechanical properties of extrusion-based 3D printed concrete. ISARC 2017 - Proc. 34th Int. Symp. Autom. Robot. Constr. (2017), pp. 240-245. https://doi.org/10.22260/ISARC2017/0032

Mechtcherine, V., Nerella, V.N., Will, F., Näther, M., Otto, J. and Krause, M. Large-scale digital concrete construction – CONPrint3D concept for on-site, monolithic 3D-printing. Autom. ConStruct., 107 (2019), p. 102933. https://doi.org/10.1016/j.autcon.2019.102933

Meng, W., Kumar, A., Khayat, K.H. Effect of silica fume and slump-retaining polycarboxylate-based dispersant on the development of properties of portland cement paste. Cement Concr. Compos., 99 (2019), pp. 181-190. https://doi.org/10.1016/j.cemconcomp.2019.03.021

Menna, C., MataFalcón, J., Bos, F.P., Vantyghem, G., Ferrara, L., Asprone, D., Salet, T., Kaufmann, W. Opportunities and challenges for structural engineering of digitally fabricated concrete. Cement Concr. Res., 133 (2020), p. 106079. https://doi.org/10.1016/j.cemconres.2020.106079

Mohan, M.K., Rahul, A.V., Van Tittelboom, K., De Schutter, G. Evaluating the Influence of Aggregate Content on Pumpability of 3D Printable Concrete. In Proceedings of the Second RILEM International Conference on Concrete and Digital Fabrication, Eindhoven, The Netherlands, 6–9 July 2020; Springer: Cham, Switzerland, (2020) pp. 333–341. https://doi.org/10.1007/978-3-030-49916-7_34

Nerella, V.N., Mechtcherine, V. Studying the printability of fresh concrete for formwork-free concrete onsite 3D printing technology (CONPrint3D) J.G. Sanjayan, A. Nazari, B. Nematollahi (Eds.), 3D Concr. Print. Technol., Butterworth-Heinemann (2019), pp. 333-347. https://doi.org/10.1016/B978-0-12-815481-6.00016-6

Nerella, V.N., Näther, M., Iqbal, A., Butler, M., Mechtcherine, V. Inline quantification of extrudability of cementitious materials for digital construction. Cem. Concr. Compos., 95 (2019), pp. 260 270. https://doi.org/10.1016/j.cemconcomp.2018.09.015

Nerella, V.N., Krause, M., Mechtcherine, V. Direct printing test for buildability of 3D-printable concrete considering economic viability. Autom. ConStruct., 109 (2020), p. 102986. https://doi.org/10.1016/j.autcon.2019.102986

Ngo, T.D., Kashani, A., Imbalzano, G., *et al.* Additive manufacturing (3D printing): a review of materials, methods, applications and challenges. Compos. Part B Eng., 143 (2018), pp. 172-196. https://doi.org/10.1016/j.compositesb.2018.02.012

Panda, B., Tan, M.J. Experimental study on mix proportion and fresh properties of fly ash based geopolymer for 3D concrete printing. Ceram. Int., 44 (2018), pp. 10258-10265. https://doi.org/10.1016/j.ceramint.2018.03.031

Panda, B., Lim, J.H., Tan, M.J. Mechanical properties and deformation behaviour of early age concrete in the context of digital construction. Compos. B Eng., 165 (2019), pp. 563-571. https://doi.org/10.1016/j.compositesb.2019.02.040

Papachristoforou, M., Mitsopoulos, V., Stefanidou, M. Evaluation of workability parameters in 3D printing concrete. Procedia Struct. Integr. 10 (2018), pp. 155–162. https://doi.org/10.1016/j.prostr.2018.09.023

Perrot, A., Rangeard D., Pierre, A. Structural built-up of cement-based materials used for 3D-printing extrusion techniques. Mater. Struct., 49 (2016), pp. 1213-1220. https://doi.org/10.1617/s11527-015-0571-0

Perrot, A., Rangeard, D. 3D Printing in Concrete: Techniques for Extrusion/Casting. In 3D Printing of Concrete; Wiley & Sons Inc.: Hoboken, NJ, USA, (2019), pp. 41–72. https://doi.org/10.1002/9781119610755.ch2

Rahul, A.V., Santhanam, M. Evaluating the printability of concretes containing lightweight coarse aggregates. Cement Concr. Compos., 109 (2020), p. 103570. https://doi.org/10.1016/j.cemconcomp.2020.103570

Rahul, A.V., Santhanam, M., Meena, H., Ghani, Z. 3D printable concrete: mixture design and test methods. Cement Concr. Compos., 97 (2019), pp. 13-23. https://doi.org/10.1016/j.cemconcomp.2018.12.014

Rahul, A.V., Sharma, A., Santhanam, M. A desorptivity-based approach for the assessment of phase separation during extrusion of cementitious materials. Cement Concr. Compos., 108 (2020), p. 103546. https://doi.org/10.1016/j.cemconcomp.2020.103546

Rehman, A.U. and Kim, J.H. 3D concrete printing: A systematic review of rheology, mix designs, mechanical, microstructural, and durability characteristics. Materials, 14(14) (2021), pp.3800. https://doi.org/10.3390/ma14143800

Roussel, N. A thixotropy model for fresh fluid concretes: theory, validation and applications. Cement Concr. Res., 36 (2006), pp. 1797-1806. https://doi.org/10.1016/j.cemconres.2006.05.025

Roussel, N. Rheological requirements for printable concretes. Cement Concr. Res., 112 (2018), pp. 76-85. https://doi.org/10.1016/j.cemconres.2018.04.005

Roussel, N., Spangenberg, J., Wallevik, J. and Wolfs, R. **Numerical simulations** of concrete processing: from standard formative casting to additive manufacturing. Cement Concr. Res., 135 (2020), p. 106075. https://doi.org/10.1016/j.cemconres.2020.106075

Rozière, E., Granger, S., Turcry, P., Loukili, A. Influence of paste volume on shrinkage cracking and fracture properties of self-compacting concrete. Cement Concr. Compos., 29 (2007), pp. 626 636. https://doi.org/10.1016/j.cemconcomp.2007.03.010

Shakor, P., Nejadi, S., Paul, G., Sanjayan, J. and Nazari, A. Mechanical properties of cement-based materials and effect of elevated temperature on three-dimensional (3-D) printed mortar specimens in inkjet 3-D printing. ACI Mater. J., 116 (2019), pp. 55-67. https://doi.org/10.14359/51714452

Shen, W., Dong, R., Li, J., Zhou, M., Ma, W., Zha, J. Experimental investigation on aggregate interlocking concrete prepared with scattering–filling coarse aggregate process. Construct. Build. Mater., 24 (11) (2010), pp. 2312-2316. https://doi.org/10.1016/j.conbuildmat.2010.04.023

Sikora, P., Chougan, M., Cuevas, K., Liebscher, M., Mechtcherine, V., Ghaffar, S.H., Liard, M., Lootens, D., Krivenko, P., Sanytsky, M. and Stephan, D. The effects of nano- and micro-sized additives on 3D printable cementitious and alkali-activated composites: A review. Appl. Nanosci, 2021. https://doi.org/10.1007/s13204-021-01738-2

Song, H., Li, X. An Overview on the Rheology, Mechanical Properties, Durability, 3D Printing, and Microstructural Performance of Nanomaterials in Cementitious Composites. Materials, 14 (2021), pp. 2950. https://doi.org/10.3390/ma14112950

Souza, M.T., Ferreira, I.M., de Moraes, E.G., Senff, L. and de Oliveira, A.P.N. 3D printed concrete for large-scale buildings: an overview of rheology, printing parameters, chemical admixtures, reinforcements, and economic and environmental prospects. J. Build. Eng., 32 (2020), p. 101833. https://doi.org/10.1016/j.jobe.2020.101833

Storch, F., Krenzer, K., Nerella, V.N., Simon, M., Will, F. and Mechtcherine, V. Development of a printhead for large-scale, extrusion-based additive manufacturing with coarse aggregate concrete. Construct. Print. Technol., 4 (2020), pp. 16-21

Suiker, A.S.J. Mechanical performance of wall structures in 3D printing processes: theory, design tools and experiments. Int. J. Mech. Sci., 137 (2018), pp. 145-170. https://doi.org/10.1016/j.ijmecsci.2018.01.010

Szostak, B., Golewski, G.L. Modification of early strength parameters of concrete by the addition of fly ash and admixture of nano CSH for application in 3D printing. In Proceedings of the MATEC Web of Conferences, Lubin, Poland, 21–23 October 2020, pp. 01016. https://doi.org/10.1051/matecconf/202032301016

Van Der Putten, J., Azima, M., Van den Heede, P., Van Mullem, T., Snoeck, D., Carminati, C., Hovind, J., Trtik, P., De Schutter, G. and Van Tittelboom, K. Neutron radiography to study the water ingress via the interlayer of 3D printed cementitious materials for continuous layering. Construct. Build. Mater., 258 (2020b), p. 119587. https://doi.org/10.1016/j.conbuildmat.2020.119587

Van Der Putten, J., De Volder, M., Van den Heede, P., De Schutter, G., Van Tittelboom, K. 3D printing of concrete: the influence on chloride penetration. F.P. Bos, S.S. Lucas, R.J.M. Wolfs, T.A.M. Salet (Eds.), Second RILEM Int. Conf. Concr. Digit. Fabr. – Digit. Concr, Springer (2020a), pp. 500-507. https://doi.org/10.1007/978-3-030-49916-7_51

Vanhove, Y., Khayat, K.H. Forced bleeding test to assess stability of flowable concrete. ACI Mater. J., 113 (2016), pp. 753-758. https://doi.org/10.14359/51689240

Vikan, H., Justnes, H. Rheology of cementitious paste with silica fume or limestone. Cement Concr. Res., 37 (2007), pp. 1512 1517. https://doi.org/10.1016/j.cemconres.2007.08.012

Wangler, T. Digital Concrete: Research and Applications. Proc. 10th Int. Concr. Congr, 35 (2019), pp. 2–12.

Wangler, T., Lloret, E., Reiter, L., Hack, N., Gramazio, F., Kohler, M., Bernhard, M., Dillenburger, B., Buchli, J., Roussel, N. and Flatt, R. Digital concrete: opportunities and challenges. RILEM Tech. Lett., 1 (2016), p. 67. https://doi.org/10.21809/rilemtechlett.2016.16

Wolfs, R.J.M., Suiker, A.S.J. Structural failure during extrusion-based 3D printing processes. Int. J. Adv. Manuf. Technol., 104 (2019), pp. 565-584. https://doi.org/10.1007/s00170-019-03844-6

Xia, M., Nematollahi, B., Sanjayan, J. Printability, accuracy and strength of geopolymer made using powder-based 3D printing for construction applications. Autom. Constr., 101 (2019), pp. 179-189. https://doi.org/10.1016/j.autcon.2019.01.013

Yazici, H. The effect of silica fume and high-volume Class C fly ash on mechanical properties, chloride penetration and freeze-thaw resistance of self-compacting concrete. Construct. Build. Mater., 22 (2008), pp. 456-462. https://doi.org/10.1016/j.conbuildmat.2007.01.002

Yu, S., Du, H., Sanjayan, J. Aggregate-bed 3D concrete printing with cement paste binder. Cement Concr. Res., 136 (2020), p. 106169. https://doi.org/10.1016/j.cemconres.2020.106169

Zareiyan, B. and Khoshnevis, B. Interlayer adhesion and strength of structures in Contour Crafting-Effects of aggregate size, extrusion rate, and layer thickness. Automation in Construction, 81 (2017), pp.112-121. https://doi.org/10.1016/j.autcon.2017.06.013

Zhang, Y., Zhang, Y., Liu, G., Yang, Y., Wu, M., Pang, B. Fresh properties of a novel 3D printing concrete ink. Construct. Build. Mater., 174 (2018), pp. 263-271. https://doi.org/10.1016/j.conbuildmat.2018.04.115

Zhang, Y., Zhang, Y., She, W., Yang, L., Liu, G., Yang, Y. Rheological and harden properties of the high-thixotropy 3D printing concrete. Constr. Build. Mater. 201 (2019), pp. 278–285. https://doi.org/10.1016/j.conbuildmat.2018.12.061

Abdelmelek Nabil (1992) is a PhD at the Department of Construction Materials and Technologies, Budapest University of Technology and Economics. His main fields of research interest are fire design and behaviour of concrete at elevated temperatures. Member of the Hungarian Group of ***fib***. abdelmelek.nabil@emk.bme.hu

György L. Balázs (1958), Civil Engineer, PhD, Dr.-habil., Professor of structural engineering at the Department of Construction Materials and Technologies of Budapest University of Technology and Economics (BME). His main fields of activities are experimental investigation and modelling of RC, PC, FRC, FRP, HSC, HPC, LWC, fire resistance and fire design, durability, sustainability, bond and cracking. He is chairman of several commissions and task groups of ***fib***. He is president of Hungarian Group of ***fib***, Editor-in-chief of the Journal "Concrete Structures". He was elected as President of ***fib*** for the period of 2011-2012. Since then, he is Honorary President of ***fib***. Chairman of ***fib*** Com 9 Dissemination of knowledge. balazs.gyorgy@emk.bme.hu

3D PRINTING TECNOLOGY IN MEDICINE - REVIEW


Marwah M. Thajeel – György L. Balázs

https://doi.org/10.32970/CS.2022.1.9

This paper presents a review of 3D printing technology in medical application, materials used in 3D bioprinting, benefits, challenges as well as the future of additive manufacturing in medicine. This technology is going to revolutionize medicine, the flexibility of 3D printing allows designers to make changes easily without the need to set up additional equipment or tools. 3D bioprinting have a promising potential in organ transplantations and help to overcome in donor shortages issue. Printed highly accurate 3D model depending on the patient's MRI or CT scans, help the surgeons to planning before surgery and have more successful operations, as well as reduce time in the operating room

Keywords: 3D bioprinting, tissue engineering, organs printing, prosthetics

1. INTRODUCTION

1.1 General

3D printing or also known as *Additive manufacturing or layered manufacturing* are used to create a physical 3D object layer by layer from computer-aided-design (CAD) software. Due to numerous benefits of this technique such as quick production with any complex shape and enhancement of printing speed and precision, has been applied to and utilized by many different industries, including medical technology. The surgical planning, preparation of organ models, fast production of personalized scaffolds, and immediate printing at the defect site can be carried out by additive manufacturing technology based on a patient's imaging data such as X-rays, computed tomography (CT) scans, magnetic resonance imaging (MRI) scans and ultrasounds (U.S. FDA, 2020), which is subsequently fed into the 3D printer (Pati et. al. 2016), printed model of congenital heart defects from CT scan data using two different 3D printing technics (*Fig. 1*).

Layered manufacturing brings new possibilities to the medical fields for building bionic organs or tissue and solving the problem of donor shortage (Kalaskar, 2017). In this regards, current paper shows the materials used in 3D printing technology in medical field, advantages, limitations, applications and the future of 3D printing technology in medicine.

1.2 3D bioprinting Materials

Generally, the 3D printed materials used in medicine must be printable, have adequate mechanical characteristics, biocompatible and biodegradable.

Bioactive and degradable materials used for drug delivery and tissue engineering applications such as ceramics, polymers and hydrogels. These materials should have the right chemical and physical qualities to support and maximize re-

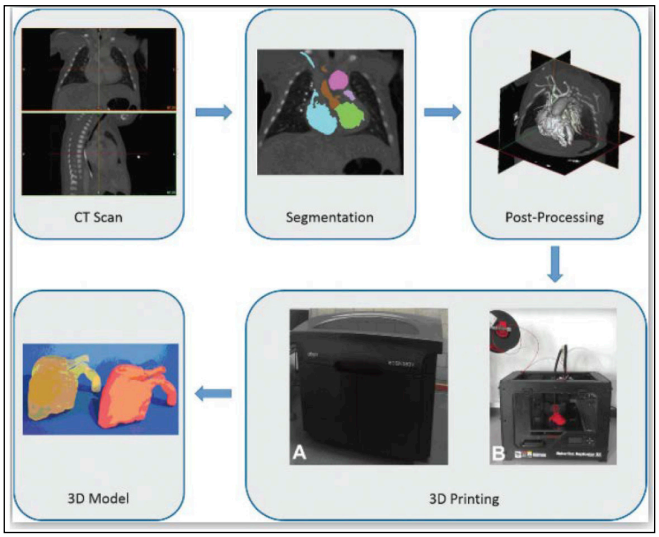

Fig. 1: 3D printed congenital heart defects model from CT scan data (Pati et. al. 2016)

generation, and it should degrade into harmless compounds that the host tissue can remove from the implantation site once the job is done (Jones, 2013; Mok et al., 2016).

Williams (2008), defines the biocompatibility as 'the ability of a biomaterial to perform its desired function with respect to a medical therapy, without eliciting any undesirable local or systemic effects in the recipient or beneficiary of that therapy, but generating the most appropriate beneficial cellular or tissue response in that specific situation, and optimizing the clinically relevant performance of that therapy'. For example, use non-degradable implants such as metals, polymers and ceramics for long term, they may corrode or wear, leading in the release of ions and wear debris, which may have undesired local or systemic consequences (Hallab et al., 2001; Gepreel and Niinomi, 2013). As a result, materials for long term use should be corrosion and wear resistant, emit little debris, and not cause the host system to react negatively.

2. ADVANTAGES

3D printing technology offers remarkable advantages for biomedical devices and tissue engineering due to its ability to produce low-volume parts that can be customized to meet the exact needs of patients. For instance, surgical implants are actually fabricated by casting in a mold for a desired part followed by chemical treatments for mechanical properties, required surface and aesthetic effects. These processes demand costly machinery, as well as the difficulty of titanium alloys crafting because of low elastic modulus, high mechanical strength and low thermal conductivity compared to steel make these material more expensive to manufacture a specific graft (Balazic et al., 2007). These operations can also produce a huge a mounts of material waste and energy intensive. 3D printing offers a new way to make a verity of practical biomedical products such as orthopedic grafts.

The advantages of using layered manufacturing technology over traditional manufacturing methods include its ability to provide designers with more freedom to create lightweight and customized implants and effectively solve the donor shortage problem for organ transplantations. Although 3D printing doesn't require specific tools or components, the cost per part remains constant. From minimally invasive surgery to cancer therapy, and from birth defect treatment to functional prostheses for amputees, all sectors of medicine and surgery are looking for advances enabled by 3D printing to improve human life quality or help patients live longer. Further development of human tissue and organs using this technology is still challenging due to its various limitations (Woodruff et al., 2012; Hutmacher et al., 2013).

3. LIMITATIONS

Despite the potential advantages of 3D printing in the medical product is still require extensive research and development to be truly effective. The lack of variety and diversity in 3D printable biomaterials is one of the major challenges. Although many printable materials have excellent properties for many other external applications, biocompatible implantable materials require specific properties that take into account both physiological conditions and interactions with the local body environment, making development much more difficult (Tasoglu and Demirci, 2013). For example, metal materials commonly used for permanent implants due to good mechanical properties, but the high elastic modulus of the metals might cause an elastic incompatible between the bone and the implant. Natural polymers such as sodium, collagen and alginate have a strong biocompatibility but low mechanical properties. Furthermore, there are no international standards for selecting medical materials for 3D printing; as a result, only synthetic evaluations based on function, structure, and clinical effects, rather than evaluations based on reliable indicators and sufficient experimental evidence.

Although cells can be directly printed at this stage, considerable work remains to be done in order to attain the aim of in vitro tissue engineering (Quan, 2015). Because the Extra Cellular Matrix (ECM) is a complex system with various components, it is challenging to reproduce its structure and biological activity in vitro. Current approaches, which predominantly stack cell-seeded hydrogels, are unable to address cellular nutrition and oxygen supply concerns. A significant number of cells cannot be provided for larger scaffolds at this time. Preprophase cells do not acquire an appropriate supply of nutrients as compared to cells that connect to the surface of scaffolds. That is, the cells persist in 3D space in a state of disequilibrium (Yan et al., 2010). For the continued development of printed scaffolds, tissues, and organs, further restrictions such as cell survival, development, differentiation, and fusion must be overcome.

4. 3D BIOPRINTING APPLICATIONS

Blood vessels, cells, cartilages, bandages, bones, maxillofacial implants and liver tissues for drug tests have all been successfully printed using 3D printing technology (Ozbolat and Yu, 2013; Ventola, 2014). In the following sub-sections will discuss the medical applications in tissues and organs printing, surgical planning, prosthetics and implants and medical training.

4.1 Tissues and organs printing

3D printing is already being utilized in studies to create tissue structures and human organ (Mannoor et al., 2013; Sawkins et al., 2015). 3D bioprinting can be combined with biocompatible microfluidics to produce highly complex structures that work similarly to natural human organs and able one to print living tissues with high speed and precision (Kolesky et al., 2014). This technology has the potential to transform medicine, printing organs directly in the body in the operating room, or printing organs that could be transferred to human donors. However, it's a challenging task to use biocompatible tissue constructs perfused with vascular network, also creates time constraints when printing living cells because to avoid cell damage due to the lack of oxygen.

One of the potential ways to print 3D cell structure is to add the cells in a scaffold. Scaffold is made out of biodegradable materials, due to facility of bio-printability and naivety of the structure, are widely used by researchers (Chua and Wai, 2015). However, it can be a challenge when use to construct small diameters blood vessels (Weinberg and Bell, 1986). (Kachouie et al., 2010) produced a new technique free from scaffold where cells encased in hydrogel were utilized to form tissue blocks that mimicked the target tissue or organ in specified geometric patterns.

Autologous grafts have traditionally been utilized to replace missing segments. These grafts are taken from another region of the patient's body, and this procedure has the potential to result in the loss of function at the donor site (Millesi, 2007). Functional nerve grafts for the treatment of peripheral nerve lesions were also produced using this technology, researchers were able to bio-print a nerve graft (Marga et al. 2012).

Faulkner et al. (2015) showed the ability of 3D bio-printing to print mini-livers using cultivated, patient-specific cells to introduce 3D objects that are function and viable for weeks after printing like a native liver. The goal of this research to develop personalized medicine and animal-free medication trials. While (Reiffel et al. 2013) showed the capability of the 3D printing technique to construct complicated geometries by printing a human-sized artificial ear.

4.2 Surgical planning

Surgical planning is one of the potential applications of 3D printing that has surfaced (*Fig. 2*). A highly trained and experienced surgeon who can make quick decisions during the operation is required for operational surgery on complex organs like the brain and heart, as well as anatomical specimens

Fig. 2: 3D printing- medical applications (a) 3D printed brain model (Ploch, et. al. 2016), (b) Patient holding her heart model used in planning for a double aortic arch surgery at Nicklaus Children's Hospital (Adams et. al., 2018)

like the pelvis and spinal cord. Surgeons can use 3D models to evaluate the damaged organs, explore various approaches, and gain hands-on experience. This approach dramatically reduces operation time and, as a result, improves the surgical outcome for patients, surgeons, and their care providers (Klein et al., 2013).

4.3 Prosthetics and implants

Recent advances in 3D printed affordable and patient custom-fit prosthetics help to improve people's life who suffered from hereditary deformity or accident (Elahinia et al., 2012) (*Fig. 3*). Within 24 hours, prosthetic limbs of any shape, size, or complexity can be created using a patient's CT or MRI pictures (Ventola, 2014).

Making customized dental implants was one of the first medical applications of 3D printing. Rapid prototypes, dental crowns and trial restorations are all regularly prepared using 3D printing technology (Eggbeer et al., 2005, Berman, 2012). The preparation of dental prosthesis can be greatly accelerated and improved with 3D printing. It was discovered that fabricating surgical guides enhanced the accuracy of dental implant placement (Liu et al., 2006).

Fig. 3: 3D printed titanium thumb prosthesis (Adams et. al., 2018)

Several cases of successful procedures using 3D printed polyetherketoneketone implants to replace parts of the skull have been described (Foletti et al., 2012). Printed cranial implants can be used to replace a patient's skull and can be designed to fit the defect properly using MRI or CT images. Plastic implants can also be manufactured more quickly than traditional titanium cranial implants. This is a significant factor since it allows patients to save time and reduces the risk of infection and brain damage.

4.4 Medical training

The use of cadaveric materials to train new medical doctors has been controversial. This is due to both ethical concerns and the high cost of the procedures. For many circumstances, including those in which using a cadaver is not an option, 3D printing technology may offer an innovative and successful substitute by replicating accurate complicated anatomical organs using high resolution MRI or CT scans. Furthermore, 3D printing's capacity to generate several replicas of any anatomical subject in various sizes provides a significant benefit in training facilities (Sheth et al., 2016).

5. 3D BIOPRINTING FUTURE

3D bioprinting of in vitro models is an exciting area of research that has yielded some promising preliminary results in recent years. The large range of 3D printing processes now accessible has enormous potential for facilitating the creation of realistic in vitro models. A comprehensive grasp of the principle, optimization, and standardization of the printing process with respect to the ultimate desired objective, as well as compliance with good manufacturing practice, are required for the effective application of 3D printed tissues as in vitro disease models. As a result, tactics aimed at understanding the various stages of disease progression and development within 3D printed tissue grafts are in high demand.

Using these revolutionary 3D printing technologies, the cost of drug screening on illness models can be significantly decreased by miniaturization while keeping its unique physiological features. The cost can be decreased even more by sharing digital data among users in research communities. 3D printed in vitro disease or tissue models, on the other hand, could be a potent substitute for in vivo animal models or even human clinical trials in drug development, cosmetics development, and toxicological testing, making it an attractive alternative for translational medical research.

Because of its adaptability, 3D printing may be used in a variety of nontraditional medical applications, including the construction of smart sensors for monitoring, precise

bio-scaffolds, mechanobiology platforms, small implanted devices, and the integration of sensing and signaling. This, however, necessitates more research into a new class of printer-friendly biomaterials. Aside from novel materials, new hardware and software interfaces are needed to print varied materials at higher spatial resolutions than are now accessible (Kalaskar, 2017).

6. CONCLUSION

The development of 3D printing applications is a significant step forward in modern biomedicine. 3D printing's flexibility allows designers to make modifications quickly and simply without the need for extra equipment or instruments. These capabilities have inspired a surge in interest in medical 3D printing. There is no doubt that 3D printing, in general, may serve hugely persisting needs in today's healthcare systems, as it is projected to facilitate the supply of necessary devices and materials, making the entire manufacturing process less time and money consuming.

When choosing a material for medical applications, a variety of factors must be considered; not only must the material properties be adequate for the use, but the host tissue reaction after implantation must also be considered. In general, materials use in 3D bioprinting should be biocompatible, biodegradable and have good mechanical properties.

3D printing technology is going to transform medicine, whether it is patient specific surgical models, custom-made prosthetics, personalized on-demand medicines, or even 3D-printed human tissue. As its core 3D printing is the use of computer guidance technology to create 3D objects.

In the future, 3D bioprinting technology may be used to create therapeutically appropriate tissues and complex organs, which could change organ transplantation by addressing challenges such as donor scarcity, rejection and infection. In an ideal world, stem cells taken from a single patient might be developed into organ-specific cells and put into a bioprinting technology to create a personalized functional organ.

In medicine, 3D bioprinting still offers a lot of potential, and it will undoubtedly transform areas like tissue engineering, drug screening, and high-throughput biological testing. Despite its enormous potential for tissue regeneration and drug screening, this technology is still in its early stages and a lot of biological and engineering challenges still have to be addressed.

7. ACKNOLEDGEMENT

Stipendium Hungaricum Scholarship Program is highly acknowledged for supporting the PhD study and research work. Authors acknowledge the support by the Hungarian Research Grant VKE 2018-1-3-1_0003 "Development of advanced concrete elements".

8. REFERENCES

Adams, J., Alexander A., et. al. (2018), *"Medical Additive Manufacturing/3D Printing"*, Faculty of Medicine, Nursing & Health Sciences, Monash University, SME Medical AM3DP Workgroup, Annual report, 2018.

Balazic, M., Kopac, J., Jackson, M.J., Ahmed, W. (2007), *"Review: titanium and titanium alloy applications in medicine"*, Int J Nano Biomater 2007;1. http://dx.doi.org/10.1504/IJNBM.2007.016517.

Berman, B. (2012), *"3-D printing: the new industrial revolution*", Bus Horiz. 2012;55(2): pp. 155–62.

Chua, C.K., Wai, Y.Y. (2015), *"Bioprinting principles and applications"*, 1st ed. World Scientific Publishing Company; 2015. 296 p. Available from: https://books.google.com/books?id=nhK3CgAAQBAJ&pgis=1.

Eggbeer, D., Bibb, R., Williams, R. (2005), *"The computer-aided design and rapid prototyping fabrication of removable partial denture frameworks"*, Proc Inst Mech Eng., 2005;219(3): pp 195–202.

Elahinia, M.H., Hashemi, M., Tabesh, M. and Bhaduri, S.B. (2012), *"Manufacturing and processing of NiTi implants: a review"*, Progress in materials science, 57(5), pp. 911-946.

Faulkner, A., Fyfe, C., Cornelissen, D.J., Gardner, J., King, J., Courtney, A. and Shu, W., (2015), *"Bioprinting of human pluripotent stem cells and their directed differentiation into hepatocyte-like cells for the generation of mini-livers in 3D"*. Biofabrication, 7(4), p. 044102.

Foletti, J.M., Lari, N., Dumas, P., Compes, P., Guyot, L. (2012), *"PEEK customized implant for skull esthetic reconstruction"*. Rev Stomatol Chir Maxillofac, 2012;113(6):468–71.

Gepreel, MA-H., Niinomi, M. (2013), *"Biocompatibility of Ti-alloys for long-term implantation"*. J Mech Behav Biomed Mater 2013; 20:407–15.

Hallab, N., Merritt, K., Jacobs, J.J. (2001), *"Metal sensitivity in patients with orthopaedic implants"*. J Bone Joint Surg Am. 2001;83(3):428.

Hutmacher, D.W (2013), *"A road map for a tissue engineering concept for restoring structure and function after limb loss"*. J Mater Sci Mater Med 2013;24(11):2659–63.

Jones, J.R. (2013), *"Review of bioactive glass: from Hench to hybrids"*. Acta Biomater 2013;9(1):4457–86.

Kachouie, N.N., Du, Y., Bae, H. (2010), *"Khabiry M, Ahari AF, Zamanian B, et al. Directed assembly of cell-laden hydrogels for engineering functional tissues"*. Organogenesis 2010;6(4):234–44.

Kalaskar, D. (2017), *"3D Printing in Medicine"*, Elsevier, 1st Edition - April 1, 2017, p 219.

Klein, G.T., Lu, Y., Wang, M.Y. (2013), *"3D printing and neurosurgery – ready for prime time?"*. World Neurosurg, 2013;80(3–4):233–5

Kolesky, D.B., Truby, R.L., Gladman, A.S., Busbee, T.A., Homan, K.A., Lewis, J.A. (2014), *"3D bioprinting of vascularized, heterogeneous cell-laden tissue constructs"*. Adv Mater, 2014;26(19):3124–30

Liu, Q., Leu, M.C., Schmitt, S.M. (2006), *"Rapid prototyping in dentistry: technology and application"*. Int J Adv Manuf Technol, 2006;29(3–4):317–35.

Mannoor, M.S., Jiang, Z., James, T., Kong, Y.L., Malatesta, K.A., Soboyejo, W., et al. (2013), *"A 3D printed bionic ear"*. Nano Lett, 23;2013:2634–9.

Marga, F., Jakab, K., Khatiwala, C., Shepherd, B., Dorfman, S., Hubbard, B., et al (2012), *"Toward engineering functional organ modules by additive manufacturing"*. Biofabrication, 2012;4(2):022001.

Millesi, H. (2007), *"Bridging defects: autologous nerve grafts"*. Acta Neurochir Suppl, 2007; 100:37–8.

Mok, S-W., Nizak, R., Fu, S-C., Ho, K-WK., Qin, L., Saris, D.B., et al. (2016), *"From the printer: Potential of three-dimensional printing for orthopaedic applications"*. J Orthopaed Transl, 2016; 6:42–9.

Ozbolat, I.T., Yu, Y. (2013), *"Bioprinting toward organ fabrication: challenges and future trends"*. IEEE Trans Biomed Eng., 2013;60(3):691–9.

Ploch, C., Mansi, C., Jayamohan, J., and Kuhl, E. (2016), *„ Using 3D Printing to Create Personalized Brain Models for Neurosurgical Training and Preoperative Planning"*, World Neurosurgery, V (90), 2016, pp. 668-674. https://doi.org/10.1016/j.wneu.2016.02.081

Quan, W. (2015), *"3D-printed alginate/hydroxyapatite hydrogel in combination of Atsttrin to repair bone defects"*. [dissertation]. Hangzhou: Zhejiang University; 2015. Chinese.

Reiffel, A.J., Kafka, C., Hernandez, K.A., Popa, S., Perez, J.L., Zhou, S., et al (2013). *"High-fidelity tissue engineering of patient specific auricles for reconstruction of pediatric microtia and other auricular deformities"*. PLoS One. 2013;8(2).

Sawkins, M.J., Mistry, P., Brown, B.N., Shakesheff, K.M., Bonassar, L.J., Yang, J. (2015),*"Cell and protein compatible 3D bioprinting of mechanically strong constructs for bone repair"*. Biofabrication, 2015;7(3):035004.

Sheth, R., Balesh, E.R., Zhang, Y.S., Hirsch, J.A., Khademhosseini, A. and Oklu, R., (2016), *"Three-dimensional printing: an enabling technology for IR"*. Journal of Vascular and Interventional Radiology, 27(6), pp. 859-865.

Tasoglu, S., Demirci, U. (2013), *"Bioprinting for stem cell research"*. Trends Biotechnol 2013;31(1):10–19.

U.S. FDA, (2020), Food and Drug Administration, *"3D Printing of Medical Devices,"* last modified March 26, 2020, https://www.fda.gov/medicaldevices/products-and-medical-procedures/3d-printing-medical-devices

Ventola, C.L. (2014), *"Medical Applications for 3D Printing: Current and Projected Uses"*. P T, 2014;39(10):704–11.

Weinberg, C.B., Bell, E. (1986), *"A blood vessel model constructed from collagen and cultured vascular cells"*. Science. 1986;231(4736):397–400

Williams, D.F. (2008), *"On the mechanisms of biocompatibility"*. Biomaterials 2008;29(20):2941–53

Woodruff, M.A., Lange, C., Reichert, J., Berner, A., Chen, F., Fratzl, P., et al. (2012), *" Bone tissue engineering: from bench to bedside"*. Mater Today 2012;15(10):430–5.

Yan, Y., Li, S., Xiong, Z., Wang, X.H., Zhang, T., Zhang, R.J. (2010), *"Fabrication technology of tissue engineering scaffold based on rapid prototyping"*. J Mech Eng 2010;46(5):93–8

Marwah M. Thajeel (1991), PhD student at the Department of Construction Materials and Technologies, Budapest University of Technology and Economics. Finished her bachelor (2012) in Civil Engineering at College of Engineering, Al-Muthanna University in Iraq and finished her master studies (2020) Master of Science in Structural Engineering at College of Engineering, Al-Qadisiyah University in Iraq. Research areas: Reinforced Concrete, Shear Strengthening, Fiber Reinforced Polymers, Fiber Reinforced Concrete. Member of the Hungarian Group of ***fib***.

György L. Balázs (1958), Civil Engineer, PhD, Dr.-habil., Professor of structural engineering at the Department of Construction Materials and Technologies of Budapest University of Technology and Economics (BME). His main fields of activities are experimental investigation and modeling of RC, PC, FRC, FRP, HSC, HPC, LWC, fire resistance and fire design, durability, sustainability, bond and cracking. He is chairman of several commissions and task groups of ***fib***. He is president of Hungarian Group of ***fib***, Editor-in-chief of the Journal „Concrete Structures". He was elected as President of ***fib*** for the period of 2011-2012. Since then, he is Honorary President of ***fib***. Chairman of ***fib*** Com 9 Dissemination of knowledge.

3D PRINTING FOR EARTH CONSTRUCTIONS – REVIEW


Marwah M. Thajeel - György L. Balázs

https://doi.org/10.32970/CS.2022.1.10

Concrete is the second frequently used material in our planet. Being the most consumed construction material for infrastructures and buildings, the demand for concrete is very high at present and expected to have the same significance in the future. On the other hand, conventional concrete could not be considered as an environmentally friendly construction material. This comes from the perspectives of reducing natural resources, high energy consumption, and produce a huge amounts of construction waste. 3D printing construction with earth materials provide the potential solutions to reshape the construction world and answering the current demands of sustainability, energy efficiency and cost in construction. This paper presents a review of 3D printed constructions made from earth materials benefits, limitations and current applications.

Keywords: 3D printing, additive manufacturing, earth materials, earthen construction

1. INTRODUCTION

Additive manufacturing also known as 3D printing was first developed in the 1980s, but at that time was a difficult and expensive operation and so had few applications. It is only since 2000 that it has become relatively straightforward and affordable and so has become viable for a wide range of uses including product design, component and tool manufacture, plastics, metalworking, aerospace engineering, dental and medical application and construction industry. 3D printing is a promising technology in construction work that can help improve the efficiency and minimize the errors of the construction and providing a matchless design freedom to designers and architects, as well as can help to optimize the structure shape by reduce the amount of the material used (Le et al., 2012, Lloret, 2015). This procedure is mainly used for minimizing the time and cost of the project (*Fig. 1*) (Nadarajah, 2018). Extrusion-deposition additive manufacturing is one of the most studied techniques. This method involves the use of multiple layers of concrete by a machine to create construction components or to print entire buildings (Lim et al., 2012, Perrot, 2016).

Constructions made from earth material are becoming more prevalent in today's energy-efficient homes and buildings. Their low ecological footprint makes them an ideal alternative to fossil fuels. At all stages of its use, clay doesn't require much energy. It can be reused, and it is easy to maintain. Also, due to its thermal inertia, mud constructions can help lower energy costs and provide a healthy indoor climate (Azeredo et al., 2008, Aubert et al., 2015). Although earth material is readily available, but its development is still limited by the high cost and the problematic durability. This issue is mainly due to the time needed for the material to harden and the labor cost to produce a good quality mud product. Many of research and experimental have been carried to improve the mix design made from earth material to have quick casting and good strength in the hardened state (Moevus et al.,2015, Landrou et al., 2017).

Digital manufacturing with earth materials could introduce the concept of traditional materials to our modern culture. This material could provide solutions to the issues of quality, cost, and efficiency. Although this technology is in its infancy, examples of digital manufacturing with earth materi-

Fig 1: 3D printing process Vs conventional construction (Nadarajah, 2018)

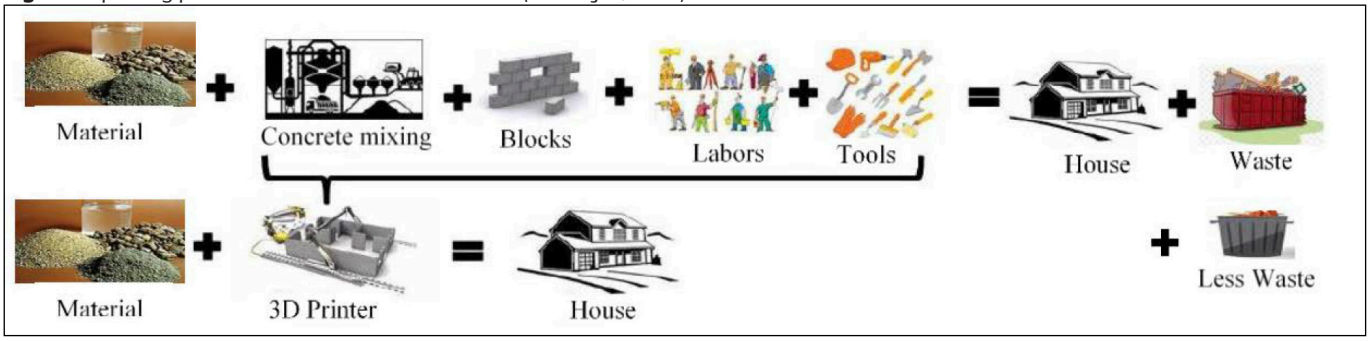

als already exist in the literature. Perrot et al. (2018) printed 3m wall made from earth material with addition of alginate to increase the strength as well as to improve the productivity. Dubor et al. (2018) tested the structural and environmental performance of full scale printed wall made of clay.

This paper aims to show the possibility of merge the 3D printing technology with natural and locally found materials to produce more economic and eco-friendly constructions.

2. 3D EARTHEN CONSTRUCTION BENEFITS AND LIMITATIONS

2.1 Advantages

Concrete is one of the most plentiful man-made composite materials worldwide that has steadily reached its popularity since its inception. It is used in buildings, roads, highways, retaining walls, dams, bridges and other all types of civil construction work, the demand for concrete is very high at present and projected to have the same importance in the future. Nevertheless, traditional concrete could not be considered as an environmentally friendly construction material. This comes from the perspectives of depleting natural resources, high energy consumption, and construction waste disposal (Ismail and Ramli, 2013). Consequently, the necessity for the utilization of renewable and recyclable resources in concrete industries is of prime importance.

In this regard, one of reasonable alternative options is the use 3D printed construction with earth materials, additive manufacturing provides a matchless freedom of form for architects of concrete members, and this can lead to reduce the construction waste since the production and management of forms, can produce a large amount of waste, particularly in the case of forms for complex structures with assembly components that are utilized just a single time, as well as reduce amount of material used by using topological optimization concept and construction time and error. Meanwhile, the earth material can reduce the demand for conventional materials, since the major constituents of concrete are the aggregates and cement and the continuous mining create the shortage problem of the construction materials, as well as cement production process responsible of about 8% of the world‘s CO2 emissions (Chatham House, 2018). To avoid this issue, it is a quite important search for alternative materials, and earth material such as clay or mud could be a good solution, since they freely available. Erath materials also offers the benefits of natural insulation, fire protection, air circulation, low first cost, 100% recyclable structures, thermal flywheel effect, low greenhouse emissions, regulating the climate and providing a healthy Indoor environment.

Earthen construction can be utilized to build the affordable housing in low-income countries and disasters refuges using soil from the surrounding area. Natural disasters thing cannot be prevented by any technology leaving the victims homeless and exposed to the external actions. According to previous disasters refuges analyses, state that to build hundreds or thousands of refuges its take years (*Fig. 2)*. Utilization of 3D printing technology with the use of local materials for construction of the refuges, this can reduce the construction time to months and reduce the cost of materials and the cost of the project in half, since the refuges are temporary, its good alternative to save money throughout the construction process.

Fig. 2: Disaster shelters (Nadarajah, 2018)

2.2 Challenges

The use of concrete for 3D printing needs a specific type of concrete. The concrete mixture should flow like a paste and harden once it has been placed. The concrete should not set too quickly while in use, since this would block the nozzle and cause the printing process to be disrupted. As a result, the concrete’s open time is critical in the printing process. Extrudability, flowability, and open time are all concepts that are intimately related to concrete consistency and setting time. Therefore, specific qualities of concrete should be adjusted and adapted for printing in order to optimize it for 3D printing settings. Another issue with using Additive Manufacturing on a wide scale is the cost of acquiring infrastructure by building companies. The cost savings obtained from this technology mainly include savings in materials, labor and time, without considering the detailed costs of the 3D printer/robot, and necessary hardware, software, training, etc. As seen in Building Information Modeling (BIM), many construction companies, especially those in developing countries, have not yet implemented the Additive Manufacturing due to huge costs engaged for hardware, software and training, etc. (Aitbayeva and Hossain, 2020).

Moreover, because of the cost, insurability issues, and poor durability due to high water sensitivity, the development of earthen building is still limited. The high cost is primarily due to the high cost of labor and the time it takes for the material to solidify, as well as a slower production rate than the concrete industry. Having a mix design that allows for both rapid casting and appropriate strength in the dry state is problematic at the moment. Therefore, more researches are need to address these problems.

3. APPLICATIONS OF 3D PRINTED EARTHEN CONSTRUCTION

In the mid-2000s researcher from the University of Southern California, Dr. Behrokh Khoshnevis developed a process called Contour Crafting (CC) that prepare for the present day’s 3D Printing Concrete (Khoshnevis, 2004). Since that several researches are engaged in the expansion of large-scale 3D printers for the construction industry, the world has now witnessed many printed structures ranging from offices, houses, bridges, shelters and many more. 3D printed constructions with earth materials are presents in the following sub sections.

Fig. 3: Gaia house (Gaia, 2018)

3.1 Gaia house

WASP (World's Advanced Saving Project), an Italian company cooperated with RiceHouse that work in the field of sustainable building by the use of waste from rice production, to build Gaia, (*Fig. 3*), the first sustainable house model with earth material from the surrounding area and natural waste materials**,** coming from the rice production chain**,** aiming to achieve an efficient product from a bio-climatic perspective.

For the construction of Gaia, RiceHouse and WASP used vegetable fibers to create a compound that included 25% of on-site soil (30% sand, 30% clay, and 40% silt), 25% rice husk, 40% straw chopped rice, and 10% hydraulic lime. The muller was used to knead the mixture, which resulted in a homogenous and workable composite.

The Crane WASP printer was created with the goal of integrating natural ventilation, thermal-acoustic insulation, and plant engineering systems all inside the same space. The deposition of raw soil, rice production waste and straw are regulated by articulated weaves capable of giving both constructive firmness and geometric diversity throughout the wall's development. The precision and speed of 3D technologies enable the diversity of computational design in building practice, allowing for intricate geometries that are impossible to recreate with traditional construction systems. The printed area was 30 square meters with wall thickness of 40 cm, the production time was only 10 days due to its masonry, it doesn't need air condition or heating system, as it keeps moderate and comfortable temperature inside both in summer and winter.

Gaia is a high-performing module in terms of energy efficiency and indoor air quality, with approximately no environmental impact. (Gaia, 2018).

3.2 Tecla house

Tecla house (the name Tecla, a combination of the words Technology and Clay), is a new circular model of housing entirely created with reusable and recyclable materials, collected from local soil**,** (*Fig. 4*). The first model was designed by the Italian architecture studio Mario Cucinella Architects (MCA) and engineered and built by Italian 3D printing specialists WASP (World's Advanced Saving Project) by April 2021, becoming the world's first house 3D-printed entirely from a mixture made from mainly local earth and water.

The material consists of local soil mixed with water, fibers from rice husks and a binder. The house is made up of two modules up to 4.2 m in height, has an area of about 60 m^3. The house was built with 200 hours of printing, formed of two connected dome-shaped volumes with a ribbed outer wall that is made up of 350 stacked layers of 3D-printed clay with thickness 12 mm, with circular open on its roof allowing light to enter the house throughout the day. The clay is arranged in undulating layers that not only provide structural stability but also to act as a thermal barrier

The prototype was constructed using a multileveled, modular 3D printer that uses two synchronized arms, each with a 50-square meter printing area that can print modules simultaneously. Tecla was the first 3D printed building that constructed by using two printers at the same time, due to WASP software capable of optimizing movements, preventing collisions, and ensuring simultaneous operation.

Tecla was developed as part of an eco-sustainability research study that looked to bioclimatic principles and vernacular architecture and construction to produce low-carbon homes. By using this technology, housing modules can be built within 200 hours while consuming an average of six kilowatts of energy for 60 m^3 of natural materials and reducing typical construction waste. WASP founder, Massimo Moretti explains, "TECLA shows that a beautiful, healthy, and sustainable home can be built by a machine, giving the essential information to the local raw material,"(Tecla, 2020).

4. CONCLUSIONS

3D construction using soil materials may become one of the important innovations in the world of construction, that combines ancient building techniques with modern technology to form recyclable, low-carbon, climate-adaptable buildings. Take the benefits of additive manufacturing in terms of freely design, reducing construction time, cost and error, as well as take the advantages of the earth materials due to unlimited existing quantity and zero environmental impact.

Erath materials also offers the benefits of natural insulation, fire protection, air circulation, low first cost, 100% recyclable structures, thermal flywheel effect, low greenhouse emissions, regulating the climate and providing a healthy Indoor environment.

Earthen construction can be utilized to build the affordable housing in low-income countries and disasters refuges.

Fig. 4: *Tecla house (Tecla, 2020)*

Utilization of 3D printing technology with the use of local materials for construction of the refuges, this can reduce the construction time from years to months and reduce the cost of materials and the cost of the project in half, since the refuges are temporary, its good alternative to save money throughout the construction process.

Moreover, the earthen construction development is still limited, due to the insurability issues, and poor durability due to high water sensitivity. Further efforts are needed to safely print more economic-sustainable construction.

5. ACKNOLEDGEMENT

Stipendium Hungaricum Scholarship Program is highly acknowledged for supporting the PhD study and research work. Authors acknowledge the support by the Hungarian Research Grant VKE 2018-1-3-1_0003 "Development of advanced concrete elements".

6. REFERENCES

Aitbayeva, D., and Hossain, M. A. (2020). "Building Information Model (BIM) Implementation in Perspective of Kazakhstan: Opportunities and Barriers" Journal of Engineering Research and Reports, 14(1), 1324, https://doi.org/10.9734/jerr/2020/v14i117113

Aubert, J.E., Maillard, P., Morel, J.C. and Al Rafii, M. (2015), "Towards a simple compressive strength test for earth bricks?" Mater Struct. 1–14 (2015), https://doi.org/10.1617/s11527-015-0601-y.

Azeredo, G., Morel, JC. and Lamarque, CH (2008). "Applicability of rheometers to characterizing earth mortar behavior. Part I: experimental device and validation". Mater Struct 41, 1465–1472 (2008). https://doi.org/10.1617/s11527-007-9343-9

Chatham House, (2018), "Why Cement is a Major Contributor to Climate Change", published12 June 2018, Available online at, https://www.chathamhouse.org/2018/06/why-cement-major-contributor-climate-change (Accessed on 27 December 2021)

Dubor, A., Cabay, E., Chronis, A. (2018),"Energy Efficient Design for 3D Printed Earth Architecture", Humanizing Digital Reality. Springer, Singapore, 2018, pp 383-393. https://doi.org/10.1007/978-981-10-6611-5_33

Gaia, (2018), "The first 3D printed house generated with the Earth", Available online at: https://www.3dwasp.com/casa-stampata-in-3d-gaia/, (Accessed on 26 December 2021).

Ismail, S. and Ramli, M. (2013), "Engineering properties of treated recycled concrete aggregate (RCA) for structural applications", Construction and Building Materials. Elsevier Ltd, 44, pp. 464–476.

Khoshnevis, B. (2004), "Automated construction by contour crafting—related roboticsand information technologies", Automation in Construction. Elsevier, 13(1), pp. 5–19.

Landrou, G., Brumaud, C., Habert, G. (2017), "Clay particles as binder for earth buildings materials: a fresh look into rheology of dense clay suspensions". In: EPJ Web of Conferences, 2017, EDP Sciences, p. 13010.

Le, T.T., Austin, S.A., Lim, S. et al. (2012), "Mix design and fresh properties for high-performance printing concrete". Mater Struct. 45, 1221–1232 (2012). https://doi.org/10.1617/s11527-012-9828-z

Lim, S., Buswell, R.A., Le, T.T., et al. (2012), "Developments in construction-scale additive manufacturing processes", Autom. Constr. 21 (2012) 262–268, https://doi.org/10.1016/j.autcon.2011.06.010

Lloret, E., Shahab, A.R., Linus, M., et al. (2016), "Complex concrete structures: Merging existing casting techniques with digital fabrication", Mater. Ecol. 60 (2015) 40– 49, https://doi.org/10.1016/j.cad.2014.02.011.

Moevus, M., Jorand, Y., Olagnon, C., et al. (2015), "Earthen construction: an increase of the mechanical strength by optimizing the dispersion of the binder phase", Mater. Struct. 1–14 (2015), https://doi.org/10.1617/s11527-015- 0595-5.

Nadarajah N. (2018), "Development of concrete 3D Printing". Master's Thesis, Aalto University, Espoo, Finland, 2018.

Perrot, A., Rangeard, D. and Pierre, A. (2016), "Structural built-up of cement-based materials used for 3D-printing extrusion techniques". Mater Struct 49, 1213–1220 (2016). https://doi.org/10.1617/s11527-015-0571-0.

Perrot, A., Rangeard, D., Courteille, E. (2018), " 3D printing of earth-based materials: Processing aspects", Construction and Building Materials, V 172, 30 May 2018, pp 670-676, https://doi.org/10.1016/j.conbuildmat.2018.04.017

Tecla, (2021), Available online at: https://www.3dwasp.com/casa-stampata-in-3d-tecla/, (Accessed on 26 December 2021).

Marwah M. Thajeel (1991), PhD student at the Department of Construction Materials and Technologies, Budapest University of Technology and Economics. Finished her bachelor (2012) in Civil Engineering at College of Engineering, Al-Muthanna University in Iraq and finished her master studies (2020) Master of Science in Structural Engineering at College of Engineering, Al-Qadisiyah University in Iraq. Research areas: Reinforced Concrete, Shear Strengthening, Fiber Reinforced Polymers, Fiber Reinforced Concrete. Member of the Hungarian Group of fib.

György L. Balázs (1958), Civil Engineer, PhD, Dr.-habil., Professor of structural engineering at the Department of Construction Materials and Technologies of Budapest University of Technology and Economics (BME). His main fields of activities are experimental investigation and modeling of RC, PC, FRC, FRP, HSC, HPC, LWC, fire resistance and fire design, durability, sustainability, bond and cracking. He is chairman of several commissions and task groups of fib. He is president of Hungarian Group of fib, Editor-in-chief of the Journal "Concrete Structures". He was elected as President of ***fib*** for the period of 2011-2012. Since then, he is Honorary President of ***fib.*** Chairman of fib Com 9 Dissemination of knowledge.

fib BULLETIN NO. 101 TITLE: PRECAST CONCRETE IN TALL BUILDINGS

Year: 2021
Pages: 234
Format approx. DIN A4 (210x297 mm)
ISBN: 978-2-88394-153-3

Abstract:
There has been continued global growth in tall building construction over recent years. The variation in the use of such buildings is remarkable, from lavish hotels and apartments to socially affordable units. As the world struggles to cope with growing numbers of people, dwindling resources and movements from rural to urban habitats it is unavoidable that population densities will increase, and more efficient use of scarce land will be needed. Taller buildings are the inevitable consequence.

Tall buildings can use several different types of material to form their framework and envelope. Those materials are mixed to provide an optimum building solution to suit client requirements such as structure, occupancy, vision, affordability, timing, sustainability and quality. Precast concrete is one of those materials, and has been used from whole frameworks to facades, and elements mixed with structural steelwork and cast in place concrete.

This state of the art report shows how precast concrete can be effectively integrated into tall buildings using modern materials and techniques, drawing on the experience and expertise that is currently available in the global precast concrete industry. The report is aimed at not only building professionals and students, but also at contractors, investors, owners, public bodies and any other parties interested in the possibilities for use of precast concrete in tall building construction. Extensive case studies at the end of the Bulletin illustrate the benefits and applications discussed in the earlier chapters.

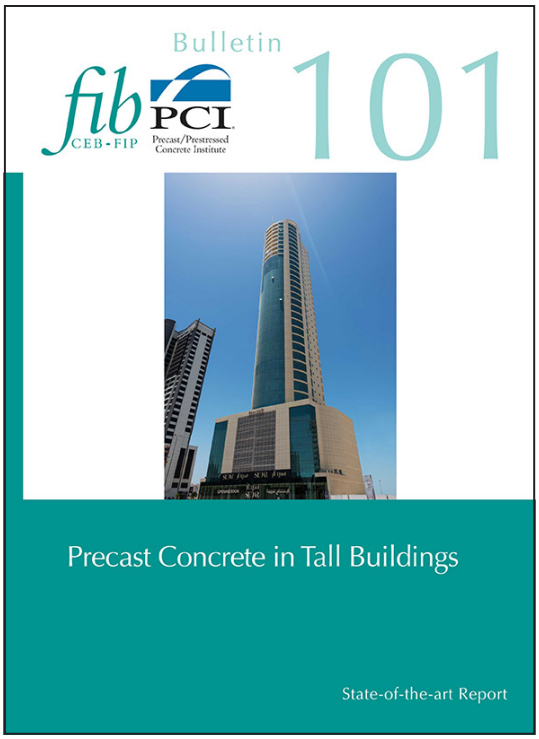

fib BULLETIN NO. 102 TITLE: GUIDE FOR PROTECTION AND REPAIR OF CONCRETE STRUCTURES

Year: 2022
Pages: 291
Format approx. DIN A4 (210x297 mm)
ISBN: 978-2-88394-155-7

Abstract:
The idea of preparing a technical document for the repairs and interventions upon concrete structures goes back to the former fib COM5: Structural Service Life Aspects, being the goal of the then TG5.9. After a long period of reduced activity, and taking into account the reorganization of fib commissions that meanwhile took place, on June 2017 a different approach was proposed to push forward the task of TG8.1 (formerly TG5.9).

The (new) goal of TG 8.1 was to deliver a 'how-to-do' guide, gathering together protection, repair, and strengthening techniques for concrete structures. Chapters are intended to provide both guidelines and case-studies, serving as support to the application of fib MC2020 pre-normative specifications.

Each chapter was written by an editorial team comprising desirably at least a researcher, a designer and a contractor. Templates have been prepared in order to harmonize the contents and the presentation of the different methods. Following the writing process, chapters were reviewed by experts and, after amendments by the authors, they underwent a second review process by COM8 and TG3.4 members, as well as by different practitioners.

For each protection, repair and strengthening method addressed in this guide, readers have a description of when to adopt it, which materials and systems are required, which techniques are available, and what kind of equipment is needed. It then presents a summary of stakeholders' roles and qualifications, design guidelines referring to most relevant codes and references, the intervention procedure, quality control measures and monitoring and maintenance activities. Due to the extent of the guide, it was decided to publish it as bulletin 102, addressing protection and repair methods, and bulletin 103, addressing strengthening methods.

We would like to thank the authors, reviewers and members of COM8 and TG3.4 for their work in developing this fib Bulletin, which we hope will be useful for professionals working in the field of existing concrete structures, especially those concerned with life-cycle management and conservation activities.

As noted above, this Bulletin is also intended to act as a background and supporting document to the next edition of the fib Model Code for Concrete Structures, which is currently under development under the auspices of TG10.1 with the working title of "fib Model Code 2020".

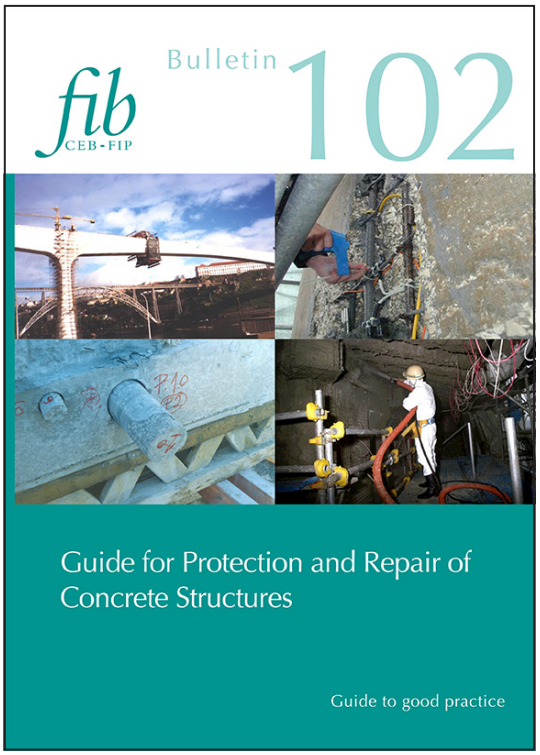

AZ NKFI ALAPBÓL MEGVALÓSULÓ PROJEKT
NEMZETI KUTATÁSI, FEJLESZTÉSI ÉS INNOVÁCIÓS HIVATAL
AZ INNOVÁCIÓ LENDÜLETE

BME, *consortium leader*
SW Umweltechnik Mo. Kft.,
ÉMI Nonprofit Kft. MC Bauchemie.
CRH Mo. Kft.

MŰEGYETEM 1782
BUDAPESTI MŰSZAKI ÉS GAZDASÁGTUDOMÁNYI EGYETEM
Építőmérnöki Kar - építőmérnöki képzés 1782 óta
Építőanyagok és Magasépítés Tanszék

National Competitiveness and Excellence Program, Subprogram B:National Program for Materials Science and Technology
Hungarian Research Grant NVKP_16-1-2016-0019
"Development of concrete products with improved resistance to chemical corrosion, fire or freeze-thaw"."
Procurement of laboratory equipment within the framework of the tender entitled

Project supervisor: Prof. György L. Balázs

Project sub-theme responsibles: Dr. Éva Lublóy, Dr. Salem G. Nehme, Dr. Katalin Kopecskó

MATERIAL SCIENTIFIC STUDIES FROM NANO-LEVEL TO MACRO-LEVEL

1. PHENOM XL Scanning Electron Microscope (SEM) with elemental analysis of EDS (energy dispersive X-ray spectroscopy) for small and large (max. 100 mm x 100 mm) samples

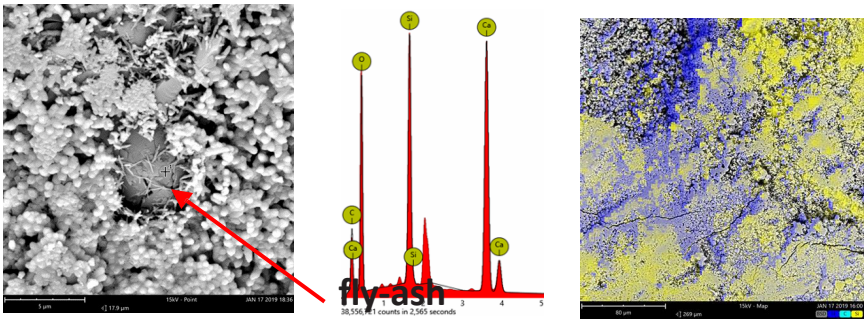

2. TAM Air 3+3 channel microcalorimeter, with 125 ml ampoulles, application range: from cement paste to concrete

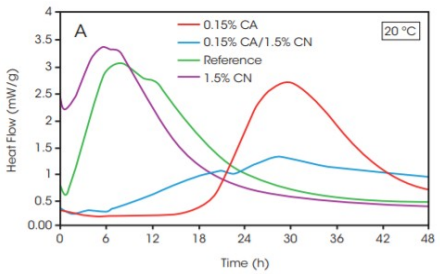

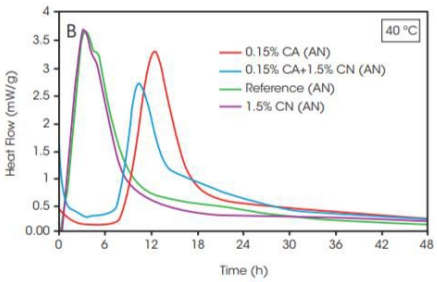

3. Zetasizer Nano ZS – Measurement of Zeta potential with titrator (variable pH range) 3,8 nm – 100 µm, particle size distribution in range 0,3 nm – 10 µm

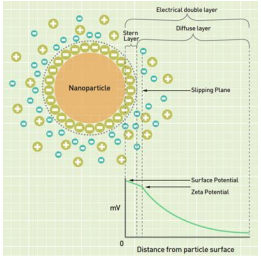

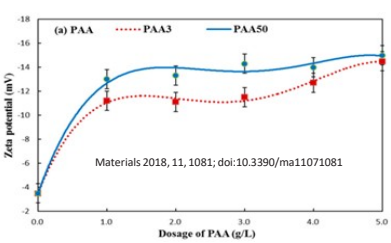

A-HÍD

CREATE THE FUTURE

A-Híd Zrt. I 1138 Budapest, Karikás Frigyes u. 20. I www.ahid.hu